UNIVERSITY OF CINCINNATI

August 30th , 20 03

I, Krishna Prasad Vummidi Murali **,**
hereby submit this as part of the requirements for the degree of:

Master of Science (M.S.)

in:

Electrical Engineering

It is entitled:

Thermionic Emission Diffusion Model of InP-based Pnp Heterojunction Bipolar Transistor with Non-Uniform Base Doping

Approved by:

Prof. Marc M. Cahay

Prof. Punit Boolchand

Prof. Kenneth P. Roenker

Thermionic Emission Diffusion Model of InP-based Pnp Heterojunction Bipolar Transistor with Non-Uniform Base Doping

A thesis submitted to the
Division of Research and Advanced Studies
of the University of Cincinnati
in partial fulfillment of the
requirements for the degree of

MASTER OF SCIENCE (M.S.)

in the Department of Electrical and Computer Engineering
and Computer Science
of the College of Engineering

2003

by

Krishna Prasad Vummidi Murali
B.E. (Instrumentation and Control Engineering)
University of Madras, Chennai, India
2000

Committee Chair: Dr. Marc M. Cahay

Abstract

In the past few years, GaAs and InP and, more recently, GaN based Npn and Pnp Heterojunction Bipolar Transistors (HBTs) have been grown and their performance has been evaluated in great details due to their potential applications in microwave, millimeter-wave, optoelectronics and high-speed applications.

This model includes the physics of hole thermionic-emission-diffusion injection at the emitter-base heterojunction and transport of holes across a linearly doped base, a calculation of the recombination currents in the base current including the effects of linear base doping, and a comparison of the effects of linear and uniform doping on current gain and base transit time.

Our simulations show that the use of non-uniform doping in the base of Pnp HBTs helps increasing the DC current gain by as much as a factor of 4. Simultaneously, we show that the base transit time, which is the major component to the overall delay time, is reduced by factor of 2. This should help increasing the unit current gain frequency and high frequency performance of Pnp HBTs.

Acknowledgements

The pursuit and completion of this study would not have been possible without the support, encouragement, and understanding of so many people. It is with great pleasure and gratitude that I take this opportunity to express my appreciation to all those who have helped me in various ways through out my course of stay at University of Cincinnati.

This thesis would not have been possible without the help, support and guidance of my advisor Dr. Marc M. Cahay. I would like to express my sincere gratitude to him for guiding me throughout the course of my thesis these two years. I would also like to thank the committee members Dr. Roenker and Dr. Boolchand.

A sincere thanks goes to all students who have endured my questions and opinions through out my stay at U.C. Thanks also go out to my friends, roommates (Bhaskar, Divakar, Jagan, Jimble, Kowta, Munish, Murali, Partha, Pradeep, Rajkumar, Shankhar, Sreeram, Sujan, Vikram and Vinodh) and colleagues (Mohan, Rajesh, Ramanujam, Venkat and Yamini) who have helped me in many ways and for making my stay in Cincinnati fun. A special thanks to Sumithra who had made my stay in Cincinnati sweet and memorable.

I have tried to include everyone, but unfortunately it is not possible to name all those who have helped me. But still a big Thanks to you all.

I am extremely greatful to my wonderful, loving parents and my sister who always had faith in my abilities and for all the sacrifices they made for me. I would not have

achieved a single thing in my life without them.

Contents

1 Introduction and Thesis outline **1**

1.1 Background 1

1.2 HBT Theory 2

1.3 InP - based HBT Technology 4

1.4 Pnp HBT Technology 7

1.5 Motivation and Organization of the Thesis 10

2 Thermionic-Emission-Diffusion Model of Pnp HBT with non-uniform base doping **13**

2.1 Introduction 13

2.2 Material Parameters 17

2.2.1 Carrier Mobility 17

2.2.2 Carrier Lifetime 19

2.3 Doping Profile in the base 24

2.4 Thermionic Emission Diffusion Model for a non-uniformly doped base . . 25

2.4.1 Effective Hole Velocities and Hole Current Density 27
2.4.2 Device Equations for the case of a non-uniformly doped base 32
2.4.3 Terminal currents and current gain 36
2.4.4 Base transit time 43
2.5 Conclusion 45

3 Results and Discussion **46**
3.1 Introduction 46
3.2 Effective Hole Velocities 47
3.3 Minority Carrier Concentration Profile in the Base 50
3.4 Terminal Currents and Current Gain 53
3.5 Base Transit Time 60

4 Summary and Suggestions for Future work. **64**
4.1 Thesis Summary. 64
4.2 Analytical Model Development 66

A Expression for built-in potential and effective velocity S_{ep} **79**

B Depletion Approximation at Emitter-Base Junction **83**

C Derivation of Current Density Across the Emitter-Base Junction of a Pnp HBT **87**

D Hole Transport Across the Base. **99**

E Recombination Current Components **107**

F Calculation of Base Transit Time **111**

List of Figures

1.1 Energy-band diagram for an abrupt Pn heterojunction typical of the emitter-base junction of a Pnp HBT. 5

2.1 Hole mobility model in $In_{0.53}Ga_{0.47}As$ as a function of doping with a fit (dashed line) to the Caughey-Thomas model (full line). 20

2.2 Electron and hole minority carrier lifetime in $In_{0.52}Ga_{0.48}As$ models as a function of doping level. The dark squares are experimental data. Below 8 x $10^{17}cm^{-3}$, τ_n and τ_p are assumed to be constant. Above 8 x $10^{17}cm^{-3}$ τ_n and τ_p are well fitted by Eq.(2.3) with the values of the parameters listed in Table 2.5 [60]. 22

2.3 Schematic energy band diagram and quasi-Fermi level variation across emitter-base heterojunction and base in a Pnp heterojunction bipolar transistor. 26

3.1 From top to bottom, Effective hole velocities base-collector saturation (v_s), quasi-neutral base diffusion (S_{dp}), thermionic emission with tunneling (S_{ip}), emitter space charge region drift diffusion (S_{ep}) and thermionic emission without tunneling in that order for InAlAs/InGaAs Pnp HBT with the parameters listed in Table 2.1 as a function of emitter-base bias V_{EB}. The results are for the case of uniform doping ($R = 1$). 49

3.2 From top to bottom, effective hole velocities [base-collector saturation (v_s^{eff}), quasi-neutral base diffusion (S_{dp}^{eff}), thermionic emission with tunneling (S_{ip}), emitter space charge region drift diffusion (S_{ep}) and thermionic emission without tunneling] for the InAlAs/InGaAs Pnp HBT with their parameters listed Table 2.1 as a function of emitter-base bias V_{EB}. The plots are for the case of maximum grading (R = 0.1), i.e, with the doping in the base region varying linearly from 10^{19} to $10^{18} cm^{-3}$ from the emitter to the collector end of the base. 51

3.3 Effective hole Saturation (v_s^{eff}) and diffusion (S_{dp}^{eff}) velocities as a function of dopant grading R. 52

3.4 Hole concentration profile across the quasi-neutral base for collector current densities of $10^3, 10^4$ and $10^5 A/cm^2$ for dopant gradings of $R = 0.9$ (top curve in each set of curves) to $R = 0.1$ (bottom curve in each set of curves) in steps of 0.1. 54

3.5 Base recombination currents: nonradiative J_{br} ($\diamond$) and radiative J_{rr} ($\circ$), space charge region J_{scr} ($\triangle$), surface J_{sr} ($\star$), emitter side interface J_{ire} ($\times$), base side interface J_{irb} ($\bigtriangledown$), electron back injection J_{ne} ($\triangleleft$), electron collector leakage J_{nc} ($\triangleright$) as a function of dopant grading R in the base for a collector current density of $10^4 A/cm^2$. 56

3.6 Base recombination currents: nonradiative J_{br} ($\diamond$) and radiative J_{rr} ($\circ$), interface J_{irb} ($\bigtriangledown$) space charge region (J_{scr}) ($\triangle$) surface J_{sr} ($\star$), as a function of dopant grading R in the base for collector current density of $10^3 A/cm^2$. 57

3.7 Base recombination currents: nonradiative J_{br} ($\diamond$) and radiative J_{rr} ($\circ$), interface J_{irb} ($\bigtriangledown$) space charge region (J_{scr}) ($\triangle$) surface J_{sr} ($\star$), as a function of dopant grading R in the base for collector current density of $10^4 A/cm^2$. 58

3.8 Base recombination currents: nonradiative J_{br} ($\diamond$) and radiative J_{rr} ($\circ$), interface J_{irb} ($\bigtriangledown$) space charge region (J_{scr}) ($\triangle$) surface J_{sr} ($\star$), as a function of dopant grading, R in the base for collector current density of $10^5 A/cm^2$. 59

3.9 Base current (J_b) and collector current (J_c) densities as function of emitter-base bias V_{EB} for two dopant gradings. The top and bottom figures correspond to R = 0.9 and 0.1, respectively. 61

3.10 DC current gain as function of collector current density (J_c) for dopant grading R varying from 0.9 (bottom) to 0.1 (top) in steps of 0.1. 62

3.11 Base transit time as function of the dopant grading R. The base transit time is relatively insensitive to the value of the collector current density. . 63

A.1 Band diagrams for two different semiconductor materials forming a heterointerface. The vacuum level is chosen as the reference energy. V_{bi} is the built in voltage. 80

List of Tables

1.1 Band Offset for GaAs and InP-based Heterostructures. 6

2.1 Summary of material parameters for the Pnp InAlAs/InGaAs heterojunction bipolar transistor studied in this thesis [37]. 16

2.2 Summary of important material parameters for InGaAs and InAlAs. . . . 18

2.3 Summary of hole mobility model parameters for InGaAs and InAlAs. . . 19

2.4 Summary of electron mobility model parameters for InGaAs and InAlAs. 21

2.5 Summary of lifetime model parameters for InGaAs [60]. 23

Chapter 1

Introduction and Thesis outline

1.1 Background

The idea that the performance of a bipolar transistor could be improved by changing the emitter material composition to increase its energy gap relative to the base is as old as the bipolar transistor itself [1,2,3]. The implementation of heterojunction approaches in bipolar devices, however, was delayed by decades from the time of initial concepts. The delay was caused by the technological problems of achieving interfaces between dissimilar materials that were free of imperfections, which could result from either impurities or structural defects due to a mismatch in lattice constant. With the advent of new fabrication techniques such as Molecular Beam Epitaxy (MBE) [4] and Metal-Organic Chemical Vapor Deposition (MOCVD) [5] in the last two decades, it has become feasible to realize heterojunction structures. In MBE, beams of ions impinge on a crystal and

epitaxial layers are grown. In MOCVD, organic precursors are combined, heated and broken down over a heated substrate to achieve epitaxial growth. Both techniques have led to the actual fabrication of Heterojunction Bipolar Transistors (HBTs) in various III - V compound systems.

In HBTs, the semiconductor or material composition is allowed to vary across the device, providing an extra degree of freedom in bipolar transistor design. By changing the band structure appropriately, the quasi-electric fields established within the HBTs exert forces on carriers. By selectively combining these forces and electrostatic forces, independent control can be exerted over the motion of electrons and holes and used to increase current gain and reduce the overall delay time [3]. The modern epitaxial growth techniques facilitates the precise control of composition in III - V semiconductor devices, giving more flexibility for designing novel device structures. In the past few years, GaAs and InP and more recently GaN based Npn and Pnp HBTs have been grown and their performance has been evaluated in great details due to their potential applications in microwave, millimeter wave, optoelectronics and high-speed applications [6,7,8,9,10,11, 12].

1.2 HBT Theory

In HBTs, a heterojunction is typically formed at the emitter-base interface with semiconductors of the same lattice constant and crystal structure, but different band-gaps.

This is illustrated in Figure 1.1 where we show the energy-band diagram of a Pn heterojunction typical of the emitter base junction for a Pnp HBT [3]. The presence of a heterojunction between the emitter and base regions results in a potential barrier which prevents the back injection of electrons from the base into the emitter and similarly for npn transistors prevents the back injection of holes from the base. The bandgap of the emitter and base affect the current gain, h_{fe}, through the emitter injection efficiency, G_e, which for the Pn junction of Figure 1.1 is given by [3]

$$G_e = \frac{p_e v_h}{n_b v_e} e^{(\Delta E_g/kT)}. \tag{1.1}$$

Here p_e is the emitter hole concentration, v_h is the effective velocity of holes injected into the base, n_b is the base electron concentration, v_e is the corresponding velocity of electrons into the emitter, and ΔE_g is the difference in bandgaps of emitter and base. From Figure 1.1, it may be seen that barriers V_n and V_p for electron and hole injection are different, $\Delta E_g = E_{ge} - E_{gb} = V_p - V_n$. In homojunction transistors, the factor $e^{(\Delta E_g/kT)}$ tends to be less than unity from bandgap narrowing effects. In HBTs, wide gap emitters materials are chosen with $\Delta E_g = 0.2$ eV or above, so that $e^{(\Delta E_g/kT)}$ can exceed 2000 or more at room temperature. As a result, emitter injection efficiency can be reached without the need of high emitter doping. Typically, base doping levels can be increased to above $10^{19} cm^{-3}$, and emitter doping dropped to 5 x $10^{17} cm^{-3}$. The high base doping leads to a low base resistance even with a thin base layer thickness and a high current gain at the same time. Futhermore, a thin base layer reduces the base

transit time so that high frequency operation is possible.

The benefits of HBTs, can be summed up as having lower base resistance, avoidance of base punch through, elimination of high injection problems, high Early voltage, reduction of B-E capacitance and potentially ultrahigh current gain. In a typical HBT design, the emitter doping and thickness must be selected to minimize the emitter resistance and emitter-base junction capacitance. Hence, base layer is heavily doped to minimize the base resistance and the base thickness is usually very thin to achieve high frequency operation. The collector layer thickness is chosen to minimize the collector transit time and collector doping is low to reduce the base collector junction capacitance to increase cut off frequency and increase the breakdown voltage.

1.3 InP - based HBT Technology

When InP is used as the substrate, the epitaxial layers that be can grown in a lattice-matched fashion are InP, $In_{0.52}Al_{0.48}As$, and $In_{0.53}Ga_{0.47}As$. InP and InAlAs have roughly the same energy gap, and energy gap of InGaAs is significantly smaller. Therefore InGaAs is used as the base layer in an InP-based HBT, and either InP or InAlAs serves as the emitter material. The collector is either, InGaAs or InP. When InGaAs is used it is a single heterojunction transistor. When InP is used, the device is Double Heterojunction Bipolar Transistor. This has been demonstrated by both MBE [13] and MOCVD [14] techniques. $In_{0.52}Al_{0.48}As$ is a welcome replacement for InP as the

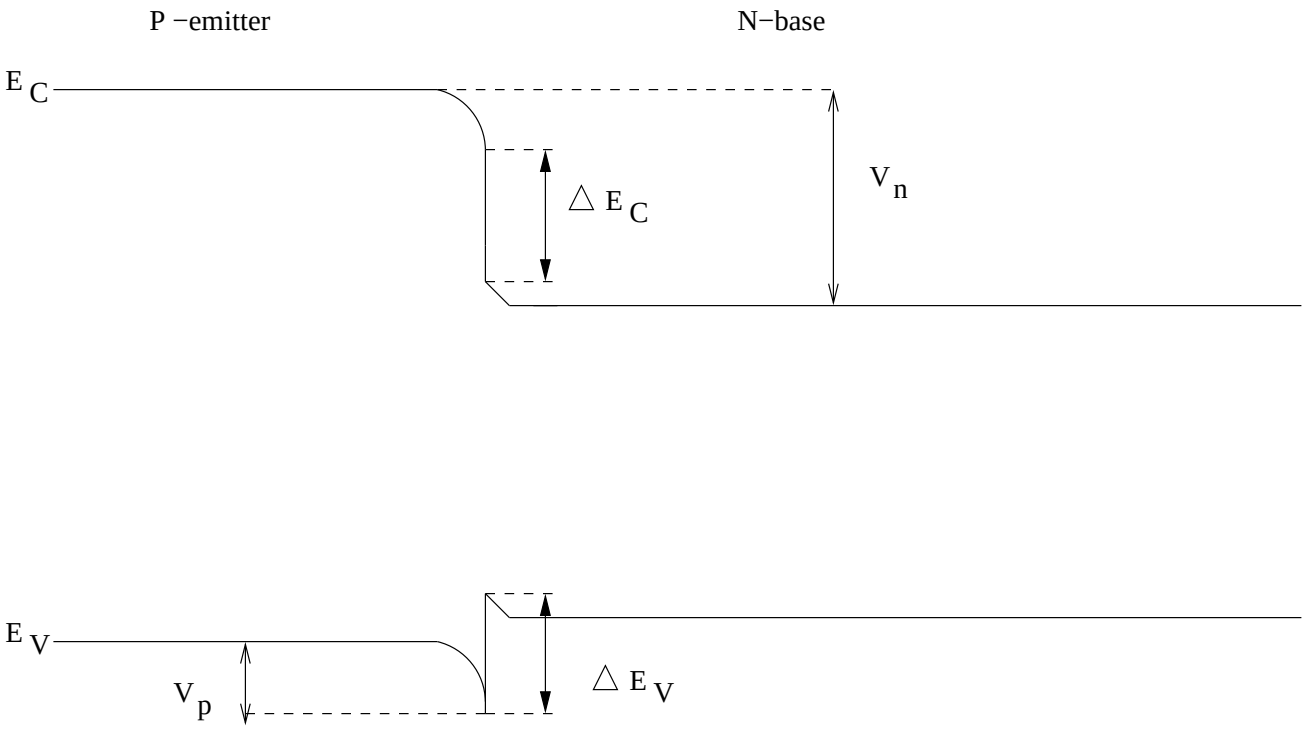

Figure 1.1: Energy-band diagram for an abrupt Pn heterojunction typical of the emitter-base junction of a Pnp HBT.

emitter material because of the difficulty in using available solid sources to grow InP emitter in MBE growth technique. Table 1.1 shows the energy bandgap and band gap discontinuities for InAlAs/InGaAs, InP/InGaAs and AlGaAs/GaAs [15] systems.

Material	E_g(eV)	E_c(eV)	E_v(eV)
InP/InGaAs	1.35/0.76	0.25	0.34
InAlAs/InGaAs	1.48/0.76	0.48	0.24
AlGaAs/GaAs	1.86/1.42	0.28	0.15

Table 1.1: Band Offset for GaAs and InP-based Heterostructures.

There are quite a few advantages of using InGaAs as the base region, and InP or InAlAs as the emitter region. First, in InP/InGaAs or InAlAs/InGaAs system the surface recombination rate is small as compared to the AlGaAs/GaAs structure, which allows higher current gain since surface recombination dominates the base current in GaAs based HBTs. Second, the electron mobility is higher in InGaAs than in GaAs, resulting in superior high frequency performance for InP-based HBT. A research group from University of California, Santa Barbara, are working towards transistors with an f_{MAX} greater than 1 THz and have reported transistors with f_{MAX} in excess of 800 GHz for an InAlAs/InGaAs HBT using transferred substrate technology [16,17].

InP based materials provide a number of advantages over competing materials for HBT implementations

1. Electron mobility is very high(higher than GaAs, with μ_n = 13,000 cm^2/Vs in

undoped layers). Similarly, the attainable values of velocity overshoot are higher, and persist over larger voltage ranges, because the energy separation of Γ and satellite valleys is higher (0.55 eV in InGaAs).

2. Larger valence band and conduction band discontinuities resulting in higher emitter-injection efficiency and non-equilibrium transport in the base.

3. The recombination velocity at free surfaces of InGaAs is lower than that in GaAs (10^3 versus 10^6 cm/sec), allowing easier scaling-down of device dimensions.

4. Lower bandgap for the InGaAs base leading to low turn-on voltage. This is useful for digital circuit operation with low power dissipation.

5. Semi-insulating substrates of InP have higher thermal conductivity than those of GaAs.

6. InP-based devices are directly compatible with optical sources and detectors for 1.3 μm and 1.55 μm radiation, which are widely used in long distance communication.

1.4 Pnp HBT Technology

The development Pnp HBTs has been lagging behind their Npn counterparts, because of apparent inferior hole properties compared to those of electrons. However, in recent years, there has been encouraging reports on Pnp HBTs fabricated in the GaAs and InP and GaN material system. It is an attractive device for use in complementary HBT-based circuit applications. There has also been good progress in the implementation

of high performance Pnp transistors along with Npns. Analysis of Pnp HBTs in the AlGaAs/GaAs material system have shown that these devices have considerable potential for microwave and millimeter-wave performance [11,18,19,20]. When the device's epitaxial structure is appropriately optimized, the performance parameters for the Pnp HBT comparable to those of Npn devices are possible [21,22,23,24] and in fact, Pnps may offer an advantage over Npn for microwave power applications due to their lower base resistances [6,8]. In recent years, there has been a number of demonstrations of Pnp GaAs-based HBTs with reports of measured cutoff frequency as high as 33 GHz and a maximum frequency of oscillation as high as 66 GHz [7,9,10,25,26]. Monolithic integration of Npns with Pnps has been demonstrated and is very useful in a number of applications where Pnp HBT could be used as a active load in feedback amplifier design or as a matched component in push-pull amplifiers [27,28].

Another III-V material of interest for high-power and high temperature applications is AlGaN/GaN heterostructures [29,30]. They are attractive because of wider bandgap, large breakdown field and a high electron saturation drift velocity. AlGaN/GaN microwave HEMTs have been reported with a record power output and power-added efficiency at moderate microwave frequencies. Heterojunction bipolar transistors may offer improved phase noise, linearity, and (output-limited) power bandwidth, but the low p-type doping thus far realized in GaN presents a formidable handicap to GaN HBT operation. Use of deep submicron emitter and collector scaling, in combination with substrate transfer processes [17], might mitigate the need for high p-type doping con-

centrations in AlGaN/GaN HBTs. Performances of pnp and npn AlGaN/GaN HBTs have been investigated with the use of 2-D device simulators [31]. It is shown that in pnp HBTs improvement in current gain could be achieved by both base reduction and compositional grading of the base. Simulated performances on pnp HBTs display frequency values one order of magnitude lower than the Npn HBT caused by the reduced minority hole transport across the base. AlGaN/GaN pnp HBTs have also been fabricated and shown to have high emitter efficiency [32].

InP-based Pnp HBTs have comparable high frequency capabilities to the Npn HBT [28], [33]. Monolithic integration of Pnps and Npns on the same substrate has been demonstrated using a merged epitaxy on a patterned, etched substrate [28],[34]. Recently, an InP based integrated HBT amplifier with Pnp active load was demonstrated for the first time using complementary HBT technology (CHBT) [35]. Stachina et al. [20, 21] have reported InAlAs/InGaAs Pnp HBTs with current gain of 170, a cut of frequency f_T of 14 GHz and maximum frequency of operation f_{MAX} of 22 GHz. Lunardi et al. [33] have reported similar results for InP/InGaAs Pnp HBTs with a current gain of 420, a cutoff frequency of f_T 10.5 GHz and maximum frequency of operation f_{MAX} of 25 GHz. A number of characteristics that make high-frequency Npn InP-based HBTs attractive, such as larger emitter-base energy bandgap differences and band discontinuities, low base-emitter turn on operating voltages, low contact resistivities, and high electron mobility, are also expected to lead performance for the InP-based Pnp HBTs comparable or superior to their GaAs based and the current GaN based HBTs.

While hole mobilities in the above mentioned material system are much lower than electron mobilities, the HBT is a device whose performance depends not only on the minority carrier transport across the narrow base region, but also on the base resistance which is dependent on the majority carrier electron mobility. For the Pnp HBT, the high electron mobility in the n-type base aids reducing the base resistance, allowing shrinkage of the base region and reduction in the base doping in order to compensate in part for the reduced hole mobility across the base. For InGaAs, the electron mobility is higher than that of GaAs so that this effect is accentuated on InP-based Pnp HBTs. This is important for power applications and contributes for higher f_{MAX} for the Pnp relative to the Npn HBT [6], [8].

1.5 Motivation and Organization of the Thesis

Most of the work done on Pnp HBTs have investigated the limitations associated with the hole's small mobility neglecting the important issues of thermionic emission and tunneling of holes across the emitter-base heterojunction and non-equilibrium hole transport in the base. They also neglected the important physics of the various recombination currents, the device parasitics and characteristically longer minority carrier lifetimes of holes relative to electrons [36]. Datta et al. have addressed some of these issues and have also investigated the device performance for a compositionally graded base [37]. The thrust of this research work is to address the above issues and develop an analytical

model for InP-based Pnp HBTs for the case of a non-uniformly doped base. The model includes the physics of hole thermionic-emission-diffusion injection at the emitter-base heterojunction and transport of holes across a linearly doped base, a calculation of the recombination currents in the base current including the effects of linear base doping, and a comparison of the effects of linear and uniform doping on current gain and base transit time.

Major efforts to improve the device performance includes reduction of the emitter-base charging time, base resistance, base transit time and improve gain. Compositionally graded base relies on bandgap engineering to create a quasi electric field to aid carrier transport and improve the device performance. An analytical model for a compositionally graded base for a InAlAs/InGaAs HBT has been presented by Datta et al. [37]. The base is linearly graded from InAlGaAs to InGaAs towards the collector. Datta et al. have shown that the base grading induces a quasi electric field which improves the overall device performance including improvements in current gain, cutoff frequency and maximum frequency of oscillation. The feasibility of the use of compositional grading in the base for Npn InP-based HBT has also been demonstrated by Kurishima et al. [38] and Ohkubo et al. [39]. using strained $In_{1-x}Ga_xAs$.

Device performance could also be improved by using non-uniformly doped base and achieve comparable results. Effects of base and emitter doping gradients for an AlGaAs/GaAs npn heterostructure have shown to improve the device performance as compared to the uniformly doped case [40], [41]. The doping dependent quasi electric field

in the base would be better than that for compositionally induced electric field because compositional grading reduces electron and hole mobilities which degrades the high frequency performance of the transistor. The non-uniform doping in the base increases the minority current in the base and reduces base transit time and improves current gain. The use of MBE and MOCVD techniques give great flexibility to design the HBT doping profile. Hence it is worth studying the performance sensitivity of non-uniform doping profiles in the base region.

This thesis is organized as follows. In chapter II, we describe an analytical thermionic-emission-diffusion model of InP-based Pnp HBTs for the case of nonuniform (linear) base doping profile. The model also includes the effects of non-uniform doping on the recombination currents. In this work, we focus on two figures of merit, the dc current gain and total base transit time. In chapter III, we apply this model to study the dc current gain and total base transit time of a specific Pnp InAlAs/InGaAs HBT as a function of the gradient of the base doping profile. We also present the results of base dopant gradient on the minority hole concentration across the base and also on the various recombination currents of a specific Pnp InAlAs/InGaAs HBT. In chapter IV, we summarize the work done and give some suggestions for future work in developing a more comprehensive model. Some of the analytical derivations in chapter II are quite lengthy and have therefore been outlined in greater details in a series of appendices.

Chapter 2

Thermionic-Emission-Diffusion Model of Pnp HBT with non-uniform base doping

2.1 Introduction

In this chapter, we describe an analytical thermionic-emission-diffusion model of Inp-based Pnp HBTs for the case of non-uniform base doping profile. Our approach follows the analytical treatment of Datta et al. [37] who have considered the influence of bandgap grading in the base on the performance of Pnp HBTs. The model matches the hole drift-diffusion current at the emitter end of the quasi neutral, non-uniformly doped base with the hole thermionic current across the valence band spike. Both hole drift-diffusion

across the emitter space charge region (SCR) and thermionic emission of the holes across the valence band discontinuity including a correction for hole tunneling are considered to determine the net hole injection across the emitter base heterojunction. Our model includes the effects of various recombination currents including the emitter-base charge region (J_{scr}), on the base side (J_{irb}), and emitter side recombination currents (J_{ire}) at the emitter-base interface, surface recombination current (J_{sr}), and the nonradiative (J_{br}), and radiative (J_{rr}) recombination currents in the base. Our model also takes into account electron back injection (J_{ne}) and electron collector leakage (J_{nc}) currents. We calculate the base and collector current densities and current gain for non-uniformly doped base and compare the results to the case of uniform doping. We also calculate the base transit time for both cases.

In the next sections, we give an outline of the model. To avoid distracting the reader with lengthy analytical derivations whenever encountered, the latter are given in a series of appendices. Appendix A gives the expression for the built-in potential following Anderson's rule, which we have used in our calculations and also shows the independence of emitter space charge drift velocity on interface dipole effect. The expressions for the electric field in the emitter base space charge region as a function of applied bias using the depletion apprroximation is given in appendix B. The expressions for the effective hole velocities describing the carrier transport process in the device and their dependence on non-uniform base doping are derived in appendices C and D. The various expressions for the recombination currents and the base transit time including the effect of non-uniform

doping are derived in appendices E and F. In this thesis, we have focussed our attention to the InP-based Pnp HBT studied by Datta et al.[37,42] so that we can compare their use of grading the electron affinity in the base to our use of non-uniform (linear) base doping profile to enhance the overall device performance. In this work, we focus on two figures of merit, the DC current gain and the base transit time.

After developing an analytical model we will apply the model to study the dc current gain and total base transit time of a specific Pnp InAlAs/InGaAs HBT as function of the gradient of the (linear) doping profile in the base. The device dimensions and doping are listed in Table 2.1. This is the same device as the one analyzed by Datta et al. [42] for the case of compositionally graded base, except for the doping in the base which was fixed at 5 x $10^{18} cm^{-3}$ in their analysis. In our simulations, we neglect compositional grading (base is made of $In_{0.53}Al_{0.47}As$) and the doping is varied from $10^{19} cm^{-3}$ at the emitter end of the base down to $10^{18} cm^{-3}$ at the collector end of the base. This case corresponds to an average of 5 x $10^{18} cm^{-3}$ in the base. To study the influence of the doping gradient, we also vary the doping at the collector end of the base from 10^{18} to $10^{19} cm^{-3}$ in steps of $10^{18} cm^{-3}$ while keeping the concentration at the emitter end fixed.

Emitter	Base	Collector
InAlAs p-type	InGaAs n-type	InGaAs p-type
$E_g = 1.47$ eV	$E_g(x_{nc}) = 0.75$ eV	$E_g = 0.75$ eV
$X_E = 4.1$ eV	$X_B(x_{nc}) = 4.58$ eV	$X_C = 4.58$ eV
$N_E = 1$ x $10^{18}/cm^3$	N_B(x) $/cm^3$	$N_C = 5$ x $10^{16}/cm^3$
$W_E = 0.14\ \mu m$	$W_B = 0.06\ \mu m$	$W_C = 0.30\ \mu m$
$L_{ne} = 0.38\ \mu m$	$L_{pb} = 0.48\ \mu m$	$L_{ne} = 5.2\ \mu m$
$\mu_h = 59\ cm^2/Vs$	$\mu_p = 100\ cm^2/Vs$	$\mu_n = 1160\ cm^2/Vs$
	$m_e^* = 0.041\ m_o$	$m_e^* = 0.041\ m_o$
$m_{pe}^* = 0.48\ m_o$	$m_{pb}^* = 0.47\ m_o$	$m_{pc}^* = 0.47\ m_o$
$n_{ie} = 9.3$ x $10^5/cm^3$	$n_{io} = 6.5$ x $10^5/cm^3$	
$s_e = 10$ cm/s	$s_b = 10$ cm/s	
		$v_s = 4.5$ x 10^6 cm/s
$\rho_{ec} = 1$ x 10^{-6} cm	$\rho_{bc} = 1$ x 10^{-7} cm	$\rho_{cc} = 1$ x 10^{-6} cm
$N_{tr} = 4$ x $10^{16}/cm^3$	B = 4.2 x $10^{11} cm^3 s$	
$\sigma = 4$ x $10^{-17} cm^2$	$s_o L_s = 2$ x $10^{-4} cm^2/s$	

Table 2.1: Summary of material parameters for the Pnp InAlAs/InGaAs heterojunction bipolar transistor studied in this thesis [37].

2.2 Material Parameters

Efficient simulation of any heterojunction based device relies critically on the accuracy of parameters used in the modeling process. In the Pnp HBT described above, materials used are $In_{0.53}Ga_{0.47}As$ (base and collector regions) and $In_{0.52}Al_{0.48}As$ (emitter), where the latter two are lattice matched to InP. Table 2.2 provides a summary of important material parameters for both these materials. Table 2.1 shows that the hole effective masses are a factor of six to ten larger than those for the electrons. Hence, the hole mobilities are correspondingly reduced. More specifically, the larger hole effective mass will decrease the hole minority carrier diffusion length in the base thereby reducing the base transport factor and current gain. It will also increase the base transit time, hence reduce the transistor's cutoff frequency. In addition, the lower majority carrier hole mobility in the emitter and collector will increase the corresponding series resistance. However, small electron effective mass gives rise to large majority carrier electron mobility in the base that reduces the base resistance, which contributes to a higher power gain and maximum frequency of oscillation and allows a reduction in the base width.

2.2.1 Carrier Mobility

The carrier mobilities are a strong function of doping level. This dependence is critical in this work because the base doping is linearly graded from the emitter end up to the collector end of the base. No distinction has been made between majority and minority

Parameter	Symbol	InGaAs	InAlAs
Permitivity	ϵ_r/ϵ_o	13.88 [43]	12.30 [44]
Energy Gap	E_g(eV)	0.75 [45]	1.47 [46]
Electron Affinity	$X(eV)$	4.58 [47]	4.1 [47]
Electron effective mass	m_n^*/m_o	0.04 [47]	0.075 [48]
Hole Effective mass	m_p^*/m_o	0.47 [47]	0.47 [44]
Light hole	m_{lh}^*/m_o	0.05 [45,47]	0.09 [44,46,48,49,50]
Heavy hole	m_{hh}^*/m_o	0.46 [45,47]	0.58 [44,48,49]

Table 2.2: Summary of important material parameters for InGaAs and InAlAs.

carrier mobility due to lack of sufficient data, though a significant difference has been reported for InGaAs material system [40]. Hereafter, we start with the Caughey-Thomas model of mobility variation versus the base doping concentration N_B [47,51,52]

$$\mu = \mu_{min} + \frac{\Delta\mu}{[1 + (\frac{N_B}{N_C})^{\alpha}]}, \tag{2.1}$$

where $\Delta\mu$ = μ_{max} - μ_{min}. The hole mobility in the $In_{0.53}Ga_{0.47}As$ base is plotted in Figure 2.3 using the parameters (μ_{min}, μ_{max} and α) listed in Table 2.4. We approximate Eq.(2.1) by a simpler analytical fit for the range of base doping of interest to us (from $10^{18}/cm^3$ to $10^{19}/cm^3$) with a formula of the type

$$\mu = \frac{\mu_o}{(N_B/N_C)^{\gamma}}. \tag{2.2}$$

The values of μ_o and γ were obtained so that Eq.(2.2) provides a good approximation

to Eq.(2.1) over that range of doping concentration. Figure 2.1 shows the fit to the Caughey-Thomas model for hole mobilities in InGaAs for μ_o and γ equal to 193 and 0.387, respectively. In Eqs.(2.1) and (2.2), N_C corresponds to the doping density above which the ionized impurity scattering becomes dominant. The values of N_C are listed in Table 2.3 for InGaAs and InAlAs. Due to larger hole effective mass than electron, the hole mobilities at low doping are more than an order of magnitude less than the corresponding electron mobility. For InGaAs and InAlAs, the latter can also be described with a Caughey-Thomas model with the fitting parameters listed in Table 2.4.

Parameter	Units	InGaAs	InAlAs
μ_{max}	$cm^2/Vsec$	331 [47,50,53]	75 [54]
μ_{min}	$cm^2/Vsec$	75	40
N_C	$1/cm^3$	1.0x10^{18}	3.8x10^{17}
α		1.37	0.79
v_s	cm/sec	4.5x10^6 [9,47]	3.0x10^6 [49]

Table 2.3: Summary of hole mobility model parameters for InGaAs and InAlAs.

2.2.2 Carrier Lifetime

The minority carrier lifetime in the base region is also critically important to the Pnp device's performance, influencing both the current gain and cutoff frequency. For modeling purposes, the doping dependence of the lifetime was included in the calculations.

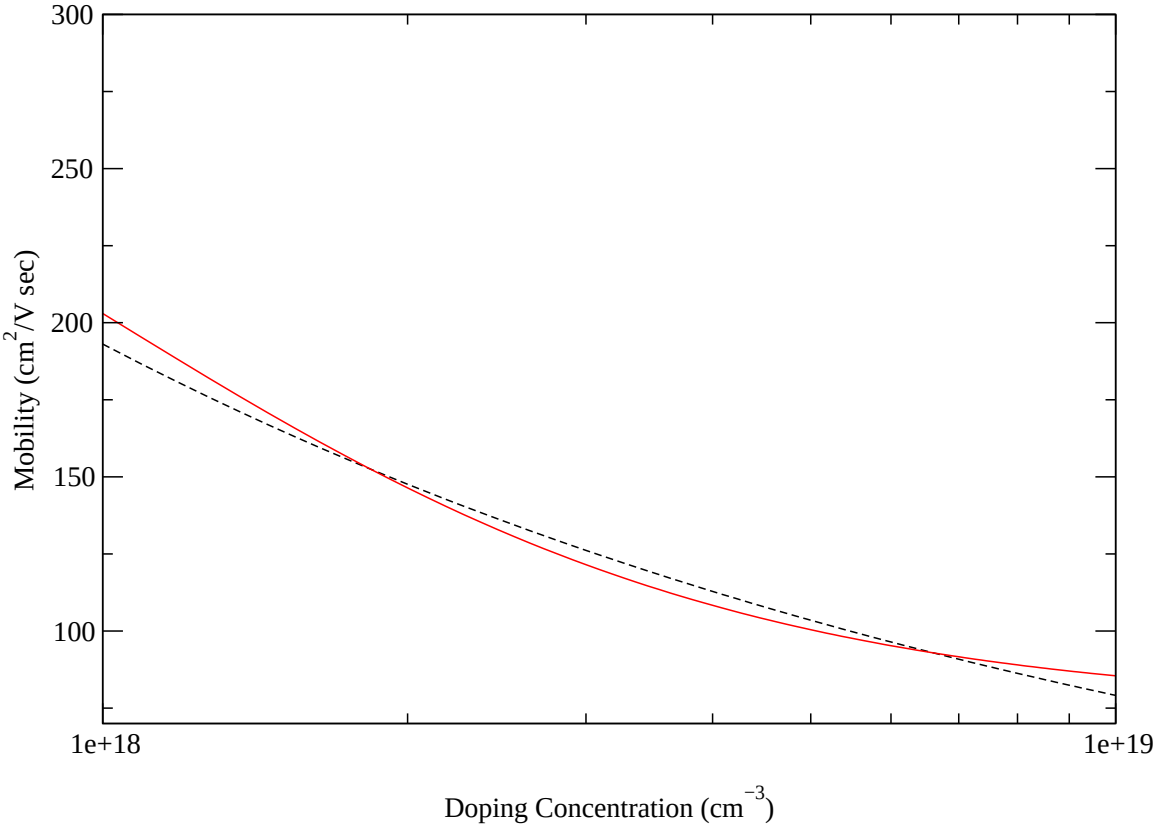

Figure 2.1: Hole mobility model in $In_{0.53}Ga_{0.47}As$ as a function of doping with a fit (dashed line) to the Caughey-Thomas model (full line).

Parameter	Units	InGaAs	InAlAs
μ_{max}	$cm^2/Vsec$	11,599 [50]	4,226 [55,56,57,58]
μ_{min}	$cm^2/Vsec$	3,372	220
N_C	$1/cm^3$	8.9x10^{16}	1.5x10^{14}
α		0.76	0.27
v_s	cm/sec	6.0x10^6 [47]	0.27 [49,56,59]

Table 2.4: Summary of electron mobility model parameters for InGaAs and InAlAs.

For n^+ InGaAs base, the hole lifetime in the base is a function of the doping and was fit to the empirical expression [60,61,62,63,64,65]

$$\tau_p(nsec) = 10^{\delta - \vartheta log N_B}, \tag{2.3}$$

where N_B is the base doping and the fitting parameters are $\delta = 22.4$ and $\vartheta = 1.20$ for $N_D \geq 8$ x $10^{17} cm^{-3}$. For smaller base dopings, a constant lifetime of 10 nsec was assumed. In the case of non-uniform base doping (linearly graded from emitter end to base collector junction), N_B would be a function of the location in the base. The minority carrier lifetime is known to be a function of the material quality and processing history so that its prediction is less certain than other material parameters. Figure 2.2 shows the electron and hole lifetimes as a function of doping in InGaAs. As can be seen, the minority carrier hole lifetime is significantly larger than that for the electron at the same doping level.

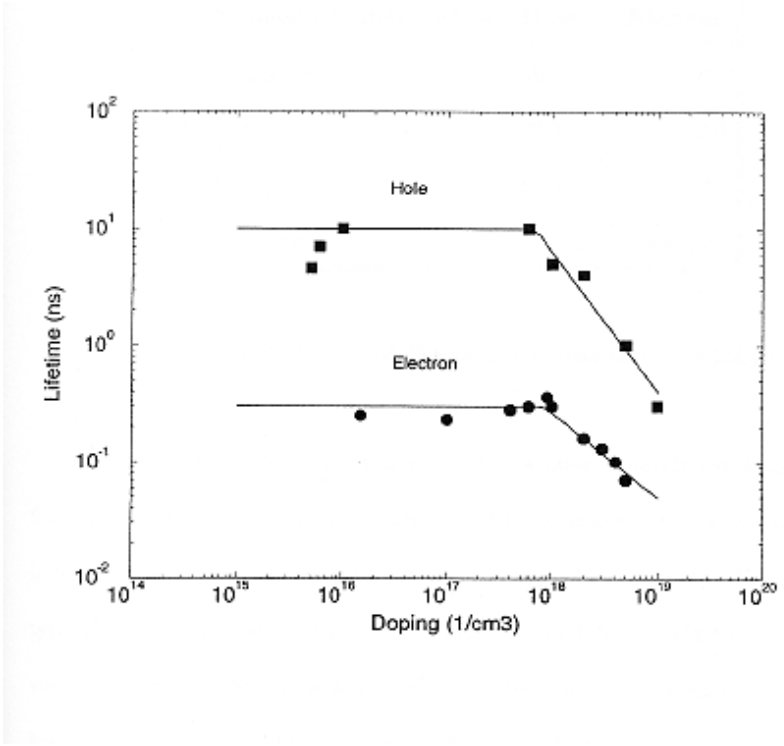

Figure 2.2: Electron and hole minority carrier lifetime in $In_{0.52}Ga_{0.48}As$ models as a function of doping level. The dark squares are experimental data. Below 8 x $10^{17}cm^{-3}$, τ_n and τ_p are assumed to be constant. Above 8 x $10^{17}cm^{-3}$ τ_n and τ_p are well fitted by Eq.(2.3) with the values of the parameters listed in Table 2.5 [60].

For hole transport across the base in Pnp HBTs, the hole diffusion length L_p is important and is related to the mobility and minority carrier lifetime by

$$L_p = \sqrt{D_p \tau_p} = \sqrt{\frac{k_B T}{q} \mu_p(N_B) \tau_p(N_B)}. \tag{2.4}$$

Combining the empirical models of the doping dependence of mobility and lifetime described above, the hole diffusion length can be calculated as a function of base doping N_B and its variation across the base.

Comparison of the electron and hole diffusion length, at a fixed doping level shows that, at doping level larger than $10^{18} cm^{-3}$, the hole diffusion length is only about a factor of two smaller than that for electron at the same doping level.

Minority Carrier Lifetime	Hole	Electron
$\tau_{max}(ns)$	10	0.3
ϑ	22.4	12.6
θ	1.2	0.73
$N_C(cm^{-3})$	8x10^{17}	8x10^{17}

Table 2.5: Summary of lifetime model parameters for InGaAs [60].

This is due to the fact that longer hole lifetime compensate in part for the lower hole mobility. For example, at a typical base doping of 1 x 10^{19} cm^{-3}, the hole mobility is only 86 cm^2/Vs compared with an electron mobility of 3590 cm^2/Vs. However, at this same doping level, the hole minority carrier lifetime is 0.40 ns vs 0.05 ns for electron.

At this doping level, the corresponding hole and electron diffusion lengths are 0.30 and 0.68 μm, respectively. This implies that the base width of Pnp HBTs needs to reduce only a factor of two smaller to that of a Npn HBT to achieve comparable current gain.

2.3 Doping Profile in the base

Modeling accurately the transport through the base of a Pnp HBT transistor is essential to assess the device performance. In this work, we examine the effects of non-uniform base doping on the minority carrier concentrations in the base, various recombination currents, the base transit time and transistor current gain. We assume that the base doping varies linearly from a high value at the emitter-base end to a lower value at the base-collector end of the base. In our simulations the doping is varied from $10^{19} cm^{-3}$ at the emitter end to $10^{18} cm^{-3}$. To characterize this doping gradient, we introduce the parameter k such that

$$k = -\frac{dN_B(x)}{dx} = \frac{N_B(x_e) - N_B(x_c)}{W_B}, \tag{2.5}$$

which is always positive since $N_B(x_e) \geq N_B(x_c)$ in our case. As will be shown below (see Eq. (2.26)), this leads to an effective electric field in the positive x-direction which facilitates hole transport across the base. From Eq.(2.5) we can write $N_B(x)$ as a

$$N_B(x) = N_B(x_e) - k(x - x_e), \tag{2.6}$$

which we will use several times in the following sections.

We also define a factor R to characterize ratio of base doping at the base-collector junction to the doping at the emitter-base junction

$$R = \frac{N_B(x_c)}{N_B(x_e)}. \tag{2.7}$$

In our numerical examples, the value of R ranges from 0.1 to 1.0. R equal to 0.1 corresponds to a maximum value of k i.e doping gradient, whereas R equal to 1 corresponds to a uniformly doped base. In this case, k is equal to zero.

2.4 Thermionic Emission Diffusion Model for a non-uniformly doped base

In modeling transport through HBTs, the principle of current balance is used to describe the emitter-base junction hole injection across the valence band discontinuity. Hole transport due to drift-diffusion across the emitter space charge region, thermionic emission (with a correction of hole tunneling) across the valence band discontinuity, and hole diffusion in the quasi-neutral base are considered following Stettler and Lundstrom for an abrupt single heterojunction Pnp HBT [66]. A schematic energy band diagram showing the energy band structure, hole quasi-Fermi level variation, and coordinate system is shown in Figure 2.3.

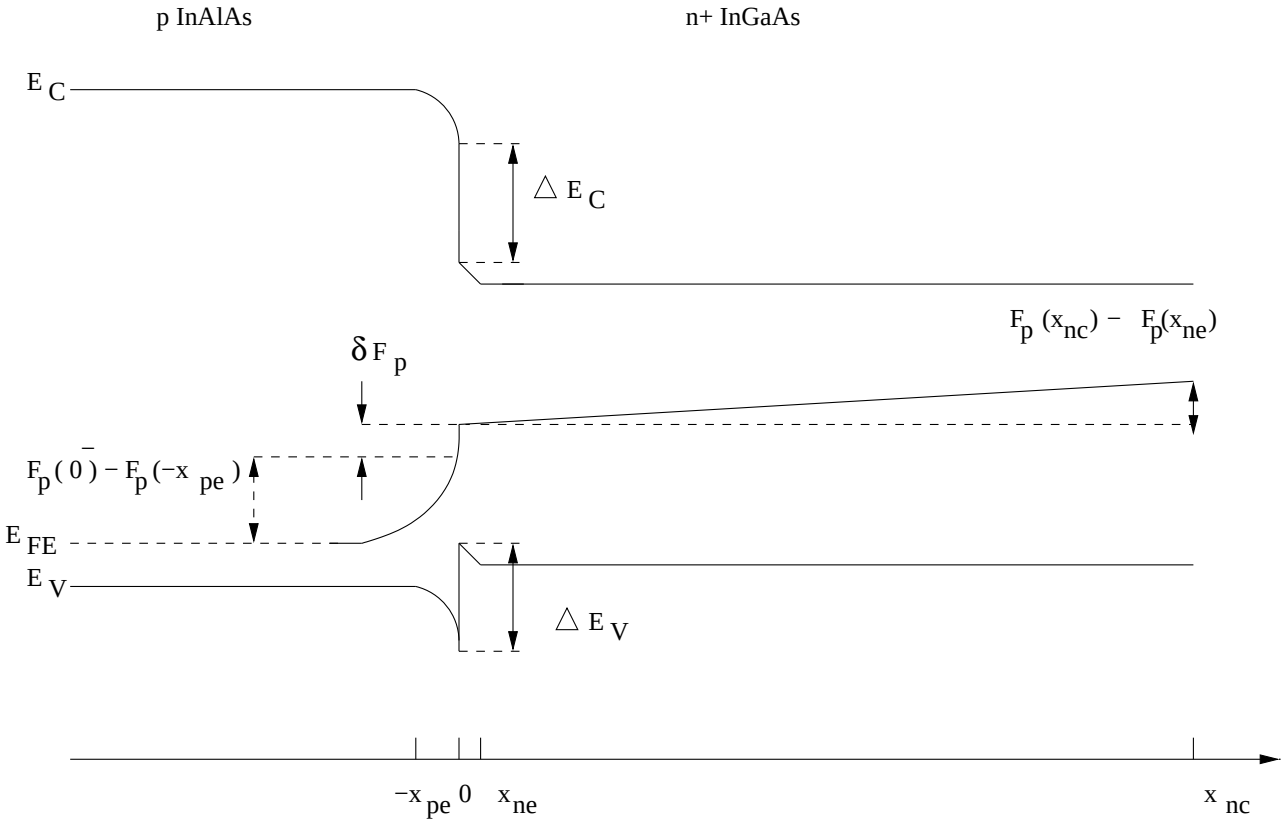

Figure 2.3: Schematic energy band diagram and quasi-Fermi level variation across emitter-base heterojunction and base in a Pnp heterojunction bipolar transistor.

First, we will describe the thermionic emission diffusion model for a constant base doping. Then, we will describe the changes necessary to treat the variation of doping across the base. We finally analyze the effects of base grading on the recombinations currents and the current gain. The effects of base grading on the base transit time is also analyzed.

2.4.1 Effective Hole Velocities and Hole Current Density

In a uniformly doped P-type emitter space-charge region, drift and diffusion contribute to the hole transport and the total hole current density J_p can be calculated as follows

$$J_p = p\mu_p \frac{dF_p}{dx}, \tag{2.8}$$

where μ_p is the low field hole mobility, p is the hole concentration and F_p is the hole quasi-Fermi level given by

$$F_p = E_v - kTln\frac{p}{N_v}, \tag{2.9}$$

where E_V is the valence band energy, N_V is the valence band effective density of states, and T is the temperature. Substituting Eq.(2.9) into Eq.(2.8) and integrating across the emitter-space charge region using the depletion approximation, the quasi-Fermi level splitting can be related to the hole current density and applied bias V_{EB} by [36,66]

$$e^{\frac{-[F_p(0^-)-F_p(-x_p)]}{kT}} = 1 - \frac{J_p e^{\frac{-qV_{EB}}{kT}}}{qS_{ep}p_{no}}, \tag{2.10}$$

where p_{no} is the thermal equilibrium minority carrier hole concentration in the base and $F_p(-x_{pe})$ and $F_p(0^-)$ are the hole quasi-Fermi levels, respectively, at the edges of the

depletion region in the emitter and at the heterojunction interface on the emitter side.

In Eq.(2.10), S_{ep} is the effective hole drift-diffusion velocity across the emitter space charge region and is given by

$$S_{ep} = \mu_p E(0_-) e^{\frac{-(\Delta E_v - qV_n)}{kT}}, \tag{2.11}$$

where ΔE_V is the valence band discontinuity at the emitter-base heterojunction and $E(0^-) = qN_a x_p/\epsilon_p$ is the electric field at the heterojunction interface on the emitter side. The Electric field at $x = 0_-$ can be calculated as a function of the applied bias. In appendix B, we show that

$$E_{0_-} = \sqrt{2(\frac{\epsilon_n}{\epsilon_p})\frac{qN_A N_B(x_{ne})(V_{bi} - V_{EB})}{(\epsilon_p N_A + \epsilon_n N_B(x_{ne})}}. \tag{2.12}$$

In Eq.(2.11), the quantity V_n corresponds to the net band bending on the base side of heterojunction and is given by

$$V_n = (\frac{\epsilon_p N_A}{\epsilon_p N_A + \epsilon_n N_B(x_{ne})})(V_{bi} - V_{EB}), \tag{2.13}$$

where N_A and $N_B(x_{ne})$ corresponds to the emitter and base doping level on the emitter side, respectively. The permitivities of the p-type emitter and the n-type base are given by ϵ_p and ϵ_n, respectively. V_{bi} is the built-in potential for the emitter-base junction taking into account the differences in permitivities across the emitter-base junction (see appendix A). The effective hole velocity across the emitter SCR given by Eq.(2.11) will be significantly less than its electron counterpart in the Npn case because of heavier hole effective masses as compared to the electrons.

Due to the presence of the valence band discontinuity, we expect a discontinuity in the hole quasi-Fermi level across the emitter-base heterojunction. The thermionic emission current is given by [36,66]

$$J_p = q\gamma_p[p(0^-)v_R(0^-) - p(0^+)v_R(0^+)e^{\frac{-\Delta E_v}{kT}}], \tag{2.14}$$

where $p(0^-)$ and $p(0^+)$ are the hole concentrations at the heterojunction interface at the emitter and base sides, respectively, and $v_R(0^+)$ and $v_R(0^+)$ are the hole velocities on the n and p side, respectively, and are defined as follows

$$v_R(0^+) = \sqrt{\frac{kT}{2\pi m^*_{p_n}}}, \tag{2.15}$$

and

$$v_R(0^-) = \sqrt{\frac{kT}{2\pi m^*_{p_p}}}, \tag{2.16}$$

where $m^*_{p_n}$ is the hole effective mass on the emitter side of the base and $m^*_{p_p}$ is the hole effective mass in the emitter.

The factor γ_p in Eq.(2.14) corresponds to a hole tunneling correction factor calculated following Grinberg et al. [67]. Using the definition for the hole quasi-Fermi level, we can write Eq.(2.14) as [36,66]

$$J_p = q\gamma_p v_R(0^+)e^{\frac{-\Delta E_v}{kT}}[e^{\delta F_p} - 1], \tag{2.17}$$

where $\delta F_p = F_p(0^+) - F_p(0^-)$ is the splitting of the quasi-Fermi level across the interface. In the limit $\delta F_p = qV_{EB}$, Eq.(2.17) gives the usual expression for the thermionic emission current.

Invoking the principle of current balance, we require the thermionic emission current density given by Eq. (2.17) to be equal to the drift-diffusion current density in the emitter space charge region in Eq. (2.10). Then using Eq. (2.14) for $p(0^+)$ and the definition of the quasi-Fermi level, we can solve Eq. (2.9) for $F_p(0^-)$ and obtain

$$e^{\frac{-\delta F_p}{kT}} = 1 - \frac{(\frac{N_{v_p}}{N_{vn}} \frac{J_p e^{\frac{-qV_{EB}}{kT}}}{qp_{no}S_{ip}})}{(1 - \frac{J_p e^{\frac{-qV_{EB}}{kT}}}{qS_{ep}p_{no}})}, \tag{2.18}$$

where S_{ip} is the effective hole velocity across the heterojunction interface given by

$$S_{ip} = v_R(0^+)e^{\frac{-(\Delta E_v - qV_n)}{kT}}. \tag{2.19}$$

Finally, we consider the hole transport across the quasi-neutral base region. For the case of uniformly doped base, in the region ($x_n \leq x \leq W_B$), diffusion of holes is the dominant mechanism. So, following Stettler and Lundstrom [66] we write

$$J_p = qD_p(\frac{p(x_{ne}) - p(x_{nc})}{W_B}), \tag{2.20}$$

where $p(x_{ne})$ and $p(x_{nc})$ are the hole concentrations at the emitter and collector ends of the base, respectively and W_B is quasi-neutral base width. Requiring that there be a finite hole concentration at the collector end of the base sufficient to carry the hole component J_p of the collector current, and neglecting hole recombination in the neutral base we require

$$J_p = qp(x_{nc})v_s, \tag{2.21}$$

where v_s is the hole saturation velocity in the base-collector space charge region and is set equal to 4.5 x 10^6 cm/s in all our simulations.

Now, using Eq.(2.20), and substituting for $p(x_{nc})$ in Eq.(2.21) we obtain

$$J_p = qS_{dp}[p(x_{ne}) - \frac{J_p}{qv_s}], \tag{2.22}$$

where we have defined a hole diffusion velocity in the base $S_{dp} = D_p/W_B$. Solving Eq.(2.21) for $p(x_{ne})$ and relating $p(x_{ne})$ to $p(0^+)$ assuming Boltzmann statistics, then using Eq.(2.14) and (2.17), we finally obtain

$$J_p = \frac{qp_{no}(\frac{N_{v_n}}{N_{v_p}})e^{\frac{qV_{EB}}{kT}}}{[\frac{1}{S_{ip}} + \frac{1}{S_{dp}} + \frac{1}{v_s} + \frac{1}{S_{ep}}(\frac{N_{v_n}}{N_{v_p}})]}, \tag{2.23}$$

where S_p is the final composite hole velocity given by

$$\frac{1}{S_p} = \frac{1}{S_{ip}} + \frac{1}{S_{dp}} + \frac{1}{v_s} + \frac{1}{S_{ep}}(\frac{N_{v_n}}{N_{v_p}}) \tag{2.24}$$

The limitation of the above equation is that we have assumed in writing Eq.(2.21) that the device is biased in the forward active mode, so our result is only good for V_{EB} greater than a few k_BT. From the above equation we can state that the hole component of the collector current is determined by the smallest effective velocity contributing to S_P. Due to the larger hole effective mass thermionic emission is not necessarily the dominant factor limiting carrier across the heterojunction as in the case of electron transport as will be shown in the numerical simulation in next chapter. A detailed derivation of Eq.(2.23) is given in appendix C. We follow a similar derivation to calculate the hole contribution to the collector current density in the case of a linear gradient across the base.

2.4.2 Device Equations for the case of a non-uniformly doped base

The analytical model for the Pnp HBT developed so far incorporated a general description of hole transport across the heterojunction. The drift diffusion of holes across the emitter space charge region is as important as thermionic field emission in limiting hole injection into the base. The drift-diffusion model is employed in this section to describe hole transport across the quasi-neutral base where the effects of non-uniform base grading have been included. This work extends the analysis of Hutchby [21], Yuan [68] and Datta et al. [37]. Shown in Figure 2.3 is the energy band diagram and coordinate system employed in the analysis. Following Ryum and Abdel-Motaleb's analysis for an Npn with a compositionally graded base [69,70], we can write for the hole and electron current densities in the base as follows

$$J_p = -\mu_p p(x)\frac{d}{dx}[qV(x) + \chi(x) + E_g(x)] - qD_p\frac{dp(x)}{dx}, \tag{2.25}$$

$$J_n = -\mu_n n(x)\frac{d}{dx}[qV(x) + \chi(x)] + qD_n\frac{dn(x)}{dx}, \tag{2.26}$$

where $V(x)$ is the electrostatic potential, q is the magnitude of the electronic charge, $\chi(x)$ is the electron affinity, $E_g(x)$ is the energy bandgap. In our case there is no bandgap variation along the base width. However, values of μ_p and D_p will be a function of x, because the doping will be varied linearly from emitter to collector in the base region.

In the case of uniform doping the majority carrier current is approximated as being

negligibly small ($J_n = 0$). Starting with Eq.(2.25), we obtain

$$\frac{k_B T}{n(x)} \frac{dn(x)}{dx} = \frac{d}{dx}[qV(x) + X(x)]. \tag{2.27}$$

Furthermore, the quasi-neutral base region, charge neutrality is satisfied,

$$p(x) + N_B(x) = n(x). \tag{2.28}$$

To account for the variation in the base doping we differentiate Eq.(2.28) and substitute the results in Eq.(2.27). The resulting equation is then used to rewrite J_p in Eq.(2.25) assuming low level injection into the base, i.e. $p(x) \ll N_B(x)$. The hole current density then becomes

$$J_p = qD_p[-\frac{dp(x)}{dx} + \frac{k}{N_B(x)} p(x)], \tag{2.29}$$

where we have used the parameter k defined in Eq.(2.5). In deriving Eq.(2.29) we have assumed Einstein's relation, $D_p = \frac{kT}{q}\mu_p$, to be valid.

The second term in Eq.(2.29) is positive and proportional to the quasi Electric field in the positive x-direction which assists the transport of holes towards the collector. It is to be noted that the D_p is also a function of the base width since mobility is a function of doping. Under steady-state conditions and neglecting hole recombination in the base, the hole continuity equation implies

$$\frac{dJ_p}{dx} = 0. \tag{2.30}$$

A second order differential equation for p(x) can be obtained by substituting Eq. (2.29)

into Eq. (2.30). This is shown explicitly in appendix D. We obtain

$$\frac{d^2p}{dx^2} + \frac{dp}{dx}[-\frac{k(1-\gamma)}{N_B(x)}] - p(x)\frac{k^2(1+\gamma)}{N_B^2(x)} = 0, \tag{2.31}$$

where γ has been defined in Eq. (2.2).

Calling $p(x_e)$ and $p(x_c)$ the hole concentrations at the emitter and collector edges of the quasi neutral base region, the solution to the differential Eq. (2.31) found to be (see appendix D)

$$p(x) = P_+[-(x-x_e)-\alpha]^{C_+} + P_-[-(x-x_e)-\alpha]^{C_-}, \tag{2.32}$$

where P_+ and P_- are defined as

$$P_+ = \frac{[p(x_e)[-(W_B+\alpha)]^{C_-} - p(x_c)[-\alpha]^{C_-}]}{(-\alpha)^{C_+}[-(W_B+\alpha)]^{C_-} - (-\alpha)^{C_-}[-(W_B+\alpha)]^{C_+}}, \tag{2.33}$$

and

$$P_- = \frac{[p(x_c)[-\alpha]^{C_+} - p(x_e)[-(\alpha+W_B)]^{C_+}]}{(-\alpha)^{C_+}[-(W_B+\alpha)]^{C_-} - (-\alpha)^{C_-}[-(W_B+\alpha)]^{C_+}}, \tag{2.34}$$

where α is given by $-N_B(x_e)/kW_B$. In Eqs. (2.32 - 2.34), the constants C_+ and C_- given by

$$\begin{aligned} C_+ &= \gamma, \\ C_- &= -1. \end{aligned} \tag{2.35}$$

Using Eq.(2.32) in (2.29) and using the fact that J_p is assumed to be constant across the base, the latter can be calculated explicitly as shown in appendix D.

$$J_p = q\frac{D_p^{eff}}{W_B}[p(x_e) - \tilde{p}(x_c)], \tag{2.36}$$

where we have introduced the new quantities

$$D_p^{eff} = D_p(x_e)(1-R)[\frac{\gamma+2}{1-R^{\gamma+2}}], \tag{2.37}$$

and

$$\tilde{p}(x_c) = Rp(x_c). \tag{2.38}$$

Equation (2.36) is an expression for hole current density analogous to the case of uniform doping discussed earlier (see Eq.(2.20)). In the non-uniform doping case, we have an effective diffusion constant D_p^{eff} and an effective saturation velocity for holes at the collector edge of the quasi-neutral base. Indeed, at the collector end of the base, we have the boundary condition given by Eq.(2.21) where v_s is the hole saturation velocity. Hence, we can write $\tilde{p}(x_c)$ as follows

$$\tilde{p}(x_c) = \frac{J_p}{qv_s^{eff}}, \tag{2.39}$$

by defining the effective saturation velocity for holes

$$v_s^{eff} = \frac{v_s}{R}. \tag{2.40}$$

Starting with Eqs.(2.36) and (2.37), it can be easily shown that, $\tilde{p}(x_c)$ tends to $p(x_c)$ and D_p^{eff} converges to $D_p(x_e)$ R tends to unity (uniform doping).

Now using Eq.(2.34) for $p(x_e)$ and relating it to $p(0^+)$ assuming Boltzman statistics, we finally obtain with the help of Eqs.(2.14) and (2.17)

$$J_p = \frac{qp_{no}(\frac{N_{vn}}{N_{vp}})e^{\frac{qV_{EB}}{kT}}}{[\frac{1}{S_{ip}} + \frac{1}{S_{dp}^{eff}} + \frac{1}{v_s^{eff}} + \frac{1}{S_{ep}}(\frac{N_{vn}}{N_{vp}})]}, \tag{2.41}$$

where S_p is the final composite hole velocity given by

$$\frac{1}{S_p} = \frac{1}{S_{ip}} + \frac{1}{S_{dp}^{eff}} + \frac{1}{v_s^{eff}} + \frac{1}{S_{ep}}(\frac{N_{v_n}}{N_{v_p}}). \tag{2.42}$$

Once again, the smallest effective hole velocities determines the collector hole current as in the case of uniformly doped base.

2.4.3 Terminal currents and current gain

As a part of the total emitter current, there is a component due to back injection of electrons from the base into the emitter which must be added to the hole component given by Eq.(2.40). Similar to the above analysis for holes, the emitter thermionic emission electron current density can be derived following Grinberg et al. [67] and is given by

$$J_{ne} = -qv_e N_{CB}[\frac{n(x_j^-)}{N_{CE}} - \frac{n(x_j^+)}{N_{CB}} e^{-\Delta E_C/k_B T}], \tag{2.43}$$

where $n(x_j^-)$ and $n(x_j^+)$ are the electron concentrations on the emitter side and the base side, respectively, of the emitter-base junction immediately adjacent to the heterojunction at x_j, N_{CE} and N_{CB} are conduction band density of states for the emitter and base regions, respectively, and ΔE_c is the conduction band discontinuity. The mean thermal electron velocity v_e in Eq.(2.42) is given by $v_e = \sqrt{\frac{k_B T}{2\pi m_e^*}}$ where m_e^* is the electron density of states effective mass in the base. Since the electron effective mass is almost a factor of two larger in the emitter than in the base for the InP-based material system, N_{CE} and N_{CB} are not equal and we cannot neglect their difference. Then, relating the electron

concentration on either side of the heterojunction to their respective values at the edges of the emitter-base space charge region using the Boltzmann relation, we get

$$n(x_j^-) = n(x_{pe})e^{\frac{qV_{jp}}{k_BT}}, \tag{2.44}$$

and

$$n(x_j^+) = n(x_{ne})e^{-\frac{qV_{jn}}{k_BT}}, \tag{2.45}$$

where $n(x_{pe})$ and $n(x_{ne})$ are the electron concentrations at the edges of the depletion region on the emitter and base sides of the heterojunction. In Eqs.(2.44 - 2.45) V_{jp} and V_{jn} are the band bendings on the emitter and base side of the heterojunction, respectively.

Using the last two relations, we can then rewrite Eq.(2.43) as follows

$$J_{ne} = qS_{in}[n_o(x_{pe})[e^{\frac{qV_{EB}}{k_BT}} - 1] - \Delta n(x_{pe})], \tag{2.46}$$

where $\Delta n(x_{pe}) = n(x_{pe})$ - $n_o(x_{pe})$ is the excess electron concentration and $n_o(x_{pe})$ is the thermal equilibrium electron concentration at the base end of the emitter space charge region.

In Eq.(2.46), S_{in} is the electron heterojunction interface velocity defined as

$$\begin{aligned} S_{in} &= v_e\frac{N_{CB}}{N_{CE}}e^{\frac{qV_{jp}}{k_BT}}, \\ &\simeq v_e\frac{N_{CB}}{N_{CE}}(\frac{N_EN_B}{n_{ie}^2})e^{-\frac{\Delta E_C}{k_BT}}e^{-\frac{qV_{EB}}{k_BT}}, \end{aligned} \tag{2.47}$$

where N_E and $N_B(x_e)$ are the emitter and base doping at the emitter edge of the base region, respectively, n_{ie} is the intrinsic carrier concentration in the emitter and V_{EB} is the applied emitter-base junction bias.

The electron minority carrier profile in the emitter is given by the usual diffusion profile so that on matching the thermionic emission and diffusion currents, the electron component of the emitter current density is given by [69]

$$J_{ne} = \frac{qS_{dne}n_o(x_{pe})}{1 + (S_{dne}/S_{in})coth(W_e/L_{ne})}(e^{qV_{EB}/k_BT} - 1), \tag{2.48}$$

where we have taken into account the finite width of the emitter W_e. In Eq. (2.48), S_{dne} is the electron diffusion velocity in the emitter given by D_{ne}/L_{ne}, where D_{ne} and L_{ne} are the electron diffusion constant and length in the emitter, respectively, and $n_o(x_{pe})$is the thermal equilibrium electron concentration in the emitter.

Regrouping the results of the previous analysis, the total emitter current density is then given by

$$\begin{aligned} J_e &= J_p + J_{ne} \\ &= qp_o(x_{ne})S_P e^{qV_{EB}/k_BT} \\ &\quad + \frac{qS_{dne}n_o(x_{pe})}{1 + (S_{dne}/S_{in})coth(W_e/L_{ne})}(e^{qV_{EB}/k_BT} - 1). \end{aligned} \tag{2.49}$$

At the base collector junction, since we have a simple p-n homojunction, the electron current density for the device in the normal, active mode is given by

$$J_{nc} = \frac{qD_{nc}}{L_{nc}}n_o(x_{pc})coth(\frac{W_c}{L_{nc}}), \tag{2.50}$$

where D_{nc} and L_{nc} are the electron diffusion constant and length in the collector, respectively, $n_o(x_{nc})$ is the thermal equilibrium electron concentration in the bulk collector and W_c is width of the neutral collector region. The total collector current is then the

sum of the hole current density given by Eq.(2.22) and electron component given by Eq.(2.48)

$$\begin{aligned} J_c &= J_p + J_{nc} \\ &= qp_o(x_{ne})S_P e^{qV_{EB}/k_BT} + \frac{qD_{nc}}{L_{nc}} n_o(x_{pc}) coth(\frac{W_c}{L_{nc}}). \end{aligned} \tag{2.51}$$

Neglecting the recombination currents, the base current density is given by the difference of the total emitter and collector current densities,

$$\begin{aligned} J_b &= J_{ne} - J_{nc} \\ &= \frac{qS_{dne}n_o(x_{pe})}{1 + (S_{dne}/S_{in})coth(W_c/L_{nc})}(e^{qV_{EB}/k_BT-1}) \\ &\quad -\frac{qD_{nc}}{L_{nc}} n_o(x_{nc}) coth(\frac{W_c}{L_{nc}}). \end{aligned} \tag{2.52}$$

We have neglected so far, particularly in the base current calculation, the contribution of various recombination mechanisms. To include the recombination currents, we follow the analysis of Ryum and Motaleb [69,70,71] and write

$$\begin{aligned} J_e &= J_p + J_{ne} + J_{scr} + J_{sr} + J_{ire} + J_{irb} + J_{br} + J_{rr}, \\ J_c &= J_p + J_{nc}, \\ J_b &= J_{ne} - J_{nc} + J_{scr} + J_{sr} + J_{ire} + J_{irb} + J_{br} + J_{rr}, \end{aligned} \tag{2.53}$$

where J_{rr} and J_{br} are the radiative and nonradiative recombination current densities on the quasi-neutral base, respectively. J_{sr} is the recombination current density at the surface, J_{scr} is the recombination current density in the emitter-base space charge

region, and J_{irb} and J_{ire} are the interface recombination current densities on the base and emitter side of the emitter-base heterojunction respectively. To calculate the various components, we must take into account the effects of linear doping across the base.

The non-radiative base recombination current is given by [69,71]

$$J_{br} = q \int_{x_e}^{x_c} \frac{[p(x) - p_o(x)]}{\tau_p(N_B(x))} dx. \tag{2.54}$$

The contribution of $p_o(x) = \frac{n_{io}^2}{N_B(x)}$ is very small in the above integral and can be omitted. The minority carrier lifetime τ_p in the base is a function of base doping as given by Eq.(2.3).

$$\tau_p(N_B(x)) = 10^{\delta - \vartheta log N_B(x)}, \tag{2.55}$$

where the constants δ and ϑ are curve fit parameters with $\delta = 22.4$ and $\vartheta = 1.2$ for $N_D \geq 8$ x $10^{17} cm^{-3}$.

For the case of linear base doping, we use Eq.(2.6)

$$N_B(x) = N_B(x_e) - k(x - x_e) \tag{2.56}$$

in Eq.(2.55) which we substitute back into Eq.(2.54). The integral in Eq.(2.54) can then be performed exactly leading to the non-radiative recombination current density.

$$J_{br} = \frac{qW_B}{\tau(x_e)} [p(x_e)A_1(R) + p(x_c)B_1(R)], \tag{2.57}$$

as shown explicitly in appendix E.

In Eq.(2.57), we have introduced the following parameters

$$A_1(R) = \frac{1}{(\gamma + \vartheta + 2)(1 - R)} \frac{(1 - R^{\gamma+\vartheta+2})}{[1 - R^{\gamma+2}]} - \frac{R^{\gamma+2}}{(1 - R)} \frac{1}{\vartheta} \frac{1 - R^{\vartheta}}{1 - R^{\gamma+2}}, \tag{2.58}$$

and

$$B_1(R) = (\frac{R}{1-R})\frac{1}{1-R^{\gamma+2}}[\frac{1-R^{\vartheta}}{\vartheta} - \frac{1-R^{\gamma+\vartheta+2}}{(\gamma+\vartheta+2)}]. \tag{2.59}$$

We see that J_{br} is a strong function of the doping gradient R. Starting with Eqs.(2.58) and (2.59), it can be shown that $A_1(R)$ and $B_1(R)$ tends to be 0.5 when R tends to unity, which corresponds to the case of uniform doping considered by Datta et al. [42].

Similarly, the radiative recombination component to the base current is given explicitly by [71].

$$J_{rr} = qB\int_{x_e}^{x_c}[N_B(x)p(x) - n_i^2(x)]dx, \tag{2.60}$$

where B is the radiative recombination coefficient. Here the second term can also be neglected in the integration since its contribution is negligible compared to the first.

Using Eqs.(2.56) and (2.32), the integration in Eq.(2.60) can be performed explicitly leading to the radiative recombination current density (see appendix E)

$$\begin{aligned} J_{rr} &= qBN_B(x_e)W_B[p(x_e)(\frac{1-R^{\gamma+3}}{(\gamma+3)(1-R)} - R^{\gamma+2})(\frac{1}{1-R^{\gamma+2}}) \\ &\quad + p(x_c)(\frac{R}{1-R^{\gamma+2}})[1 - \frac{1-R^{\gamma+3}}{(1-R)(\gamma+3)}]. \end{aligned} \tag{2.61}$$

For the case of uniform doping (R tends to unity), the coefficients of $p(x_e)$ and $p(x_c)$ in Eq.(2.60) tends to 0.5. In this case, J_{rr} reduces to its expression for uniformly doped base derived by Datta et al. [42].

The emitter-base space charge recombination current J_{scr} is given by [69,71]

$$J_{scr} = \frac{1}{2}qN_{tr}\sigma\upsilon_e W_o\sqrt{n(x_e)p(x_e)}, \tag{2.62}$$

where $n(x_e) = N_B(x_e)$ and $p(x_e)$ is given by

$$p(x_e) = p_o(x_e)\frac{S_p}{S_{dp}}e^{\frac{qV_a}{kT}}, \tag{2.63}$$

where $p_o(x_e) = n_{in}^2(x_e)/N_B(x_e)$ and

$$W_o = W_{scr}[\frac{\pi k_B T}{q(V_{bi} - V_{EB})}]. \tag{2.64}$$

where W_0 is the fraction of the width of the emitter-base space charge region W_{scr} in which recombination predominately occurs. Using the above results we get

$$J_{scr} = \frac{1}{2}qN_{tr}\sigma\upsilon_e W_o n_{io}\sqrt{\frac{S_P}{S_{dp}^{eff}}}e^{qV_{BE}/2k_BT}, \tag{2.65}$$

where σ is the carrier capture cross section, N_{tr} is the recombination trap density given in Table 2.1, υ_e is the electron thermal velocity defined earlier.

Similarly, the surface recombination current can be written as [69,71]

$$J_{sr} = qs_o L_s\frac{P_E}{A_E}n_{io}\sqrt{\frac{S_P}{S_{dp}^{eff}}}e^{qV_{BE}/2k_BT}, \tag{2.66}$$

where $P_E(A_E)$ is the emitter mesa perimeter (area), s_o is the surface recombination velocity and L_s is the surface diffusion length.

Finally, J_{ire} and J_{irb} associated with recombination at the E-B interface on the emitter and base sides, respectively, are given by [69,71]

$$J_{ire} = qs_e p_o(x_{pe})e^{-qV_p/k_BT}[\frac{S_P}{S_{dp}^{eff}}e^{qV_{BE}/k_BT} - 1], \tag{2.67}$$

and

$$J_{irb} = qs_b p_o(x_{ne})e^{qV_n/k_BT}[\frac{S_P}{S_{dp}^{eff}}e^{qV_{BE}/k_BT} - 1], \tag{2.68}$$

where s_e and s_b are the interface recombination velocities on the emitter and base sides of the heterojunction, respectively, and V_p and V_n are the fractions of built-in potential on the emitter and base sides of the emitter-base heterojunction, respectively. The material parameters used in calculations are listed in Table 2.1 and the device is structure is that of Stanchina et al. [28]. Regrouping all the results above, we can calculate the small signal current gain as J_c/J_b including the various recombination currents. The relative magnitudes of the various recombination currents will be examined for a specific device in the next chapter.

2.4.4 Base transit time

Because of the quasi electric field due to the varying doping profile in the base which helps hole transport across the base, the base transit time is expected to be reduced compared to the case of uniform doping. This should benefit the high frequency performance capabilities of the device because, in a Pnp HBT, the low hole diffusion constant in the base makes the hole base transit time a dominant component in the emitter-to-collector delay time. Following Pulfrey [72] et al. [73], we calculate the base transit time as follows

$$\tau_b = \int_{x_e}^{x_c} \frac{dx}{v(x)}, \tag{2.69}$$

where $v(x)$ is the average velocity of holes across the base and is related to the hole current J_p as follows

$$v^{-1}(x) = \frac{q}{J_p}(p(x) - p_o(x)). \tag{2.70}$$

Since $p(x)$ is a function of the grading factor R, the base transit time will be affected by the linear doping across the base. In Eq.(2.70), the contribution of equilibrium hole concentration $p_o(x)$ is significantly less and can be ignored.

Using the expression for p(x) in Eq.(2.32), the base transit time is calculated explicitly in appendix F and found to be

$$\tau_b = \frac{W_B^2}{2\tilde{D}_p} + \frac{W_B}{\tilde{v_s}}, \tag{2.71}$$

where

$$\tilde{D}_p = \frac{D_p^{eff}}{f(R)}, \tag{2.72}$$

and

$$\tilde{v_s} = \frac{v_s}{[Rf(R) - g(R)]}. \tag{2.73}$$

In Eqs.(2.72) and (2.73), the functions $f(R)$ and and $g(R)$ are functions of R and are given explicitly in appendix F. The case of uniform base doping, (R = 1) it can be shown that the base transit time τ_b in Eq.(2.71) reduces to the well known expression [**?**]:

$$\tau_b = \frac{W_B^2}{2D_p} + \frac{W_B}{v_s}. \tag{2.74}$$

2.5 Conclusion

In this chapter, we have developed an analytical model of Pnp HBT that takes into account current thermionic-emission-diffusion of holes across the emitter-base heterojunction and matches this injection current to the drift diffusion current in the linearly doped base to determine self-consistently the collector and base current densities as a function of the applied emitter-base bias. The effects of linear base doping were incorporated in the determination of the various recombination currents in the base and emitter-base space charge region, current gain and base transit time.

For simplicity, the model of tunneling and thermionic emission used in this work assumes an effective mass of carriers equal to the density of states effective mass for holes. A more through investigation should include an independent calculation of light and heavy hole tunneling currents across the emitter-base junction following the scattering matrix approach of Ekbote et al. [74].

Chapter 3

Results and Discussion

3.1 Introduction

In the previous chapter, we have derived an analytical model of a Pnp HBT in the case of linear variation of the doping across the base. In this chapter, we apply this model to study the DC current gain and the total base transit time of a specific Pnp InAlAs/InGaAs HBT as a function of the gradient of the (linear) doping profile in the base. The parameters of the device are listed in Table 2.1 on page 17. This is the same device as the one analyzed by Datta et al. [42] for the case of a compositionally graded base. In their case, the doping in the base was kept fixed at 5 x $10^{18} cm^{-3}$. In our simulations, we neglect compositional grading (base is made of $In_{0.53}Ga_{0.47}As$) and the doping is varied from $10^{19} cm^{-3}$ at the emitter end of the base down to $10^{18} cm^{-3}$ at the collector end of the base. This case corresponds to an average of 5 x $10^{18} cm^{-3}$ in

the base. To study the influence of the doping gradient, we also vary the doping at the collector end of the base from 10^{18} to $10^{19}cm^{-3}$ in steps of $10^{18}cm^{-3}$ while keeping the concentration at the emitter end fixed.

The analytical equations derived in the previous chapter were programmed using Matlab. In the following sections, we present the results of various effects of base doping on the device performance, focusing on the DC current gain and base transit time. In writing the boundary condition at the collector we neglect the effect of V_{CB}. This assumption is not accurate for the device operating in the forward saturation mode.

3.2 Effective Hole Velocities

In chapter II, we show that the collector current density of the typical Pnp HBT considered here can be calculated as the sum of J_p and J_{nc} where

$$J_p = \frac{qp_{no}(\frac{N_{v_n}}{N_{v_p}})e^{\frac{qV_{EB}}{kT}}}{[\frac{1}{S_{ip}} + \frac{1}{S_{dp}^{eff}} + \frac{1}{v_s^{eff}} + \frac{1}{S_{ep}}(\frac{N_{v_n}}{N_{v_p}})]}, \tag{3.1}$$

where $p_o(x_{ne})$ is the thermal equilibrium hole concentration at the emitter end of the quasi-neutral base v_s^{eff} corresponds to the effective saturation velocity of holes in the base-collector space charge region assuming the device is biased in the forward active mode and the S's are the effective hole velocities: S_{ip} is the effective hole interface velocity, S_{ep} is the hole drift-diffusion velocity in the emitter space charge region and S_{dp} is the effective hole velocity associated with drift diffusion across the quasi-neutral base region.

From Eq.(3.1), we see that the smallest of the four velocities will control the current flow through the emitter-base heterojunction. First, we discuss the results for a uniformly doped base and then we discuss the effects of base grading and its effects on hole velocities. Shown in Figure 3.1 is a plot of all four velocities as a function of emitter-base bias for the device structure of Stanchina et al. [28], with no dopant grading in the base. The base doping is kept at a constant value of 1 x $10^{19} cm^{-3}$. The hole saturation velocity v_s (4.5 x $10^6 cm/s$) is smaller than that of electrons ($10^7 cm/sec$), but much larger than other velocities and so is less important in determining the hole injection current. Similarly the hole diffusion velocity S_{dp} is also larger than both S_{ip} and S_{ep} which are the two velocities determining the hole current density. Shown in Figure 3.1 is the thermionic emission velocity S_{ip} with and without the inclusion of hole tunneling factor γ_p. The effect of hole tunneling is to enable additional hole injection across the heterojuntion so that it effectively raises the velocity S_{ip} by more than a factor of 10 at low bias and by a factor of 3 at high bias. For holes, the low field mobility is much smaller than for electrons so that the velocity prefactor in Eq.(2.10) still makes S_{ep} smaller and comparable to the thermionic-emission velocity S_{ip} including the tunneling factor as seen in Figure 3.1. As a result, the drift diffusion of holes across the emitter space charge region and the thermionic emission of holes across the valence band discontinuity are the two major physical mechanisms limiting hole injection across the emitter-base junction.

As discussed in chapter II, the effect of dopant grading enhances both the hole effective diffusion coefficient across the base and leads to an effective saturation velocity

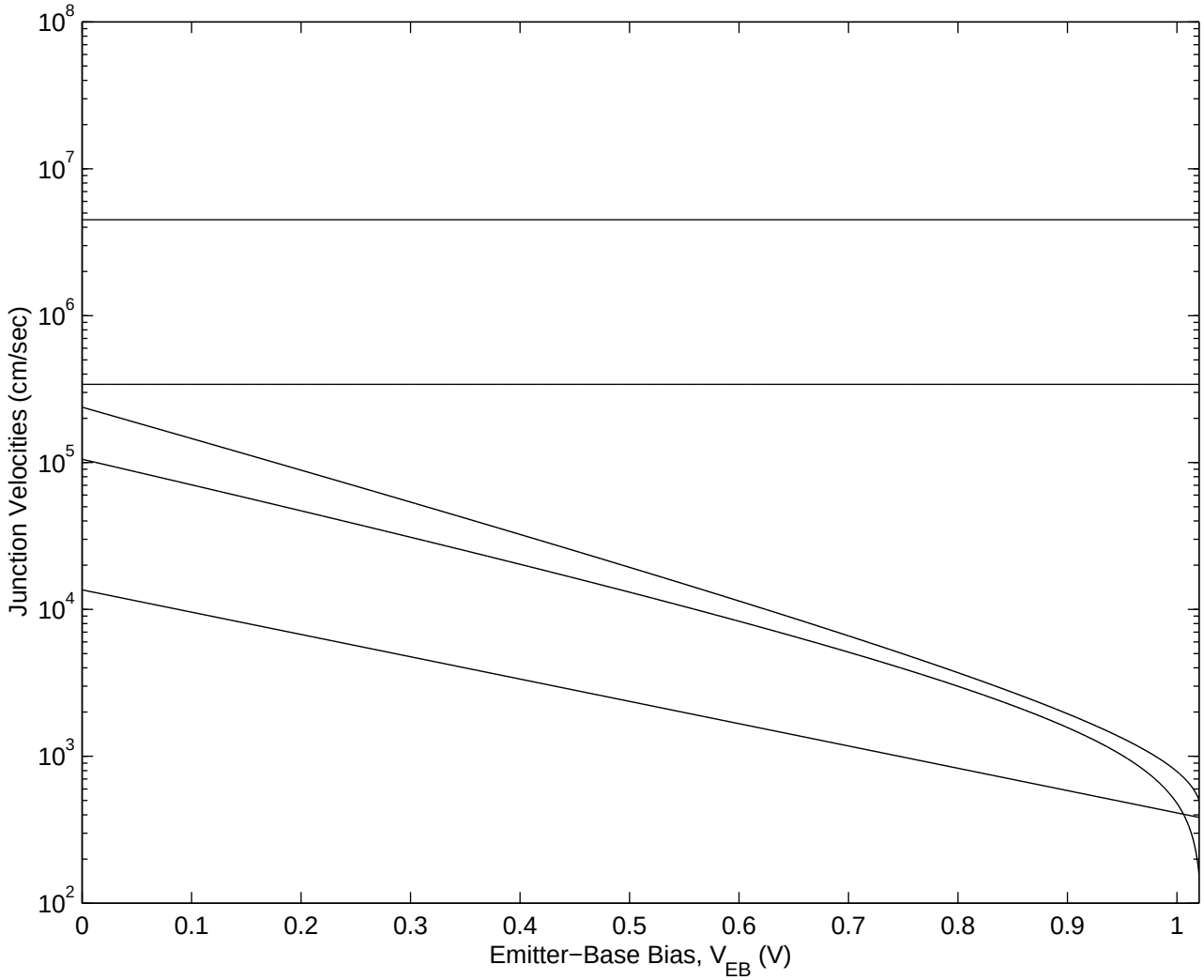

Figure 3.1: From top to bottom, Effective hole velocities base-collector saturation (v_s), quasi-neutral base diffusion (S_{dp}), thermionic emission with tunneling (S_{ip}), emitter space charge region drift diffusion (S_{ep}) and thermionic emission without tunneling in that order for InAlAs/InGaAs Pnp HBT with the parameters listed in Table 2.1 as a function of emitter-base bias V_{EB}. The results are for the case of uniform doping ($R = 1$).

of holes v_s^{eff} much larger than v_s at the base-collector junction. This is illustrated in Figure 3.2 where we plot all four velocities as function of emitter base bias for a maximum dopant grading, (R = 0.1) across the base. Now the new hole diffusion velocity S_{dp}^{eff} is enhanced by a factor of 2 and the saturation velocity by a factor of 10 ($v_s^{eff} = 10$) due to the dopant grading. The two other velocities S_{ip} and S_{ep} are unaffected by the dopant grading. So, both these velocities remain less than S_{dp}^{eff} and v_s^{eff} and continue to control the current flow across the emitter-base heterojunction. This trend was found to be valid for all intermediate values of R from 0.1 to 1. Figure 3.3 is a plot of effective hole diffusion coefficient and hole effective saturation velocities as a function of dopant grading R, as calculated using Eqs.(2.37) and (2.39).

3.3 Minority Carrier Concentration Profile in the Base

Figure 3.4 shows the calculated hole profile across the base region for different base dopant gradings at collector current densities of 10^3, 10^4 and 10^5 A/cm^2, respectively. For a weak grading ($R = 0.9$), the hole profile is the normal decreasing hole concentration since the hole diffusion process is primarily responsible for carrier transport across the base. It can also be seen that for an increased grading, the hole concentration at the emitter end decreases. As a result, for a strong grading ($R = 0.1$), the slope of the profile is much smaller as compared to $R = 0.9$ and also shows an accumulation at the collector

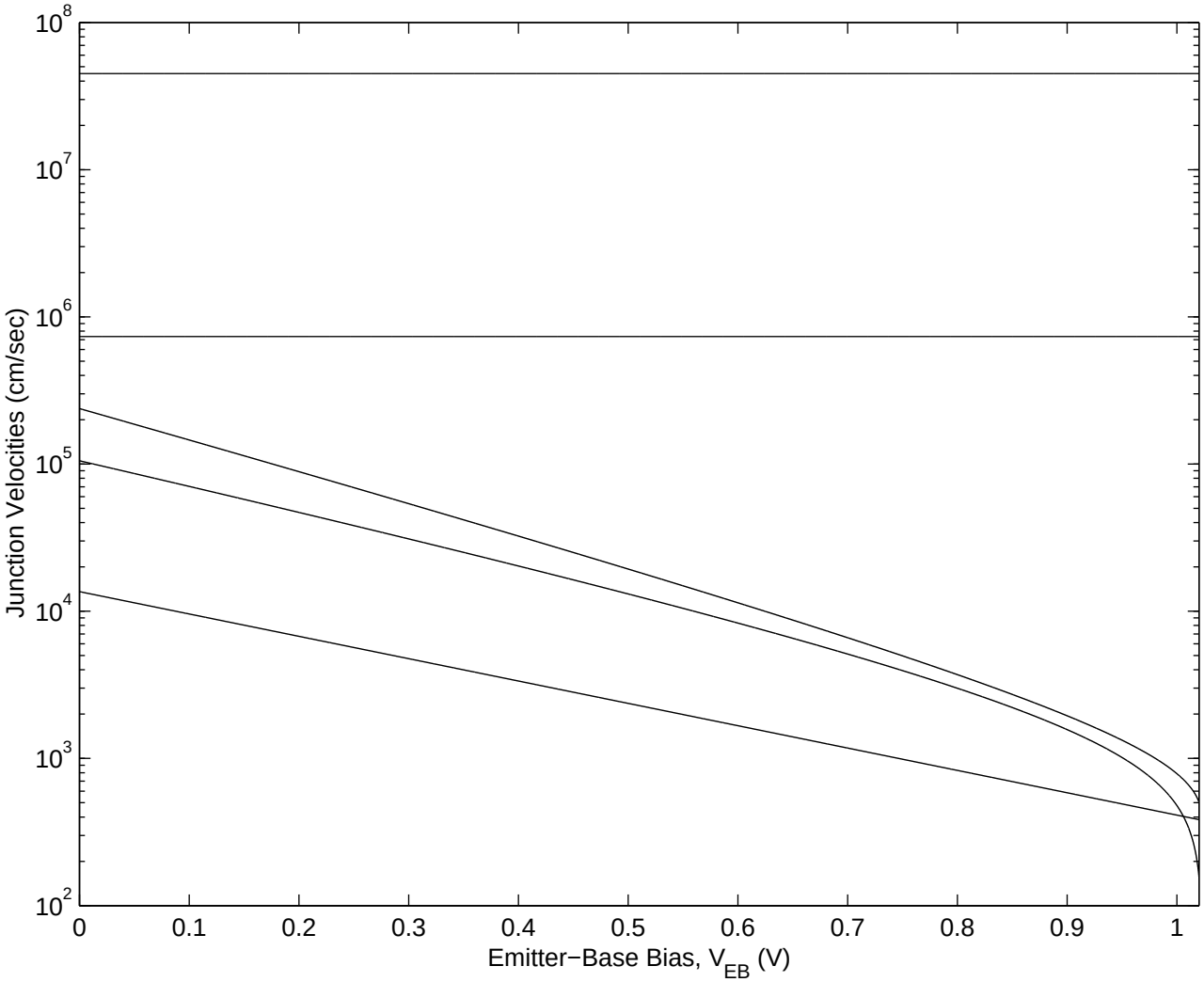

Figure 3.2: From top to bottom, effective hole velocities [base-collector saturation (v_s^{eff}), quasi-neutral base diffusion (S_{dp}^{eff}), thermionic emission with tunneling (S_{ip}), emitter space charge region drift diffusion (S_{ep}) and thermionic emission without tunneling] for the InAlAs/InGaAs Pnp HBT with their parameters listed Table 2.1 as a function of emitter-base bias V_{EB}. The plots are for the case of maximum grading (R = 0.1), i.e, with the doping in the base region varying linearly from 10^{19} to $10^{18} cm^{-3}$ from the emitter to the collector end of the base.

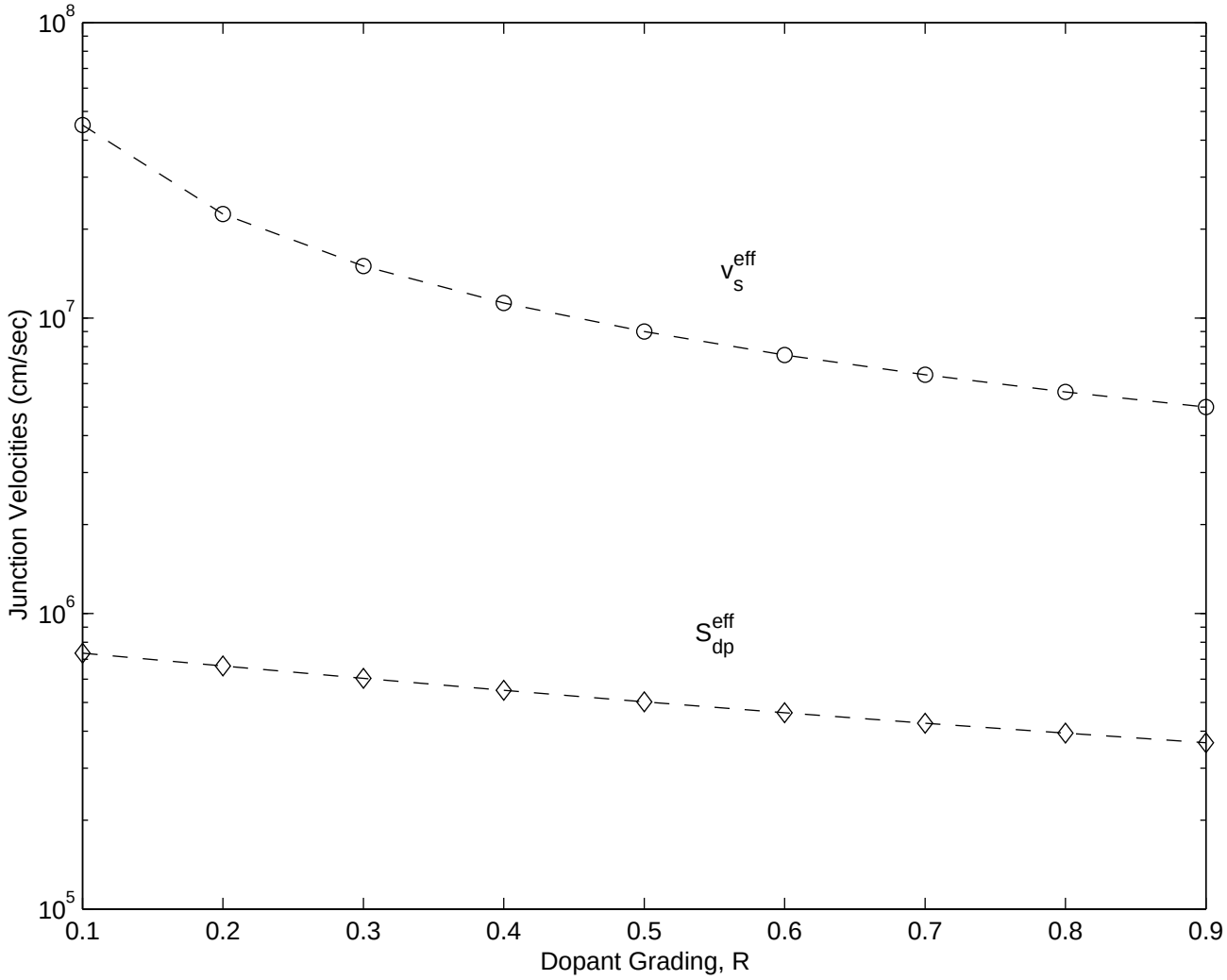

Figure 3.3: Effective hole Saturation (v_s^{eff}) and diffusion (S_{dp}^{eff}) velocities as a function of dopant grading R.

end of the base. This trend is due to the more efficient transport of holes as a result of the additional drift component of the hole transport due to the quasi electric field arising from the dopant grading. It should be noted that there is almost no variation in collector current density with respect to the dopant grading. This is because the collector current density is predominantly dominated by the thermionic-field emission (S_{ip}) and hole drift diffusion in the emitter space charge region (S_{ep}), as discussed earlier. As will be shown next, the base current density J_b, which includes the various recombination currents, is more dependent on the dopant grading and decreases with the increase in the dopant grading.

3.4 Terminal Currents and Current Gain

In the absence of dopant grading, the base current is dominated by non-radiative recombination in the quasi-neutral base. As the grading increases, the non-radiative current as well as most of the other recombination current components decrease in size, as shown in Figure 3.5, which is a plot of various contributors to the base current as function of dopant grading R, at a constant collector current density of $10^4 A/cm^2$. This results from the fact that with increased dopant grading the quasi-electric field is enhanced and holes are effectively swept out of the quasi-neutral base reducing the hole concentration across the entire width of the base, as seen in Figure 3.4. This effect reduces not only non-radiative (J_{br}) and radiative (J_{rr}) components, but also the interface and space charge

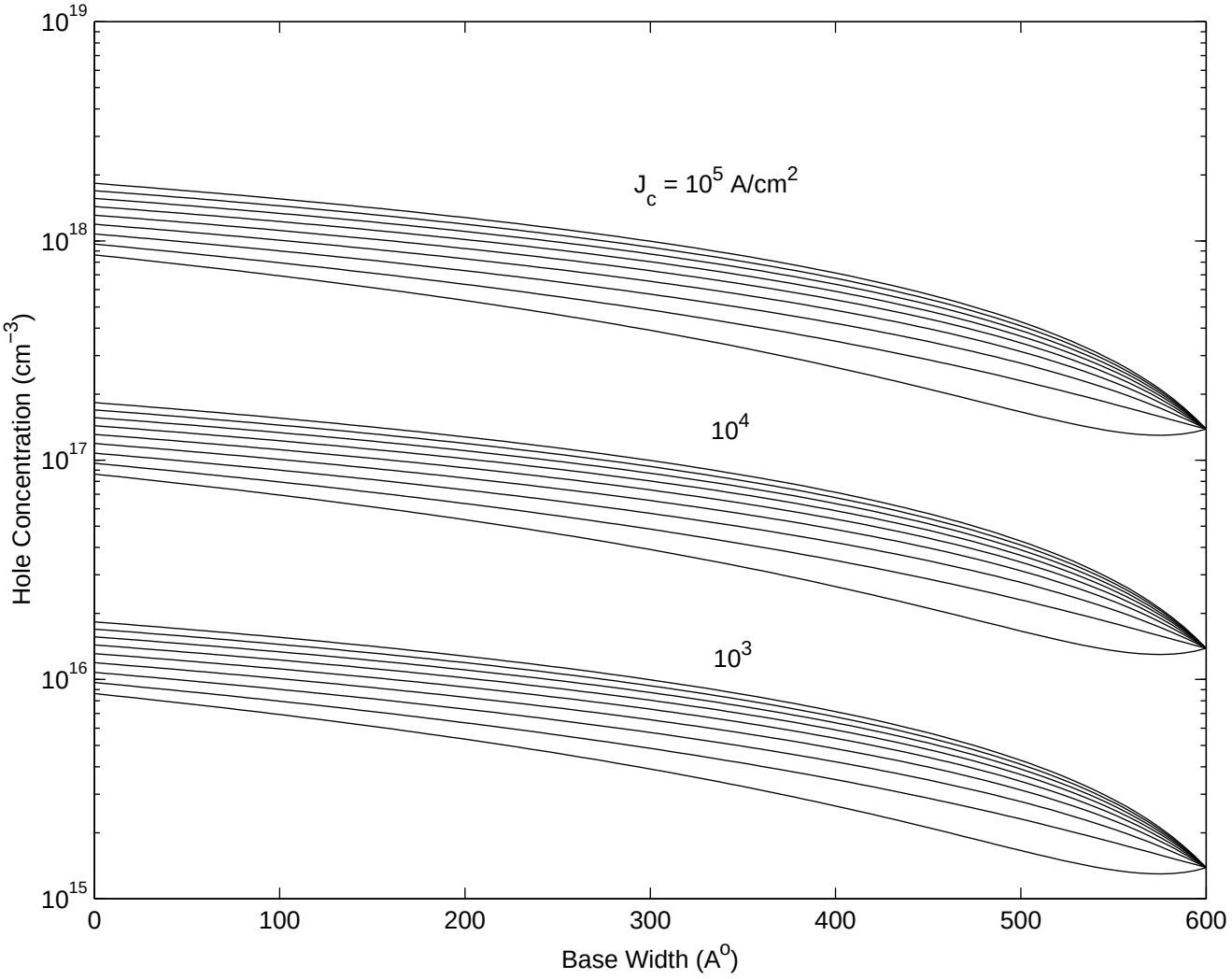

Figure 3.4: Hole concentration profile across the quasi-neutral base for collector current densities of $10^3, 10^4$ and $10^5 A/cm^2$ for dopant gradings of $R = 0.9$ (top curve in each set of curves) to $R = 0.1$ (bottom curve in each set of curves) in steps of 0.1.

region components. With increase in the quasi electric field, the hole concentration at the emitter end of the base $p(x_e)$ is reduced, as seen in Figure 3.4, which leads to a smaller space charge recombination current (J_{scr}). Similarly, increasing the quasi-field increases the effective hole diffusion velocity in the base S_{dp}^{eff}, as seen in Figure 3.3, which causes the interface recombination currents (J_{ire} and J_{irb}) to decrease. The quasi-field in the base also drives the holes away from the exposed base surface between the emitter mesa and the base metal contact and so reduces the base surface recombination current J_{sr}. The dopant grading has no effect on the emitter back injection current (J_{ne}), as it is mostly dependent on conduction band discontinuity which is affected by compositional grading rather than dopant grading [37]. Finally, J_{nc} is given by the normal forward current for a simple p-n junction, which is independent of the dopant grading. Also plotted in Figures (3.6 - 3.8) are the five major recombination currents for collector current densities of 10^3, 10^4 and 10^5 A/cm^2, respectively. It is evident from these figures that each of these components increase by a factor of 10 for higher collector current densities in agreement with Figure 3.4, where the area under the curve $p(x)$ also increases by a factor of 10.

Figure 3.9 is a plot of J_c and J_b for case of maximum ($R = 0.1$) and minimum ($R = 0.9$) dopant gradings. As noted that there is almost no variation of the collector current density with dopant grading. This is because J_c is predominantly dominated by the combination of thermionic-field emission (S_{ip}) and hole drift diffusion in the emitter space charge region (S_{ep}). Effective hole diffusion S_{dp}^{eff} and hole saturation v_s^{eff}

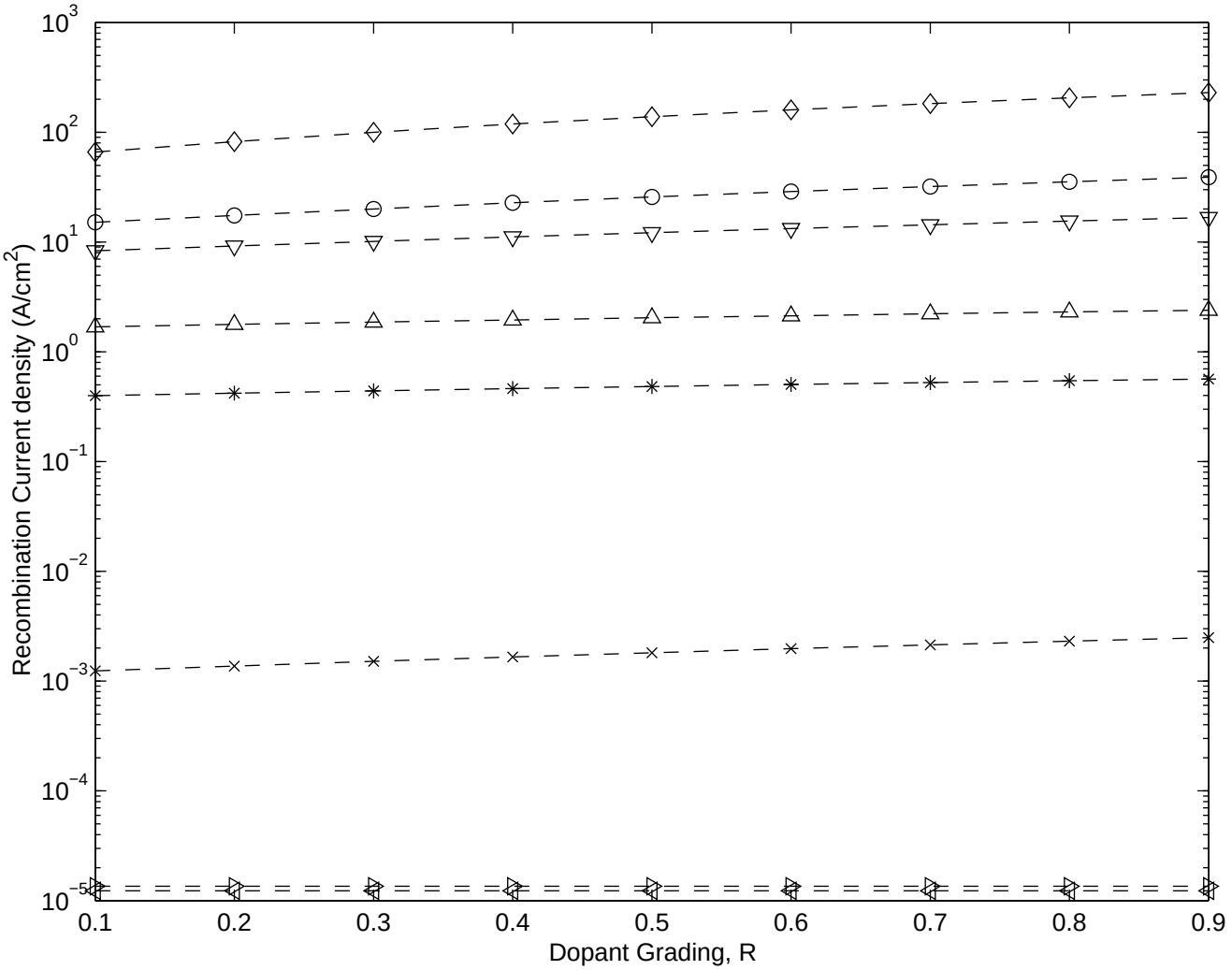

Figure 3.5: Base recombination currents: nonradiative J_{br} ($\diamond$) and radiative J_{rr} ($\circ$), space charge region J_{scr} ($\triangle$), surface J_{sr} ($\star$), emitter side interface J_{ire} ($\times$), base side interface J_{irb} ($\triangledown$), electron back injection J_{ne} ($\triangleleft$), electron collector leakage J_{nc} ($\triangleright$) as a function of dopant grading R in the base for a collector current density of $10^4 A/cm^2$.

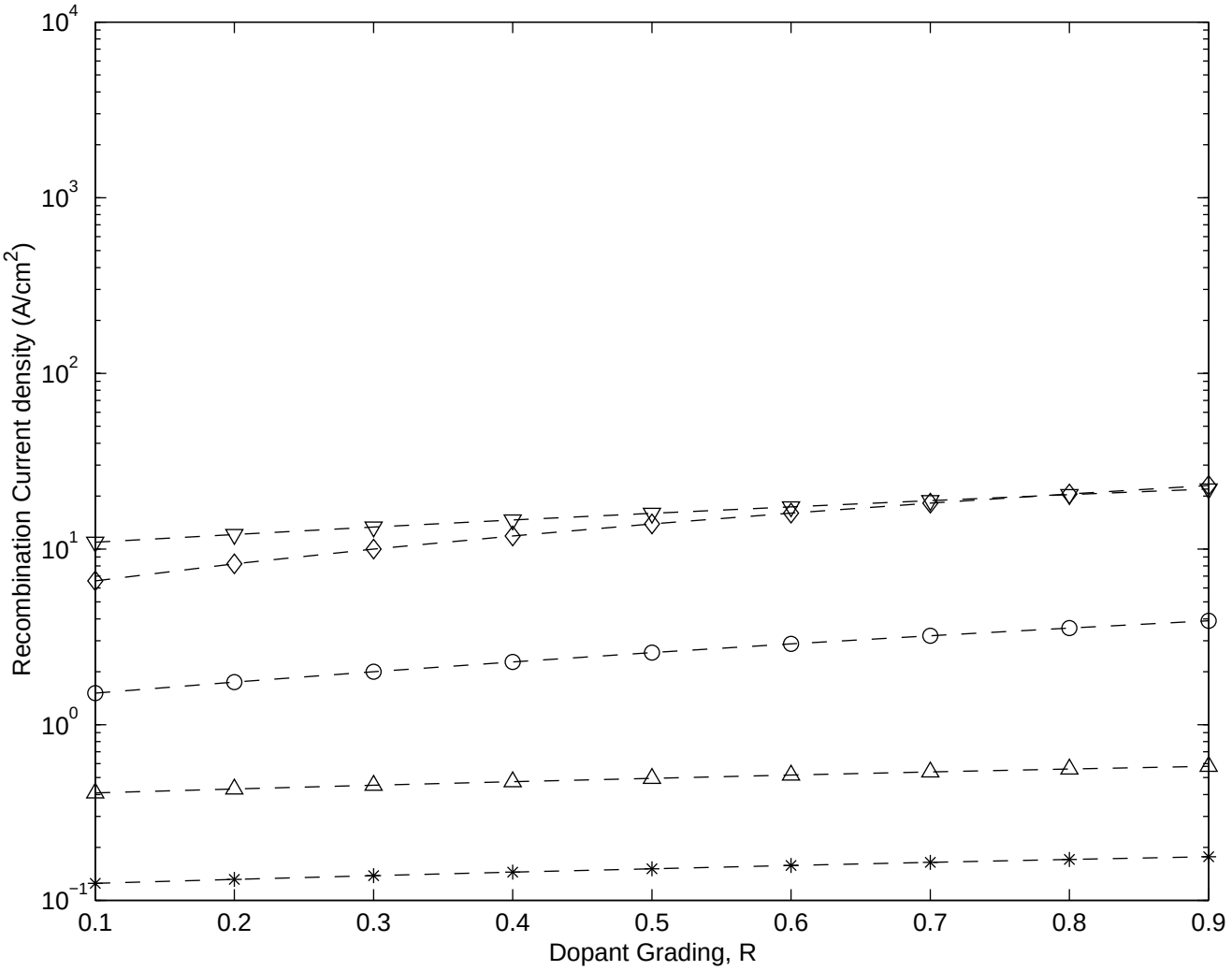

Figure 3.6: Base recombination currents: nonradiative J_{br} ($\diamond$) and radiative J_{rr} ($\circ$), interface J_{irb} ($\bigtriangledown$) space charge region (J_{scr}) ($\bigtriangleup$) surface J_{sr} ($\star$), as a function of dopant grading R in the base for collector current density of $10^3 A/cm^2$.

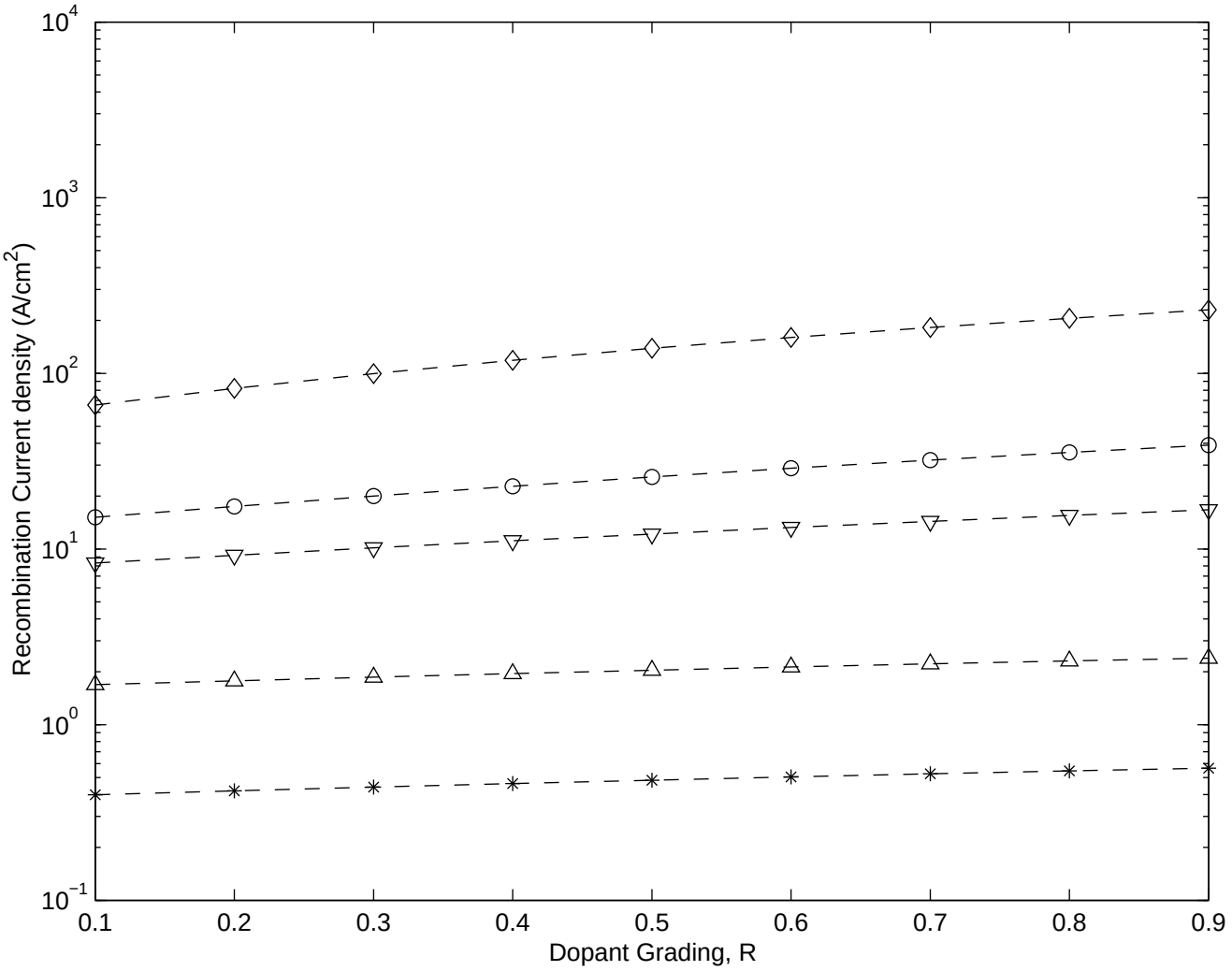

Figure 3.7: Base recombination currents: nonradiative J_{br} ($\diamond$) and radiative J_{rr} ($\circ$), interface J_{irb} ($\bigtriangledown$) space charge region (J_{scr}) ($\bigtriangleup$) surface J_{sr} ($\star$), as a function of dopant grading R in the base for collector current density of $10^4 A/cm^2$.

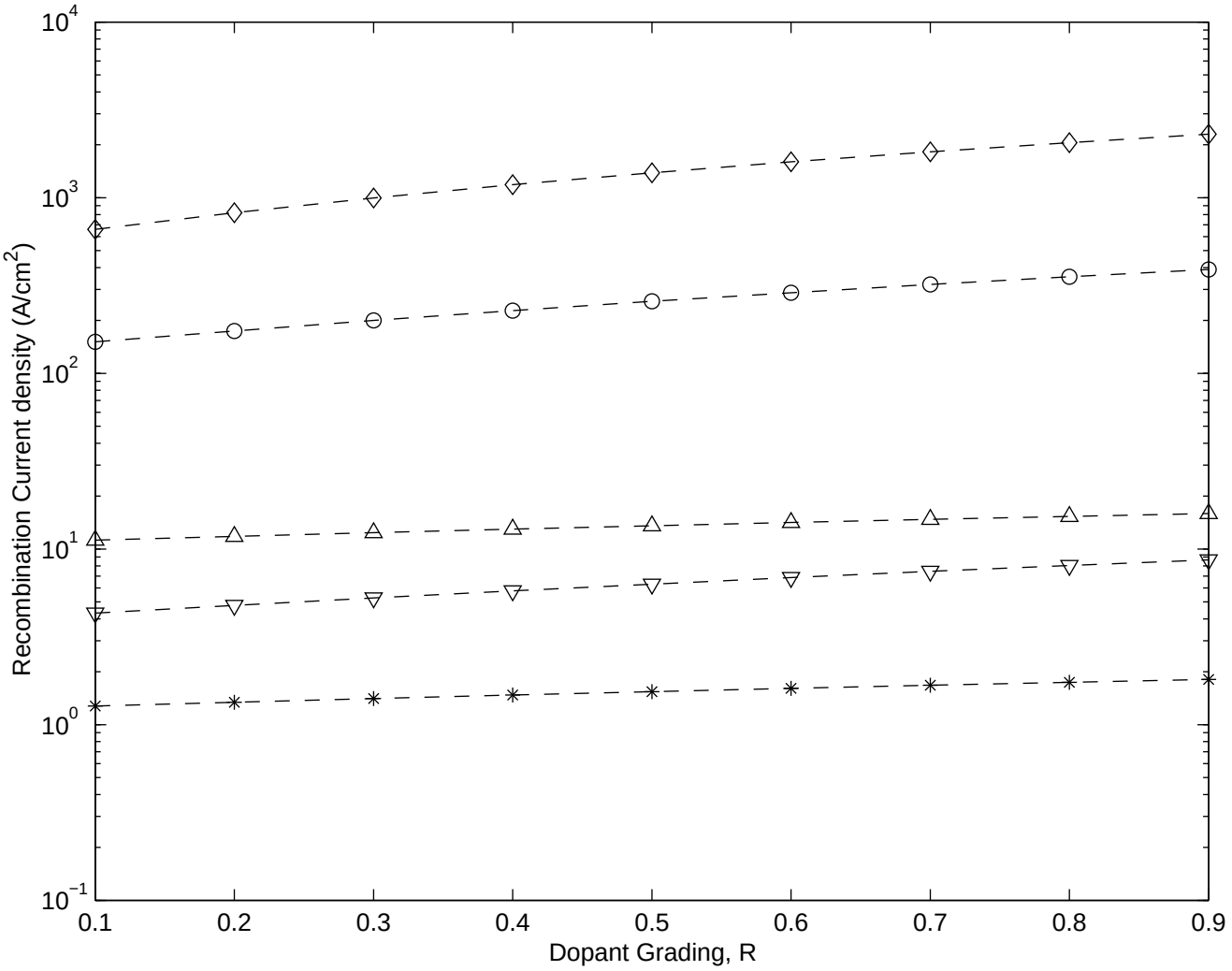

Figure 3.8: Base recombination currents: nonradiative J_{br} ($\diamond$) and radiative J_{rr} ($\circ$), interface J_{irb} ($\bigtriangledown$) space charge region (J_{scr}) ($\bigtriangleup$) surface J_{sr} ($\star$), as a function of dopant grading, R in the base for collector current density of $10^5 A/cm^2$.

velocities, which are grading dependent does not determine the value of J_p. The base current density J_b, which includes the various recombination currents, is more dependent on the dopant grading and decreases with the increase in the grading. As a result of these two observations, the DC current gain, when plotted as a function of collector current density, is strongly dependent on the dopant grading factor R. This is illustrated in Figure 3.10. As expected we see that there is maximum gain when the dopant grading is the largest. At current densities between 10^4 to $10^5 A/cm^2$, the DC current gain is nearly constant and is about a factor 4 larger for R = 0.1 compared to R = 0.9.

3.5 Base Transit Time

Incorporation of dopant grading impacts the base transit time (τ_b) and so the high frequency performance capabilities of the device. Figure 3.11 shows the plot of τ_b as a function of dopant grading. The base transit time τ_b decreases from around 10 ps to about 4 ps when the dopant grading (R) is increased from 0.9 to 0.1. This is again an illustration of the benefit of a quasi electric field in the base helping holes to cross the base more rapidly.

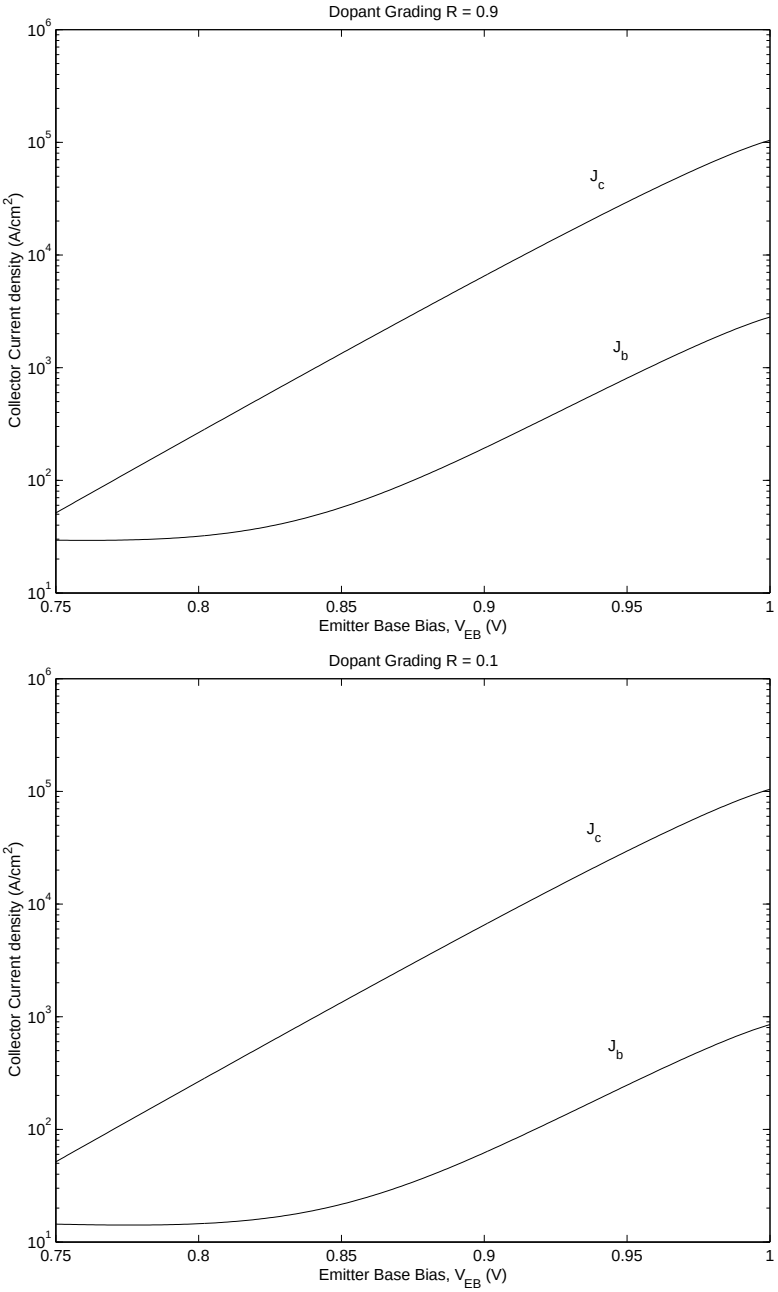

Figure 3.9: Base current (J_b) and collector current (J_c) densities as function of emitter-base bias V_{EB} for two dopant gradings. The top and bottom figures correspond to R = 0.9 and 0.1, respectively.

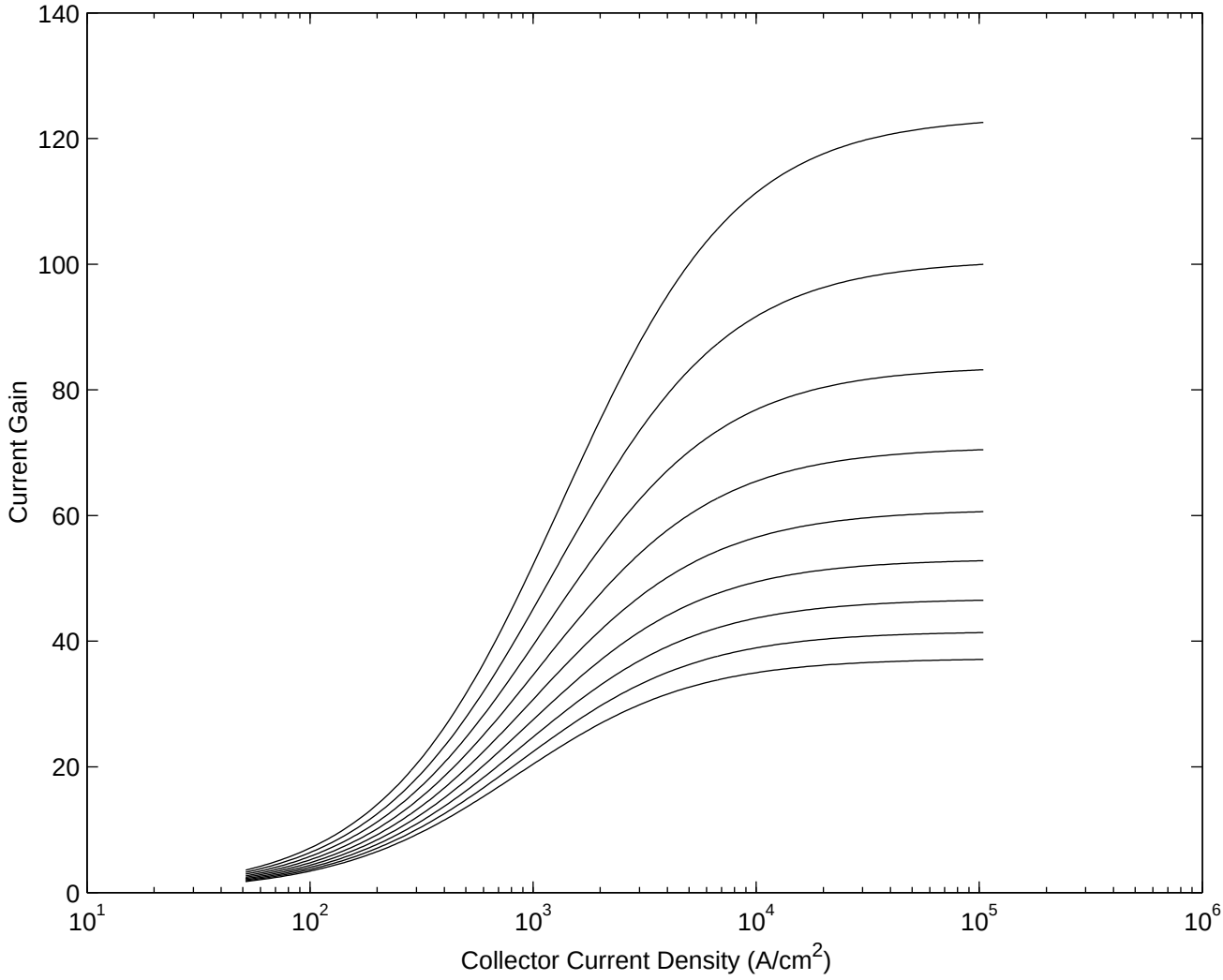

Figure 3.10: DC current gain as function of collector current density (J_c) for dopant grading R varying from 0.9 (bottom) to 0.1 (top) in steps of 0.1.

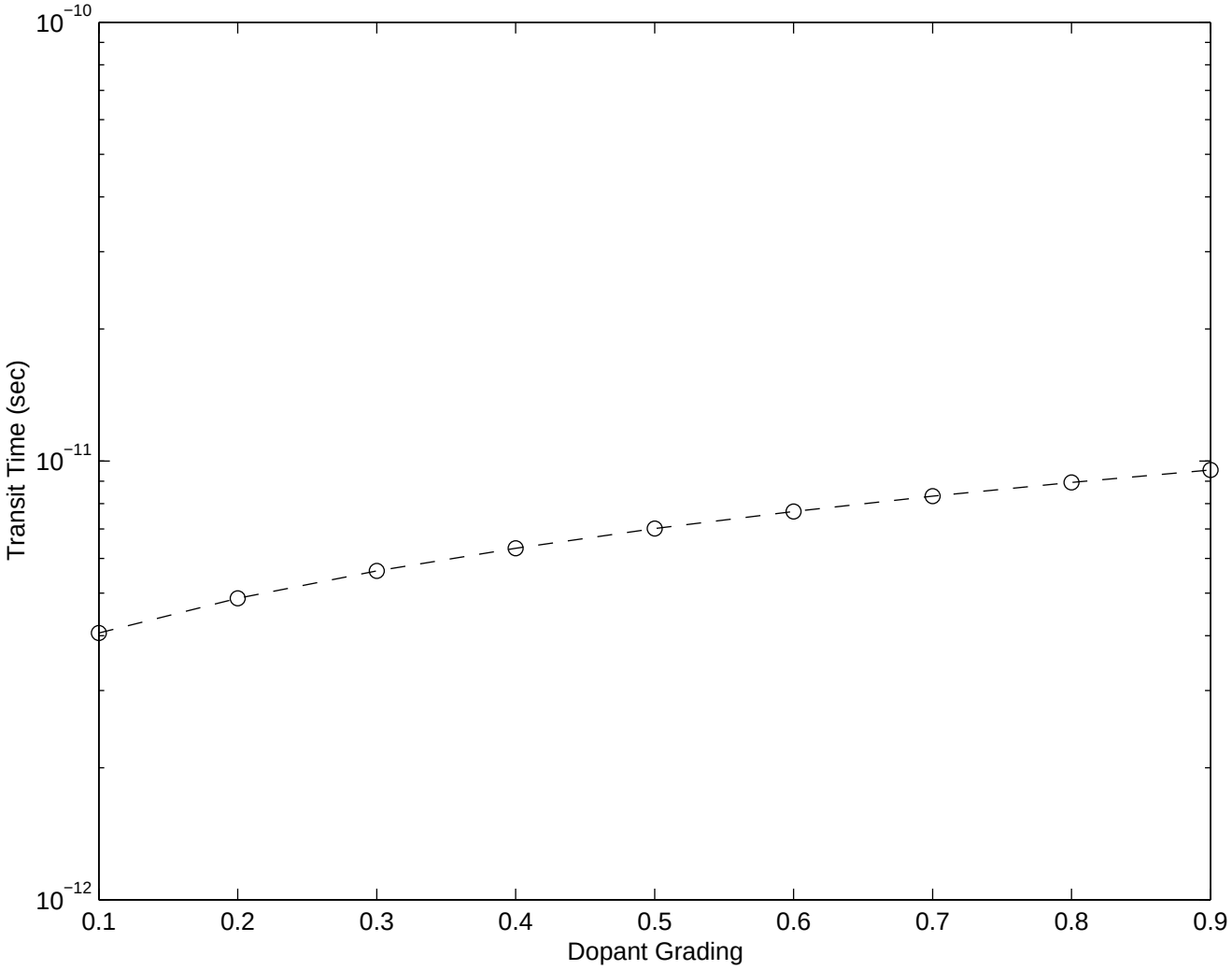

Figure 3.11: Base transit time as function of the dopant grading R. The base transit time is relatively insensitive to the value of the collector current density.

Chapter 4

Summary and Suggestions for Future work.

4.1 Thesis Summary.

In this thesis, we have developed an analytical model of Pnp HBTs with a linear doping profile across the base. The model incorporates a thermionic-emission-diffusion model of hole injection across the heterojunction and matches the hole flux with a drift-diffusion model of current in the base. It includes the effects of quasi Fermi level splitting at the emitter-base heterojunction and its influence on thermionic emission, tunneling and recombination currents. Our model includes the effects of various recombination currents in: the emitter-base space charge region (J_{scr}), on the base side (J_{irb}) and emitter side (J_{ire}) of the emitter-base interface. The model also includes surface recombination

current (J_{sr}), the nonradiative (J_{br}) and radiative (J_{rr}) recombination currents in the base, and the electron back injection (J_{ne}) and electron collector leakage (J_{nc}) currents.

First we investigated the effects of non-uniform doping on hole effective velocities. It was shown that linear doping enhances both the hole effective diffusion coefficient S_{dp}^{eff} across the base and also leads to an effective saturation velocity of holes v_s^{eff} at the base collector junction much larger than the measured saturation velocity v_s of holes in the bulk. The two other effective velocities S_{ip} and S_{ep} are unaffected by dopant grading and remain less than S_{dp}^{eff} and v_s^{eff}. So, both S_{ip} and S_{ep} remain the velocities controling the current flow across the emitter-base heterojunction.

We then investigated the effect of dopant gradient on the minority carrier profile in the base. For a strong dopant grading the slope of the minority carrier profile in the base is much smaller than for weak grading. This minority carrier profile also shows accumulation at the collector end of the base. This trend is due to the more efficient transport of holes across the base. This also led to a lower base transit time which is an illustration of the benefit of a quasi electric field in the base helping holes to cross the base more rapidly. We also show that the incease in current gain was due to the fact that the dopant gradient reduces the various recombination currents that contributes to the base current and, in effect loweres the base current. As a result, the DC current gain, when plotted as a function of collector density, is strongly dependent on the dopant gradient. There is a maximum gain when the dopant gradient is the largest.

4.2 Analytical Model Development

The Thermionic-emission-diffusion model could be further extended to a more general charge control based Gummel-Poon model [75]. This would incorporate the high current effects such as base pushout and series resistance effect which would lead to device degradation at high current density device operation. A more advanced Gummel-Poon model could be developed by incorporating the recombination currents while matching up the hole flux across the heterojunction with the hole drift-diffusion in the base. This will result in a more accurate calculation of the hole injection from the emitter into the base and a more accurate determination of the device gain and frequency performance. Similar to the dopant gradient in the base, the emitter doping could also be varied linearly to create a retarding field for minority carrier transport in the emitter which in turn would increase the current gain.

More sophisticated doping profiles in the base (piecewise linear or quadratic) could be investigated to try to minimize the base transit time. This may lead to untractable analytical solutions of the minority carrier (hole) distribution profile across the base. However, the hole distribution and all recombination currents could still be evaluated numerically, as well as the base transit time. The latter would need to be minimized by varying the parameters describing the doping profile across the base. However, the shape of the analytical curve describing the base doping profile should be kept simple enough so that it can eventually be realized experimentally.

Another step in further developing the analytical model will be a better description of the hole tunneling current across the emitter-base junction. For instance, Ekbote et al. [74] have investigated the effects of band mixing between light-holes and heavy-holes in the tunneling properties of holes at the emitter-base heterojunction using a scattering matrix approach. Following their analysis, an effective tunneling factor including the effects of band-mixing can be derived for incorporation in our analytical model. Moreover since Pnp HBTs employ a narrow base width (30 nm typically), the effects of ballistic transport in the base and velocity overshoot in the base collector region could be analyzed through Monte Carlo simulation. Based on Monte Carlo results, an effective diffusion constant in the base and an effective saturation velocity in the base collector space charge region could be determined and incorporated in our analytical model.

Bibliography

[1] W.Shockley, *US Patent No. 2569347*, 1866 (1961).

[2] H.Kroemer, "Theory of a wide-gap emitter for transistors", *Proc. IRE.*, **45**, p.1535, (1957).

[3] H. Kroemer, "Heterojunction bipolar transistors and integrated circuits", *Proc. IEEE*, **70**, p. 13, (1982).

[4] A.Y.Cho and J.R.Arthur, "Molecular Beam Epitaxy", *Proc. Solid State Chem.*, **10**, Pt. 3, p. 157, (1975).

[5] R. D. Dupuis, L. A. Moudy and P. D. Dapkus, "Preparation and properties of GaAlAs-GaAs heterojunction grown by metal-organic chemical vapour deposition", *Galium-Arsenide and Related Compounds, 1st Phys. Conf.*, **45**, p. 1, (1979).

[6] W. Liu and C. Dai, "An advantage of pnp over npn AlGaAs/GaAs heterojunction bipolar transistors for microwave power applications", *J. of Appl. Phys.*, **31**, p. 452, (1992).

[7] W. Liu, D. Hill, D. Costa, and J. S. Harris, "High performance microwave AlGaAs/InGaAs pnp HBT with high dc current gain", *IEEE Microwave Guided Wave Lett.*, **2**, p.331, (1992).

[8] G. B. Gao, D. J. Roulston and H. Morkoc, "Is npn or pnp the better choice for millimeter-wave AlGaAs/GaAs heterojunction bipolar transistors", *Solid State Electron.*, **33**, p. 1209, (1990).

[9] D. G. Hill, T. S. Kim and H. Q. Tserng, "X-band power AlGaAs/InGaAs pnp HBTs", *IEEE Electron Device Lett.*, **14**, p. 185, (1993).

[10] B. Bayraktaroglu, N. Camilleri and S. A. Lambert, "Microwave performances of npn and pnp AlGaAs/GaAs heterojunction bipolar transistors", *IEEE Trans. Microwave Theory Tech.*, **36**, p. 1869, (1988).

[11] H. Beneking and L. M. Su, "AlGaAs/GaAs heterojunction microwave bipolar transistor", *Electron Lett.*, **17**, p.301, (1981).

[12] L. S. McCarthy, I. P. Smorchkova, H. Xing, P. Kozodoy, P. Fini, J. Limb, D. Pulfrey, J. Speck, M. J. W. Rodwell, S. P. DenBaars, U. K. Mishra, "GaN HBT: Toward an RF Device", *IEEE Trans. Electron Devices*, **48**, p. 543 (2001).

[13] M. B. Panish, "Gas source molecular beam epitaxy of GaInAs(P): gas source, single quantum-well, superlattice p-i-n's and bipolar transistor", *J. Cryt. Growth*, **81**, p. 249, (1987).

[14] P. A. Houston, "Double heterojunction bipolar transistors in InP/InGaAs grown by metal-organic chemical vapour deposition", *Electron Lett.*, **23**, p. 931, (1987).

[15] B. Jalali, R. N. Nottenburg, A. F. J. Levi, A. Y. Cho and M. B. Panish, "Base doping limits in heterostructure bipolar transistors", *Appl. Phys. Lett.*, **56**, p. 391, (1989)

[16] Q. Lee et al.,"Submicron transfered-substrate heterojunction bipolar transistors with greater than 1 Thz fmax", *In Proc. IEEE Device Research Conf.*, Santa Barbara, CA, June 1999.

[17] Q. Lee et al., "Submicron transferred-substrate heterojunction bipolar transistors", *IEEE Electron Device Lett.*, **20** p. 396 (1999).

[18] M. Konnzai, K. Katsukawa and K. Takahashi, "AlGaAs/GaAs heterojunction phototransistors with high current gain", *J. Appl. Phys.*, **48**, p. 4389, (1977).

[19] D. Ankri and A. Scarennec, "Design and evaluation of a planar AlGaAs/GaAs bipolar transistor", *Electron Lett.*, **16**, p. 41, (1980).

[20] S. Tiwari, S. L. Wright and A. W. Kleinsasser, "Transport and related properties of AlGaAs/GaAs double heterojunction bipolar transistors", *IEEE Trans. Electron Devices*, **34**, p. 185, (1987).

[21] J. A. Hutchby, "High-performance p-n-p AlGaAs/GaAs heterojunction bipolar transistors: A theoritical study", *IEEE Electron Device Lett.*, **7**, p. 108, (1986).

[22] D. A. Sunderland and P. D. Dapkus, "Optimizing n-p-n and p-n-p heterojunction bipolar transistors for speed", *IEEE Trans. on Electron Devices*, **34**, p. 367, (1987).

[23] J. S. Yuan, "High- performance p-n-p heterojunction bipolar transistor design", *Solid State Electron.*, **34**, p.1347, (1991).

[24] M. E. Kim, B. Bayraktroglu and A. Gupta, "HBT devices and circuit applications," in *HEMTs and HBTs: Devices, Fabrication and Circuits*, F. Ali and A. Gupta, Eds. Boston, MA: Artech House, p. 318, (1991).

[25] D. B. Slater, P. M. Enquist, J. A. Hutchby, A. S. Morris and R. J. Trew, "pnp HBT with 66 Ghz f_{max}", *IEEE Electron Device Lett.*, **15**, p. 91, (1994).

[26] G. J. Sullivan, M. F. Chang, N. H. Sheng, R. J. Anderson, N. L. Wang, K. C. Wang, J. A. Higgins, and P. M. Asbeck, "AlGaAs/GaAs Pnp HBTs with high maximum frequency of oscillation", *IEEE Electron Device Lett.*, **11**, p. 463, (1990).

[27] P. M. Enquist, D. B. Slater and J. W. Swartz, "Complementary AlGaAs/GaAs HBT I^2L(CHI^2L) technology", *IEEE Electron Device Lett.*, **13**, p. 180, (1992).

[28] W. E. Stanchina, R. A. Metzger, M. W. Pierce, J. F. Jensen, L. G. McCray, R. Wong-Quen and F. Williams, "Monolithic fabrication of npn and pnp AlInAs/GaInAs HBTs", *Proc.* 5^{th} *Intl. Conf. InP and Rel. Materials*, p. 569, (1993).

[29] J. Pankove, S. S. Chang, H. C. Lee, R. J. Molnar, T. D. Moustakas, and B. Van Zeghbroeck, "High-temperature GaN/SiC heterojunction bipolar transistor with high gain",*IEDM Tech. Dig.*, p. 389 (1994).

[30] S. T. Sheppard, K. Doverspike, W. L. Pribble, S. T. Allen, J. W. Palmour, L. T. Kehias, and T. J. Jenkins, "High power microwave GaN/AlGaN HEMTs on silicon carbide",*56th Annu. Device Res. Conf. Dig.* (Late News), (1998).

[31] C. Monier, F. Ren, J. Han, P. Chang, R. J. Shul, K. Lee, A. Zhang, A. G. Baca, S. Pearton, "Simulaiton of NPN amd PNP AlGaN/GaN Heterojunction Bipolar Transistors Performance: Limiting factors and optimum Design", *IEEE Trans, on Electron Dev.*, **48**, p. 427 (2001).

[32] A. P. Zhang, G. T. Dang, and F. Ren, "Direct-current characteristics of pnp AlGaN/GaN heterojunction bipolar transistors", *Appl. Phys. Lett.*, **76**, p. 2943 (2000).

[33] L. M. Lunardi, S.Chandrasekhar, and R. A. Hamm, "High-speed, high-current-gain pnp InP/InGaAs heterojunction bipolar transistors", *IEEE Electron Device Lett.*, **14**, p. 19, (1993).

[34] W. E. Stanchina, R. A. Metzger, D. B. Rensh, L. M. Burns, J. F. Jensen, R. H. Walden, L. E. Larson, and P. T. Greiling, "InP-based technology for monolithic multiple-device, multiple-function IC's", *GOMAC-91 Dig. Papers*, p. 385 (1991).

[35] D. Cui, D. Palvidis, S. S. H. Hsu. D. Sawadi, P. Chin, and T. Block, "First demonstration of monolithic InP-based HBT amplifier with PNP active load", *IEEE Electron Dev. Lett.*, *23*, p. 114 (2002).

[36] S. Datta, K. P. Roenker, M. Cahay, "Hole Tranport and Quasi-Fermi Level Splitting at the Emitter-Base Junction in Pnp Heterojunction Transistors", **85**, p. 1949, (1999).

[37] S. Datta, S. Shi, K. P. Roenker, M. Cahay, "A Thermionic-Emission-Diffusion Model for the Graded Base Pnp Heterojunction Transistors", *J. of Appl. Phys.*, **83**, p. 8036, (1998).

[38] K. Kurishima, H. Nakajima, S. Yamahata, T. Kobayashi, and Y. Matsuoka, *J. Appl. Phys.*, **34**, p. 1221, (1995).

[39] M. Ohkubo, J. Osabe, N. Ikeda, and T. Ninomiya, *Proceedings of the Ninth International Conference on Indium Phosphide and Related Materials*, 1997, p. 641.

[40] S. N. Mohammad, J. I. Chyi, J. Chen, and H. Morkoc, "Influence of nonunifrom doping on the uniformity of current gain, base transit time, and related properties of AlGaAs/GaAs heterojunction bipolar transistors", *J. Appl. Phys.*, **78**, p. 2105, (1990).

[41] J. H. Ning, J. S. Yuan, and J. Song, "Effects of base and emitter doping gradients on the electrical performance of heterojunction bipolar transistors", *Solid-State Electron.*, **41**, p. 1263 (1997).

[42] S. Datta, S. Shi, K. P. Roenker, M. Cahay, W. E. Stanchina, "Simulation and Design of InAlAs/InGaAs Pnp Heterojunction Bipolar Transistors", *IEEE Trans. on Electron Devices.*, **45**, p. 1643, (1998).

[43] S. R. Ahmed, B. R. Nag, and M. D. Roy, "Hot electron transport in $In_{0.53}Ga_{0.47}As$", *Solid State Electron.*, **28**, p. 1193 (1985).

[44] J. Bohrer, M. Grundmann, U. Lienert, D. Bimberg, H. Ishikawa, M. Kanada, and N. Watanabe, "Determination of band discontinuity of MOCVD grown $In_{1-x}Ga_xAs/In_{1-y}Al_yAs$ heterostructures with optical and structural methods", *J. Cryst. Growth.*, **107**, p. 555 (1991).

[45] M. Shur, *Physics of Semiconductor Devices*, Englewood Cliffs, NJ, Prentice Hall, pp. 627 (1990).

[46] W. Lee and C. G. Fonstad, "$In_{0.52}Al_{0.48}As/In_{0.53}Ga_{0.47}As/In_{0.52}Ga_{0.48}As$ abrupt double heterojunction bipolar transistors", *IEEE Electron Device Lett.*, **7**, p. 683 (1986).

[47] S. Adachi, "Material properties of $In_{1-x}Ga_xAs_yP_{1-y}$ and related binaries", *J. Appl. Phys.*, **53**, p. 8775 (1988).

[48] S. Hiyamizu, T. Fujii, S. Muto, T. Inata, Y. Nakata, Y. Sugiyama, and S. Sasa, "MBE growth of InGaAs-InAlGaAs heterostructures for applications to high speed devices", *J. Cryst. Growth*, **81**, p. 349 (1987).

[49] I. S. Ashour, H. E. Kadi, K. Sherif, J. P. Valcout, and D. Decoster, "Cutoff frequency and responsivity limitation of AlInAs/GaInAs MSM PD using a two-dimensional bipolar physical model", *IEEE Trans. Electron Devices*, **42**, p. 231 (1995).

[50] L. Y. Leu, J. T. Gardner and S. R. Forrest, "A high-gain, high bandwidth $In_{0.53}Ga_{0.47}As/InP$ heterojunction phototransistor fof optical communication", *J. Appl. Phys.*, **69**, p. 1052, (1991).

[51] D. M. Caughey and R. E. Thomas, "Carrier mobilities in silicon empirically related to doping and field", *Proc. IEEE*, **55**, p. 2192 (1967).

[52] S. Selberherr, "Analysis and Simulation of Semiconductor devices", Vienna, Springer Verlag, 1984, p. 80.

[53] T. P. Pearsall and J. P. Hirtz, "The carrier mobilities in $Ga_xIn_{1-x}As$ grown by organo-metallic CVD and liquid-phase epitaxy", *J. Cryst. Growth*, **54**, p. 127 (1981).

[54] M. J. Martinez, D. C. Look, J. R. Sizelove, and F. L. Schuermeyer, "Monte Carlo simulation of hole transport in $Al_xGa_{1-x}As, In_{1-x}Al_xAs$ and $GaAs_xSb_{1-x}$", *J. Appl. Phys.*, **77**, p. 661 (1995).

[55] J. M. Golio, Microwave MESFETs and HEMTs Boston, MA: Artech House, 1991, p. 8-25.

[56] M. A. Littlejohn, K. W. Kim, and H. Tian, "High field transport in InGaAs and related heterostructures", *Properties of Lattice-Matched and Strained Indium Gallium Arsenide*, P. Bhattacharya, Ed. London. U.K. INSPEC, p. 107 (1993).

[57] G. J. Davies, T. Kerr, C. G. Tuppen, B. Wakefield, and D. A. Andrews, "The growth and characterization of minimally doped $Al_{1-x}In_xAs$ growth by molecular beam epitaxy", *J. Vac. Sc. Technol.*, B, p. 219 (1984).

[58] K. Y. Cheng, A. Y. Cho, and W. R. Wagner, "Tin doing in $Ga_{0.47}In_{0.53}As$ and $Al_{0.48}In_{0.52}As$ grown by molecular beam epitaxy", *J. Appl. Phys.*, **52**, p. 6328 (1985).

[59] E. Y. Wu, "A Monte Carlo study of steady state electron transport in uncompensated $Al_{0.25}In_{0.75}As$", *J. Appl. Phys.*, **67**, p. 6899 (1987).

[60] S. Datta, S. Shi, K. P. Roenker, M. Cahay, W. E. Stanchina, "Implications of Hole versus electron transport Properties for High Speed Pnp Heterojunction Bipolar Transistors", *Solid-State Elecron.*, **43**, p. 73, (1999).

[61] M. M. Tashima, L. W. Cook, and G. E. Stillman, "Room-temperature electron diffusion lenghts in liquid phase epitaxial InGaAsP and InGaAs", *Appl. Phys. Lett.*, **39**, p. 960 (1981).

[62] J. E. Ehrlich, D. T. Neilson, A. C. Walker, G. T. Kennedy, R. S. Grant, W. Sibbett, and M. Hopkinson, "Carrier lifetimes in MBE and MOCVD InGaAs quantum wells", *Semicond. Sci. Technol.*, **8**, p. 307 (1993).

[63] B. Sermage, H. J. Eichler, J. P. Heritage, R. J. Nelson, and N. K. Dutta, "Photoexcited carrier lifetime and Auger recombination in 1.3 μm InGaAsP", *Appl. Phys. Lett.*, **42**, p.259 (1983).

[64] C. R. Selvakumar, "A new minority carrier lifetime model for heavily doped GaAs and InGaAsP to obtain analytical solutions", *Solid State Electron.*, **30**, p. 773 (1987).

[65] N. Chand, "Carrier diffusion lengths and lifetimes in InGaAs", *Properties of Lattice-Matched and Strained Indium Gallium Arsenide*, P. Bhattacharya, Ed. London, U.K. :INSPEC, 1993, p.127.

[66] M. A. Stettler and M. S. Lundstrom, "A detailed investigation of heterojunction transport using a rigorous solution of the Boltzmann equation", *IEEE Trans. Electron Devices*, **41**, p. 592 (1994).

[67] A. A. Grinberg, M. S. Shur, R. J. Fischer and H. Morkoc, "An investigation of the effect of graded layers and tunneling on the performance of AlGaAs/GaAs heterojunction bipolar transistors", *IEEE Trans. Electron Devices*, **31**, p. 1758 (1984).

[68] J. S. Yuan, "Hole tunneling through the emitter-base junction of a heterojunction bipolar transistor", *Solid State Electron.*, **34**, p. 1347, (1991)

[69] B. R. Ryum and I. M. Abdel-Motaleb, "An analytical all-injection charge-based model for graded-base HBTs", *Solid State Electron.*, **34**, p. 1125 (1991).

[70] B. R. Ryum and I. M. Abdel-Motaleb, "A Gummel-Poon model for abrupt and graded heterojunction bipolar transistors (HBTs)", *Solid State Electron.*, **33**, p. 869 (1990).

[71] B. R. Ryum and I. M. Abdel-Motaleb, "Effects of recombination current on current gain of HBTs", *IEEE Proc.- G: Circuits, Devices Syst.*, **138**, p. 115 (1991).

[72] D. L. Pulfrey and S. Searless, "Electron quasi-Fermi level splitting at the base-emitter junction in pnp heterojunction bipolar transistors", *J. of Appl. Phys.*, **85**, p. 1949 (1999).

[73] D. K. Ferry, L. A. Akers, and E. W. Greeneich, in *Ultra Large Scale Integrated Microelectronics*, (Prentice Hall, Englewood Cliffs, N.J. 1988), p. 112.

[74] S. Ekbote, M. M. Cahay, and K. P. Roenker, "Influence of the spin-orbit split-off band on the tunneling properties of holes through heterostructures", *Phys. Rev. B.*,

[75] S. Datta, K. P. Roenker, M. M. Cahay, "A Gummel-Poon model for pnp heterojunction bipolar transistors with a compositionally graded base", *Solid-State Electron.*, **44**, p. 991, (2000).

Appendix A

Expression for built-in potential and effective velocity S_{ep}

The builtin potential is the difference of the field-free work functions of the two semiconductor materials. Referring to Figure A.1, the builtin potential is found to be equal to

$$V_{bi} = -\frac{1}{q}(\chi_n - \chi_p) - \frac{1}{2q}(E_{gn} - E_{gp}) + (\phi_n + \phi_p), \tag{A-1}$$

where χ_n and χ_p are the electron affinities, and ϕ_n and ϕ_p are the separation of the Fermi potential from the midgap on the n-type and p-type materials, respectively.

Depending on the materials forming the heterostructure, we have typically

$$\chi_n - \chi_p = y(E_{gn} - E_{gp}), \tag{A-2}$$

where y = 1 corresponds to Anderson's rule and y=0.65 is valid for an AlGaAs/GaAs

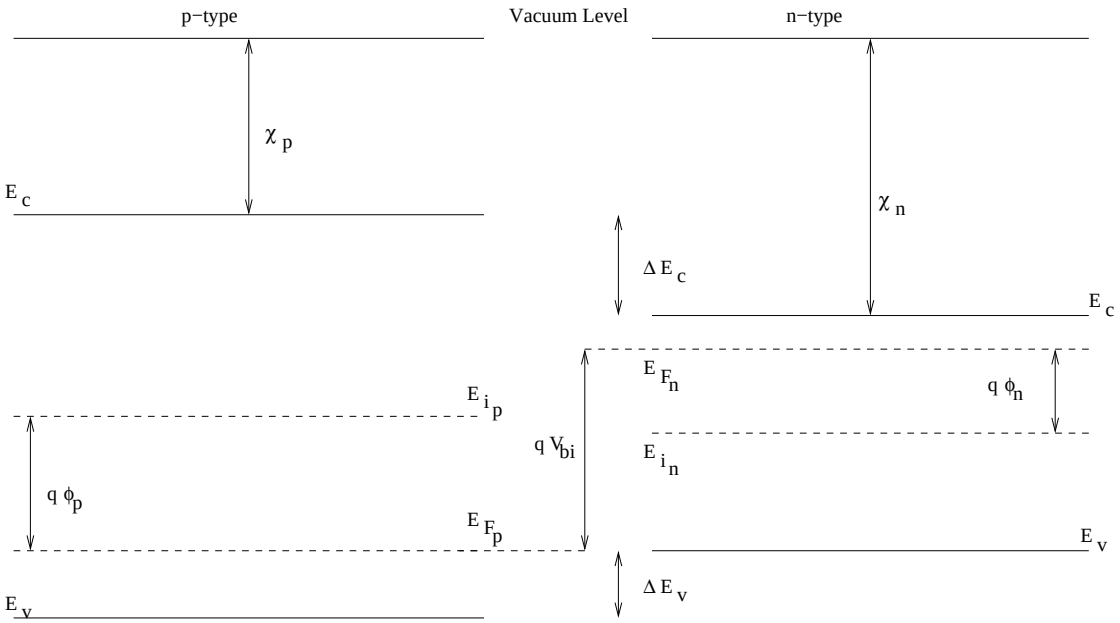

Figure A.1: Band diagrams for two different semiconductor materials forming a heterointerface. The vacuum level is chosen as the reference energy. V_{bi} is the built in voltage.

heterointerface. Substituting Eq.(A-2) into Eq.(A-1), we get

$$V_{bi} = -\frac{y}{q}(E_{gn} - E_{gp}) - \frac{0.5}{q}(E_{gn} - E_{gp}) + (\phi_n + \phi_p), \tag{A-3}$$

or

$$V_{bi} = -\frac{1}{q}(y - 0.5)(\Delta E_c + \Delta E_v) + \frac{kT}{q}(\frac{N_A N_D}{n_{in} n_{ip}}). \tag{A-4}$$

The last term can be rewritten as follows

$$\frac{N_A N_D}{n_{in} n_{ip}} = \frac{p(-x_p) N_D}{n_{in} n_{ip}} = \frac{p(-x_p)}{p_{no}} \frac{n_{in}}{n_{ip}}, \tag{A-5}$$

where p_{no} is the hole equilibrium concentration on the n-side of the heterojunction. Further more we have

$$n_{in} = \sqrt{N_{cn} N_{vn}} e^{-\frac{E_{gn}}{2kT}}, \tag{A-6}$$

and

$$n_{ip} = \sqrt{N_{cp} N_{vp}} e^{-\frac{E_{gp}}{2kT}}. \tag{A-7}$$

Hence,

$$\frac{n_{in}}{n_{ip}} = e^{\frac{(E_{gp} - E_{gn})}{2kT}}, \tag{A-8}$$

where we have assumed that the difference between the density of states of the sides of the heterojunction is negligible.

Substituting Eq.(A-8) in Eq.(A-5), the built in potential becomes

$$V_{bi} = \frac{(1 - y)}{q}(\Delta E_c + \Delta E_v) + \frac{kT}{q} ln(\frac{p(-x_p)}{p_{no}}). \tag{A-9}$$

Therefore

$$p(-x_p) = p_{no} e^{(V_{bi} - \frac{1}{q}(1-y)(\Delta E_c + \Delta E_v))}. \tag{A-10}$$

Earlier, we have shown that (See Eq.(2.10)) in chapter II)

$$e^{F_p(-x_p)-F_p(0_-)} = 1 - (\frac{J_p e^{\frac{qV_p}{kT}}}{q\mu_p p(-x_p)E(0_-)}). \tag{A-11}$$

Since for an applied bias V_{EB} across the heterojunction we have

$$V_{bi} - V_{EB} = V_p + V_n. \tag{A-12}$$

We can use Equations (A-10) and (A-12) to rewrite Eq.(A-11) as follows

$$e^{F_p(-x_p)-F_p(0_-)} = 1 - (\frac{J_p e^{\frac{q}{kT}(V_{bi}-V_a-V_n)}}{q\mu_p E(0_-)p_{no}e^{\frac{qV_{bi}}{kT}}e^{-(1-y)(\frac{\Delta E_v+\Delta E_c)}{kT})}}). \tag{A-13}$$

Simplifying, we get

$$e^{F_p(-x_p)-F_p(0_-)} = 1 - \frac{J_p e^{-\frac{qV_a}{kT}}}{qS_{ep}p_{no}}, \tag{A-14}$$

where we have introduced the effective velocity

$$S_{ep} = \mu_p E(0_-)e^{-(\frac{\Delta E_v - qV_n}{kT})}e^{\frac{y\Delta E_v-(1-y)\Delta E_c}{kT}}. \tag{A-15}$$

However,

$$\Delta E_v = (1-y)\Delta E_g, \tag{A-16}$$

and

$$\Delta E_c = y\Delta E_g, \tag{A-17}$$

therefore the numerator in the last exponential in Eq.(A-15) reduces to unity and S_{ep} is given by

$$S_{ep} = \mu_p E_(0_-)e^{-(\frac{\Delta E_v - qV_n}{kT})} \tag{A-18}$$

The explicit expressions for $E(0^-)$ and V_n are given in appendix B.

Appendix B

Depletion Approximation at Emitter-Base Junction

We model the space-charge region across the emitter-base interface of a Pnp HBT using the depletion approximation. In this case, the space-charge distribution on both sides of the interface is given by

$$\rho(x) = -qN_A, \tag{B-1}$$

for $-x_p < x < 0$, and

$$\rho(x) = +qN_D, \tag{B-2}$$

for $0 < x < x_n$.

Starting with Poisson's equation, we get

$$\frac{dE}{dx} = -q\frac{N_A}{\epsilon_p}, \tag{B-3}$$

in the emitter region and

$$\frac{dE}{dx} = +q\frac{N_D}{\epsilon_n}, \tag{B-4}$$

in the base region where ϵ_p and ϵ_n are the dielectric constants of the emitter and base, respectively.

Integrating Eq.(B-3) across $[-x_p, x]$ and Eq.(B-4) across $[x, x_p]$, we get

$$E(x) = -\frac{qN_A}{\epsilon p}(x + x_p), \tag{B-5}$$

on the p-side (emitter), and

$$E(x) = -\frac{qN_D}{\epsilon n}(x - x_n), \tag{B-6}$$

on the n-side (base).

The electrostatic potential $V(x)$ on either side of the junction is then found by integrating the previous results starting with

$$\frac{dV}{dx} = -E(x). \tag{B-7}$$

This leads to

$$V(x) = \frac{qN_D}{2\epsilon_n}(x - x_n)^2, \tag{B-8}$$

on the base side and

$$V(x) = \frac{qN_A}{2\epsilon_p}(x + x_p)^2, \tag{B-9}$$

on the emitter side.

The built-in potential on the emitter side is therefore

$$V_p = \frac{qN_A}{2\epsilon_p}x_p^2, \tag{B-10}$$

and, on the base side, it is given by

$$V_n = \frac{qN_D}{2\epsilon_n} x_n^2. \tag{B-11}$$

The total built-in potential V_{bi} across the space-charge region is therefore given by

$$V_{bi} = V_n + V_p = \frac{q}{2}(\frac{N_D}{\epsilon_n} x_n^2 + \frac{N_A}{\epsilon_p} x_p^2), \tag{B-12}$$

$$V_{bi} = \frac{q}{2\epsilon_n} N_D x_n^2 [1 + (\frac{N_A}{N_D})(\frac{\epsilon_n}{\epsilon_p})(\frac{x_p}{x_n})^2]. \tag{B-13}$$

From the space charge neutrality condition, we have

$$qN_D x_n = qN_A x_p. \tag{B-14}$$

With the last equation, we can rewrite the built-in potential as

$$V_{bi} = \frac{q}{2\epsilon_n} N_D x_n^2 [\frac{\epsilon_p N_A + \epsilon_n N_D}{\epsilon_p N_A}]. \tag{B-15}$$

Hence the width of the depletion region on the base side is

$$x_n = \sqrt{\frac{2\epsilon_n \epsilon_p N_A V_{bi}}{qN_D[\epsilon_p N_A + \epsilon_n N_D]}}. \tag{B-16}$$

Similarly, we can write an expression for the width of the depletion region on the emitter side

$$x_p = \sqrt{\frac{2\epsilon_n \epsilon_p N_D V_{bi}}{qN_A[\epsilon_p N_A + \epsilon_n N_D]}}. \tag{B-17}$$

Plugging back the expressions of x_n and x_p in Eqs.(B-10) and (B-11), we obtain

$$V_n = \frac{\epsilon_p N_A V_{bi}}{(\epsilon_p N_A + \epsilon_n N_D)}, \tag{B-18}$$

and

$$V_p = \frac{\epsilon_n N_D V_{bi}}{(\epsilon_p N_A + \epsilon_n N_D)}. \tag{B-19}$$

If a forward bias V_{EB} is applied across the emitter-base junction, the equations above stay valid after replacing V_{bi} by $V_{bi} - V_{EB}$. The Electric field at $x = 0_-$ can then be calculated as a function of the applied bias

$$E(0_-) = \sqrt{2(\frac{\epsilon_n}{\epsilon_p})\frac{qN_A N_D(V_{bi} - V_{EB})}{(\epsilon_p N_A + \epsilon_n N_D)}}. \tag{B-20}$$

This last equation is used in Chapter II to derive an expression of the current density across the emitter-base junction.

Appendix C

Derivation of Current Density Across the Emitter-Base Junction of a Pnp HBT

On the p-side in the space charge region ($-x_p \leq x \leq 0$), we assume hole transport is governed by drift-diffusion and we write the sum of drift and diffusion currents as follows

$$J_p = p\mu_p \frac{dF_p}{dx}, \tag{C-1}$$

where F_p is the hole quasi-fermi level defined by

$$F_p = E_v - kT \ \ ln\frac{p}{N_v}, \tag{C-2}$$

and

$$p = N_v e^{\frac{-(F_p - E_v)}{kT}}, \tag{C-3}$$

where N_v is the density of states in the valence band in the emitter. Substituting Eq.(C-2) in Eq.(C-1) we get

$$\frac{J_p}{\mu_p p(x)}dx = dF_p = d[E_v - kTln\frac{p}{N_v}]. \tag{C-4}$$

Integrating both sides across the p-side space charge region (-x_p to 0^-) we get

$$\frac{J_p}{\mu_p}\int_{-x_p}^{0^-} dx = [E_v(x) - kTln\frac{p(x)}{N_v}]_{-x_p}^{0^-} = [E_v(0^-) - E_v(-x_p)] + kTln(\frac{p(-x_p)}{p(0^-)}), \tag{C-5}$$

which is also equal to $F_p(0^-)$ - $F_p(-x_p)$. To calculate $p(-x_p)/p(0^-)$ on the righthand side of Eq.(C-5), we use

$$J_p = qp(x)\mu_p E(x) - qD_p\frac{dp(x)}{dx}, \tag{C-6}$$

where $E(x)$ is the electric field in the p-side space charge region which we calculated in the the depletion approximation. On the emitter side of the space-charge region ($-x_p \leq x \leq 0^-$),

$$E(x) = E(0^-)(1 + \frac{x}{x_p}), \tag{C-7}$$

where

$$E(0^-) = -\frac{qN_A x_p}{\epsilon_p}. \tag{C-8}$$

$E(x)$ at x = 0^- is negative since the direction of the field is to the left.

Substituting Eq.(C-8) into Eq.(C-7) we get

$$-\frac{J_p}{\mu_p kT} = \frac{q}{kT}p(x)E(0^-)[1 + \frac{x}{x_p}] + \frac{dp}{dx}. \tag{C-9}$$

This is in the form of the generic first order differential equation

$$\frac{dy}{dx} + P(x)y = Q(x), \tag{C-10}$$

where

$$\begin{aligned} y(x) &= p(x), \\ P(x) &= \frac{qE(0^-)}{kT}[1 + \frac{x}{x_p}], \\ Q(x) &= -J_p/\mu_p\, kT. \end{aligned} \tag{C-11}$$

The general solution of Eq.(C-10) is

$$y(x) = e^{-\int P(x)dx}\{\int Qe^{\int P(x)dx}dx + c\}. \tag{C-12}$$

We first calculate $\int P(x)dx$

$$\int P(x)dx = \frac{qE(0^-)}{kT}\int_{-x_p}^{x}[1 + \frac{x}{x_p}]dx = \frac{qE(0^-)x_p}{2kT}[1 + \frac{x}{x_p}]^2. \tag{C-13}$$

Using the definition of Debye length on the p-side :

$$L_{D_p} \equiv \sqrt{\frac{\epsilon_p k_B T}{q^2 N_A}}, \tag{C-14}$$

then the prefactor in Eq.(C-13) becomes

$$\frac{qE(0^-)x_p}{2kT} = \frac{qx_p}{2kT}(\frac{qN_A x_p}{\epsilon_p}) = (\frac{q^2 N_A}{\epsilon_p kT})\frac{x_p^2}{2} = \frac{x_p^2}{2L_{D_p}^2}, \tag{C-15}$$

and therefore

$$\int P(x)dx = \frac{(x + x_p)^2}{2L_{D_p}^2}. \tag{C-16}$$

Substituting Eq.(C-16) in Eq.(C-12) gives

$$p(x) = e^{-\frac{(x+x_p)^2}{2L_{D_p}^2}} \{\frac{-J_p}{\mu_p kT} \int_{-x_p}^{x} e^{\frac{(x+x_p)^2}{2L_{D_p}^2}} dx + c\}. \tag{C-17}$$

At $x = -x_p$, the integral goes to zero, the exponential goes to 1 and we get $c = p(-x_p)$. In the absence of any current, $p(-x_p) = p_o(-x_p)$ the equilibrium hole concentration in the emitter:

$$p_o(x) = p_o(-x_p) e^{-\frac{(x+x_p)^2}{2L_{D_p}^2}}. \tag{C-18}$$

Rearranging Eq.(C-19) we get an expression for $\frac{1}{p(x)}$ that is substituted back into Eq.(C-5) leading to

$$\frac{1}{p(x)} = \frac{e^{\frac{(x+x_p)^2}{2L_{D_p}^2}}}{\frac{-J_p}{\mu_p kT} \int_{-x_p}^{x} e^{\frac{(x+x_p)^2}{2L_{D_p}^2}} dx + p(-x_p)}. \tag{C-19}$$

Integrating this last expression across $[-x_p, 0^-]$ we get

$$\int_{-x_p}^{0^-} \frac{dx}{p(x)} = \int_{-x_p}^{0^-} \frac{e^{\frac{(x+x_p)^2}{2L_{D_p}^2}}}{\frac{-J_p}{\mu_p kT} \int_{-x_p}^{x} e^{\frac{(x+x_p)^2}{2L_{D_p}^2}} dx + p(-x_p)} dx. \tag{C-20}$$

Letting $g(x) = \frac{(x+x_p)^2}{2L_{D_p^2}}$ and $u(x) = e^{g(x)}$, the integral on the RHS can be rewritten as

$$RHS = \int \frac{u(x)dx}{Q \int u(x)dx + c}, \tag{C-21}$$

using the identity

$$\frac{d}{dx}\{ln[Q \int u(x)dx + c]\} = \frac{Qu(x)}{Q \int u(x)dx + c}. \tag{C-22}$$

we can rewrite Eq.(C-21) as follows

$$\int \frac{u(x)dx}{Q \int u(x)dx + c} = \frac{1}{Q} ln[Q \int u(x)dx + c]. \tag{C-23}$$

and Eq.(C-20) becomes

$$\int_{-x_p}^{0^-} \frac{1}{p(x)}dx = (\frac{-\mu_p kT}{J_p})ln[(\frac{-J_p}{\mu_p kTp(-x_p)})\int_{-x_p}^{0^-} e^{\frac{(x+x_p)^2}{2L_{D_p}^2}}\,dx + 1]. \tag{C-24}$$

Using the expression in Eq.(C-5) we can write

$$e^{\frac{-[F_p(0^-)-F_p(-x_p)]}{kT}} = 1 - (\frac{J_p}{\mu_p kTp(-x_p)})\int_{-x_p}^{0^-} e^{\frac{(x+x_p)^2}{2L_{D_p}^2}}\,dx. \tag{C-25}$$

To solve the integral on the RHS of this last equation, we follow Lundstrom and use the approximation [66]

$$\int_0^{y_n->\alpha} e^{y^2}dy = \frac{e^{y_n^2}}{2y_n}. \tag{C-26}$$

Letting $y = \frac{x+x_p}{\sqrt{2}L_{D_p}}$, we get

$$\int_{-x_p}^{0^-} e^{\frac{(x+x_p)^2}{2L_{D_p}^2}} = \sqrt{2}L_{D_p}\int_0^{y_p} e^{y_p^2}\,dy = \frac{L_{D_p}^2}{x_p}e^{\frac{x_p^2}{2L_{D_p}^2}} \tag{C-27}$$

where we introduced $y_p = \frac{x_p}{\sqrt{2}L_{D_p}}$.

Using Eq.(C-27) in Eq.(C-25) we get

$$e^{\frac{-(F_p(0^-)-F_p(-x_p))}{kT}} = 1 - \frac{J_p}{\mu_p kTp(-x_p)}\frac{L_{D_p}^2}{x_p}e^{\frac{x_p^2}{2L_{D_p}^2}}. \tag{C-28}$$

Now substituting the definition of L_{D_p} and expressing the result in terms of $E(0_-)$ we get

$$\frac{L_{D_p}^2}{x_p} = \frac{kT}{qE(0_-)}. \tag{C-29}$$

So Eq.(C-29) becomes

$$e^{\frac{-(F_p(0^-)-F_p(-x_p))}{kT}} = 1 - \frac{J_p}{q\mu_p p(-x_p)E(0^-)}e^{\frac{x_p^2}{2L_{D_p}^2}}. \tag{C-30}$$

Next we can write the exponent in terms of $V_{bi} - V_{EB}$ using the results of appendix B and get

$$y_p^2 = \frac{x_p^2}{2L_{D_p}^2} = \frac{q}{kT}(\frac{N_D}{N_A + N_D})(V_{bi} - V_{EB}) \tag{C-31}$$

So, Eq.(C-30) becomes

$$e^{\frac{-(F_p(0^-)-F_p(-x_p))}{kT}} = 1 - \frac{J_p}{q\mu_p p(-x_p)E(0^-)}e^{\frac{qV_p}{kT}}, \tag{C-32}$$

where we have used $V_{bi} - V_{EB} = V_n + V_p$ and $V_p = (\frac{\epsilon_n N_D}{\epsilon_p N_A + \epsilon_n N_D})(V_{bi} - V_{EB})$ and $V_n = (\frac{\epsilon_p N_A}{\epsilon_p N_A + \epsilon_n N_D})(V_{bi} - V_{EB})$.

Following Stettler and Lundstrom [66], we can relate $p(-x_p)$ to minority carrier equilibrium concentration on the n-side using

$$p(-x_p) = p_{no}e^{\frac{qV_{bi}-\Delta E_v}{kT}}, \tag{C-33}$$

where $p_{no} = \frac{n_{in}^2}{N_D}$ is the thermal equilibrium carrier concentration on the n-side where n_{in} is the intrinsic concentration on the n-side. Substituting Eq.(C-33) into Eq.(C-32) gives

$$e^{\frac{-(F_p(0^-)-F_p(-x_p))}{kT}} = 1 - \frac{J_p e^{\frac{qV_p}{kT}}}{q\mu_p p_{no}E(0^-)e^{\frac{qV_{bi}-\Delta E_v}{kT}}}. \tag{C-34}$$

Recalling that $V_{bi} - V_{EB} = V_p + V_n$ and using the definition S_{ep}

$$S_{ep} \equiv \mu_p E(0^-)e^{\frac{-(\Delta E_v - qV_n)}{kT}}, \tag{C-35}$$

Eq.(C-33) can be rewritten in the very compact form

$$e^{\frac{-(F_p(0^-)-F_p(-x_p))}{kT}} = 1 - \frac{J_p e^{\frac{-qV_{EB}}{kT}}}{qS_{ep}p_{no}}. \tag{C-36}$$

This expression gives the relationship between the separation of the quasi-Fermi levels of holes at the two ends of the emitter-base space-charge region as a function of the bias V_{EB} and current J_p. This is analogous to the results of Stettler and Lundstrom derived for Np emitter-base junction [66].

Next, we consider the hole thermionic emission current across the emitter-base heterojunction interface. The hole current density across the interface is the difference of the fluxes of the two thermionic currents in the opposite direction:

$$J_p = q[p(0^-)v_R(0^-) - p(0^+)v_R(0^+)e^{\frac{-\Delta E_v}{kT}}], \tag{C-37}$$

where

$$v_R(0^+) = \sqrt{\frac{kT}{2\pi m^*_{p_n}}}, \tag{C-38}$$

and

$$v_R(0^-) = \sqrt{\frac{kT}{2\pi m^*_{p_p}}}, \tag{C-39}$$

where $m^*_{p_n}$ and $m^*_{p_p}$ are the hole effective masses on the n-side and p-side, respectively.

At thermal equilibrium, $J_p = 0$, so we get

$$p_o(0^-)v_R(0^-) = p_o(0^+)v_R(0^+)e^{\frac{-\Delta E_v}{kT}}, \tag{C-40}$$

where $p_o(0^-)$ and $p_o(0^+)$ are the equilibrium values on either side of the heterojunction. Recalling the definitions of the hole quasi-Fermi levels, we can write

$$p(0^+) = N_{v_n}e^{\frac{-(F_p(0^+)-E_v(0^+))}{kT}}, \tag{C-41}$$

and

$$p(0^-) = N_{v_p} e^{\frac{-(F_p(0^-)-E_v(0^-))}{kT}}. \tag{C-42}$$

Since, at thermal equilibrium $F_p(0^-) = F_p(0^+) = E_F$, we have

$$p_o(0^+) = N_{v_n} e^{\frac{-(E_F-E_v(0^+))}{kT}}, \tag{C-43}$$

and

$$p_o(0^-) = N_{v_p} e^{\frac{-(E_F-E_v(0^-))}{kT}}. \tag{C-44}$$

Substituting these results into Eq.(C-40) leads to

$$N_{v_p} v_R(0^-) = N_{v_n} v_R(0^+). \tag{C-45}$$

Using Eqs.(C-45), (C-41) and (C-42) in Eq.(C-37) gives

$$J_p = qN_{v_n} v_R(0^+) e^{\frac{-\Delta E_v}{kT}} e^{\frac{-(F_p(0^+)-E_v(0^+))}{kT}} [e^{\frac{\delta F_p}{kT}} - 1], \tag{C-46}$$

where we use the notation $\delta F_p = F_p(0^+) - F_p(0^-)$, to define the jump in the hole quasi-Fermi level across the emitter-base junction. Using Eq.(C-41), we write Eq.(C-44) as follows

$$J_p = qp(0^+) v_R(0^+) e^{\frac{-\Delta E_v}{kT}} [e^{\frac{\delta F_p}{kT}} - 1]. \tag{C-47}$$

From Eq.(C-48) we can solve for $p(0^+)$

$$p(0^+) = \frac{J_p}{qv_R(0^+)} e^{\frac{\Delta E_v}{kT}} \frac{1}{[e^{\frac{\delta F_p}{kT}} - 1]}. \tag{C-48}$$

Another expression for $p(0^+)$ can be derived starting with Eq.(C-37)

$$p(0^+) = [-\frac{J_p}{qv_R(0^+)} + \frac{p(0^-)v_R(0^-)}{v_R(0^+)}] e^{\frac{\Delta E_v}{kT}}. \tag{C-49}$$

Since

$$p(0^-) = N_{v_p} e^{\frac{-(F_p(0^-)-E_v(0^-))}{kT}} = N_{v_n} \frac{v_R(0^+)}{v_R(0^-)} e^{\frac{-(F_p(0^-)-E_v(0^-))}{kT}}, \tag{C-50}$$

we substitute this result into Eq.(C-49) and obtain

$$p(0^+) = [-\frac{J_p}{qv_R(0^+)} + N_{v_n} e^{\frac{-(F_p(0^-)-E_v(0^-))}{kT}}] e^{\frac{\Delta E_v}{kT}}. \tag{C-51}$$

Next, we make use of Eq.(C-36) which we write as follows

$$e^{\frac{-F_p(0^-)}{kT}} = e^{\frac{-F_p(-x_p)}{kT}} [1 - \frac{J_p e^{\frac{-qV_a}{kT}}}{qS_{ep}p_{no}}]. \tag{C-52}$$

Substituting Eq.(C-52) into Eq.(C-51) gives

$$p(0^+) = e^{\frac{\Delta E_v}{kT}} [\frac{-J_p}{qv_R(0^+)} + N_{v_n} e^{\frac{E_v(0^-)}{kT}} e^{\frac{-F_p(x_p)}{kT}} \{1 - \frac{J_p e^{\frac{-qV_a}{kT}}}{qS_{ep}p_{no}}\}]. \tag{C-53}$$

Now at x = -x_p we have from Eq.(C-41)

$$p(-x_p) = N_{v_p} e^{\frac{-(F_p(-x_p)-E_v(-x_p))}{kT}}, \tag{C-54}$$

and therefore

$$e^{\frac{-F_p(-x_p)}{kT}} = \frac{p(-x_p)}{N_{v_p}} e^{\frac{-E_v(-x_p)}{kT}}. \tag{C-55}$$

From Eq.(C-33), we have

$$p(-x_p) = p_{no} e^{\frac{qV_{bi}-\Delta E_v}{kT}}. \tag{C-56}$$

So Eq.(C-53) becomes

$$e^{\frac{-F_p(-x_p)}{kT}} = \frac{p_{no}}{N_{v_p}} e^{\frac{qV_{bi}-\Delta E_v}{kT}} e^{\frac{-E_v(-x_p)}{kT}}. \tag{C-57}$$

and substituting Eq.(C-57) into Eq.(C-53) finally leads to

$$p(0^+) = e^{\frac{\Delta E_v}{kT}} [\frac{-J_p}{qv_R(0^+)} + N_{v_n} e^{\frac{E_v(0^-)}{kT}} e^{\frac{qV_{bi}-\Delta E_v}{kT}} e^{\frac{-E_v(-x_p)}{kT}} \{1 - \frac{J_p e^{\frac{-qV_a}{kT}}}{qS_{ep}p_{no}}\}]. \tag{C-58}$$

Since $E_v(0^-) - E_v(-x_p) = -qV_p$ and $V_{bi} - V_{EB} = V_n + V_p$, the second expression for $p(0^+)$ becomes

$$p(0^+) = \frac{e^{\frac{\Delta E_v}{kT}}}{qv_R(0^+)}[-J_p + qv_R(0^+)\frac{N_{v_n}}{N_{v_p}}p_{n_o}e^{\frac{-qV_p}{kT}}e^{\frac{qV_{bi}-\Delta E_v}{kT}}\{1 - \frac{J_p e^{\frac{-qV_a}{kT}}}{qS_{ep}p_{no}}\}]. \tag{C-59}$$

Defining an effective velocity for holes across the heterojunction interface as

$$S_{ip} \equiv v_R(0^+)e^{\frac{-(\Delta E_v - qV_n)}{kT}}, \tag{C-60}$$

Eq.(C-59) can then be written as

$$p(0^+) = \frac{e^{\frac{\Delta E_v}{kT}}}{qv_R(0^+)}[-J_p + qS_{ip}\frac{N_{v_n}}{N_{v_p}}p_{n_o}\{1 - \frac{J_p e^{\frac{-qV_a}{kT}}}{qS_{ep}p_{no}}\}]. \tag{C-61}$$

Setting the expressions for $p(0^+)$ in Eq.(C-48) and Eq.(C-61) equal and simplifying we get

$$e^{\frac{-\delta F_p}{kT}} = 1 - \frac{(\frac{N_{v_p}}{N_{v_n}}\frac{J_p e^{\frac{-qV_a}{kT}}}{qp_{no}S_{ip}})}{(1 - \frac{J_p e^{\frac{-qV_a}{kT}}}{qS_{ep}p_{no}})}. \tag{C-62}$$

This is analogous to Stettler and Lundstrom's Eq.(7) in ref [66], except for the additional factor $\frac{N_{v_p}}{N_{v_n}}$ and the difference in the signs.

In the quasi-neutral base region ($x_n \leq x \leq W$), the transport of holes is governed by the following equation derived in appendix D

$$J_p = qD_p^{eff}(\frac{p(x_e) - \tilde{p}(x_c)}{W_B}). \tag{C-63}$$

Satisfying the boundary condition at the collector requires

$$J_p = qp(x_c)v_s, \tag{C-64}$$

where v_s is hole saturation velocity. We can write Eq.(C-63) as

$$J_p = qS_{dp}^{eff}[p(x_e) - \frac{J_p}{qv_s^{eff}}], \tag{C-65}$$

where $S_{dp}^{eff} = S_{dp}/R$ and $v_s^{eff} = v_s/R$ are the effective hole diffusion and saturation velocities due to the linear doping across the base, R is the value of dopant ratio $N_B(x_c)/N_B(x_e)$.

Assuming the n-side to be heavily doped, the hole quasi-Fermi level is constant across the n side of the SCR and

$$p(x_n) = p(0^+)e^{\frac{-qV_n}{kT}}. \tag{C-66}$$

So arranging Eq.(C-65) gives $\frac{J_p}{qS_{dp}^{eff}} = p(x_e) - \frac{J_p}{qv_s^{eff}}$ and

$$p(x_e) = \frac{J_p}{q}[\frac{1}{S_{dp}^{eff}} + \frac{1}{v_s^{eff}}]. \tag{C-67}$$

Substituting Eq.(C-66) into this last result gives an approximation for $p(0^+)$

$$p(0^+) = \frac{J_p}{q}e^{\frac{qV_n}{kT}}[\frac{1}{S_{dp}^{eff}} + \frac{1}{v_s^{eff}}]. \tag{C-68}$$

Setting this expressions for $p(0^+)$ equal to the one obtained in Eq.(C-48) leads to

$$\frac{e^{\frac{\Delta E_v}{kT}}}{v_R(0^+)}\frac{1}{(e^{\frac{\delta F_p}{kT}} - 1)} = e^{\frac{qV_a}{kT}}[\frac{1}{S_{dp}^{eff}} + \frac{1}{v_s^{eff}}]. \tag{C-69}$$

Using the definition of S_{ip} in Eq.(C-60), we get

$$\frac{1}{(e^{\frac{\delta F_p}{kT}} - 1)} = S_{ip}[\frac{1}{S_{dp}^{eff}} + \frac{1}{v_s^{eff}}], \tag{C-70}$$

which can be rearranged as follows

$$\frac{1}{S_{ip}}(\frac{1}{e^{\frac{\delta F_p}{kT}} - 1}) = (\frac{1}{S_{ip}} + \frac{1}{S_{dp}^{eff}} + \frac{1}{v_s^{eff}}). \tag{C-71}$$

which with the help of Eq.(C-62) finally leads to

$$J_p = \frac{qp_{no}(\frac{N_{vn}}{N_{vp}})e^{\frac{qV_{EB}}{kT}}}{[\frac{1}{S_{ip}} + \frac{1}{S_{dp}^{eff}} + \frac{1}{v_s^{eff}} + \frac{1}{S_{ep}}(\frac{N_{vn}}{N_{vp}})]}. \tag{C-72}$$

This last Equation gives the current across the emitter base junction as controlled by the four effective velocities limiting the current flow on the either side of the junction. Equation(C-72) shows that the smallest of the four velocities is the one controlling the intensity of the current across the emitter-base junction.

Appendix D

Hole Transport Across the Base.

Following [69,70], the hole and electron drift and diffusion currents in the quasi-neutral base region are given by

$$J_p = -\mu_p p(x)\frac{d}{dx}[qV(x) + \chi(x) + E_g(x)] - qD_p\frac{dp(x)}{dx}, \tag{D-1}$$

and

$$J_n = -\mu_n n(x)\frac{d}{dx}[qV(x) + \chi(x)] + qD_n\frac{dn(x)}{dx}. \tag{D-2}$$

In our case, μ_p and D_p will be a function of x because the doping will be assumed to vary linearly from emitter to collector in the base region. In the linearly doped base, the majority carrier current is approximated as being negligibly small so $J_n = 0$. Therefore Eq.(D-2) leads to

$$\frac{k_B T}{n(x)}\frac{dn(x)}{dx} = \frac{d}{dx}[qV(x) + X(x)], \tag{D-3}$$

where we have used Einstein's relation, $D_n = \frac{k_B T}{q}\mu_n$.

Furthermore, in the quasi-neutral base region, we have charge neutrality

$$p(x) + N_B(x) = n(x). \tag{D-4}$$

So we can write

$$\frac{dp(x)}{dx} + \frac{dN_B(x)}{dx} = \frac{dn(x)}{dx}. \tag{D-5}$$

Substituting Eq.(D-5) into Eq.(D-3), we get

$$\frac{k_B T}{p(x) + N_B(x)}[\frac{dp(x)}{dx} + \frac{dN_B(x)}{dx}] = \frac{d}{dx}[qV(x) + \chi(x)]. \tag{D-6}$$

Since, we have no energy gap variation in the base, we substitute Eq.(D-6) into Eq.(D-1) and get

$$J_p = -\mu_p k_B T[\frac{p(x)}{p(x) + N_B(x)}]\frac{dp(x)}{dx} - qD_p\frac{dp(x)}{dx}. \tag{D-7}$$

Rearranging and assuming Einstein's relation to be valid for hole transport, we get

$$J_p = -qD_p[\frac{2p(x) + N_B(x)}{p(x) + N_B(x)}]\frac{dp(x)}{dx} - qD_p[\frac{p(x)}{p(x) + N_B(x)}]\frac{dN_B}{dx}. \tag{D-8}$$

We assume a linear grading of the doping in the base region and define a parameter k as follows

$$k = -\frac{dN_B(x)}{dx} = \frac{N_B(x_e) - N_B(x_c)}{W_B}, \tag{D-9}$$

which is positive since $N_B(x_e) > N_B(x_c)$. Hence, the base grading leads to an effective electric field helping the holes to cross the base faster.

Assuming low level injection into the base, i.e, $p(x) << N_B(x)$ we rewrite Eq.(D-8) as

$$J_p = qD_p[-\frac{dp(x)}{dx} + \frac{k}{N_B(x)}p(x)]. \tag{D-10}$$

Neglecting hole recombination in the base and under static conditions, the hole continuity equation implies

$$\frac{dJ_p}{dx} = 0. \tag{D-11}$$

Using Eq.(D-10) we get

$$\frac{dJ_p}{dx} = -q\frac{dD_p}{dx}\frac{dp}{dx} - qD_p\frac{d^2p}{dx^2} + q\frac{dD_p}{dx}\frac{k}{N_B(x)}p(x) + qD_p[-\frac{k}{N_B^2(x)}\frac{dN_B}{dx}p(x) + \frac{k}{N_B(x)}\frac{dp}{dx}] = 0. \tag{D-12}$$

Rearranging the terms, we obtain a second order differential equation for $p(x)$

$$\frac{d^2p}{dx^2} + \frac{dp}{dx}[\frac{1}{D_p}\frac{dD_P}{dx} - \frac{k}{N_B(x)}] + p(x)[-\frac{1}{D_p}\frac{k}{N_B(x)} + \frac{k}{N_B^2(x)}\frac{dN_B}{dx}] = 0. \tag{D-13}$$

If we are in the range of N_B ($10^{18}\ \ cm^{-3} < N_B < 10^{19}\ \ cm^{-3}$) curve fitting parameter γ can be introduced to approximate the mobility dependence on doping

$$\mu = \mu_o(\frac{N_B}{N_C})^{-\gamma}, \tag{D-14}$$

as discussed in Chapter 2 in section 2.2.1. Then using Einstein's relation we derive

$$\frac{1}{D_p}\frac{dD_p}{dx} = \frac{1}{\mu_p}\frac{d\mu_p}{dx} = -\gamma\frac{1}{N_B}\frac{dN_B}{dx}. \tag{D-15}$$

The coefficient of dp/dx in Eq.(D-13) becomes

$$\frac{1}{D_p}\frac{dD_p}{dx} - \frac{k}{N_B} = -\frac{1}{N_B}[\gamma\frac{dN_B}{dx} + k] = -\frac{k'}{N_B(x)}, \tag{D-16}$$

where $k' = k + \gamma\frac{dN_B}{dx} = k(-\gamma+1)$. Similarly, the coefficient of $p(x)$ in Eq.(D-13) becomes

$$-\frac{1}{D_p}\frac{dD_p}{dx}\frac{k}{N_B} + \frac{k}{N_B^2}\frac{dN_B}{dx} = \frac{k}{N_B^2}\frac{dN_B}{dx}(\gamma+1). \tag{D-17}$$

Using, Eq.(D-17), Eq.(D-13) can be rewritten as follows

$$\frac{d^2p}{dx^2} - \frac{dp}{dx}[\frac{k(1-\gamma)}{N_B(x)}] - p(x)\frac{k^2(1+\gamma)}{N_B^2(x)} = 0. \tag{D-18}$$

Introducing a new dimensionless variable y such that

$$y = \frac{x - x_e}{W_B} - \frac{1}{k}\frac{N_B(x_e)}{W_B} = -\frac{N_B(x)}{kW_B}, \tag{D-19}$$

we have

$$\frac{dp}{dx} = \frac{dp}{dy}\frac{dy}{dx} = \frac{dp}{dy}\frac{1}{W_B}, \tag{D-20}$$

and

$$\frac{d^2p}{dx^2} = \frac{d^2p}{dy^2}\frac{1}{W_B^2}. \tag{D-21}$$

Using Eqs.(D-20) and (D-21) we rewrite Eq.(D-18) after multiplying throughout by W_B^2

$$\frac{d^2p}{dy^2} + (1-\gamma)\frac{1}{y}\frac{dp}{dy} - (1+\gamma)\frac{1}{y^2}p(y) = 0. \tag{D-22}$$

Introducing the new parameters $A = 1 - \gamma$ and $B = -(1 + \gamma)$ and multiplying on both sides by y^2, we obtain

$$y^2\frac{d^2p}{dy^2} + Ay\frac{dp}{dy} + Bp(y) = 0. \tag{D-23}$$

This differential equation can be solved exactly if we make the following additional transformation

$$y = -e^v. \tag{D-24}$$

The choice of the minus sign is because y defined in Eq.(D-19), is negative over the neutral base region $[x_e, x_c]$.

Using Eq.(D-24), we obtain

$$\frac{dp}{dy} = -e^{-v}\frac{dp}{dv}, \tag{D-25}$$

and

$$\frac{d^2p}{dy^2} = e^{-2v}[\frac{d^2p}{dv^2} - \frac{dp}{dv}]. \tag{D-26}$$

Substituting back these derivatives in Eq.(D-23), we obtain

$$\frac{d^2p}{dv^2} + \gamma\frac{dp}{dv} - (1+\gamma)p(v) = 0, \tag{D-27}$$

which is a second order differential equation with constant coefficients. Assuming a solution of the form $p = e^{Cv}$, the characteristic equation leads to the two solutions

$$C_+ = \gamma + 1, \tag{D-28}$$

and

$$C_- = -1. \tag{D-29}$$

Therefore, the general solution of Eq.(D-27) is of the form

$$p(v) = D_1 e^{C_+ v} + D_2 e^{C_- v}. \tag{D-30}$$

Hence,

$$p(y) = D_1(-y)^{C_+} + D_2(-y)^{C_-} \tag{D-31}$$

Defining $\alpha = -N_B(x_e)/k$, we obtain

$$p(x_e) = D_1(-\frac{\alpha}{W_B})^{C_+} + D_2(-\frac{\alpha}{W_B})^{C_-} \tag{D-32}$$

and

$$p(x_c) = D_1[-(\frac{W_B+\alpha}{W_B})]^{C_+} + D_2[-(\frac{W_B+\alpha}{W_B})]^{C_-}. \tag{D-33}$$

The last two equations are two equations with two unknowns (D_1, D_2) which must be determined from the boundary conditions $p(x_e)$, $p(x_c)$. Using Cramer's rule we find

$$D_1 = \frac{p(x_e)[-(\frac{W_B+\alpha}{W_B})]^{C_-} - p(x_c)[-(\frac{\alpha}{W_B})]^{C_-}}{D}, \tag{D-34}$$

and

$$D_2 = \frac{p(x_c)[-(\frac{\alpha}{W_B})]^{C_+} - p(x_e)[-(\frac{W_B+\alpha}{W_B})]^{C_+}}{D}, \tag{D-35}$$

where

$$D = (-\frac{\alpha}{W_B})^{C_-}[-(\frac{W_B+\alpha}{W_B})^{C_-}] - (-\frac{\alpha}{W_B})^{C_-}[-(\frac{W_B+\alpha}{W_B})^{C_+}]. \tag{D-36}$$

Using definition (D-19) for the variable y, Eq.(D-31) becomes

$$p(x) = D_1[-(\frac{x-x_e}{W_B}) - \frac{\alpha}{W_B}]^{C_+} + D_2[-(\frac{x-x_e}{W_B}) - \frac{\alpha}{W_B}]^{C_-}. \tag{D-37}$$

Using Eqs.(D-34) and (D-35), we finally obtain

$$p(x) = P_+[-(x-x_e) - \alpha]^{C_+} + P_-[-(x-x_e) - \alpha]^{C_-}, \tag{D-38}$$

where

$$P_+ = \frac{[p(x_e)[-(W_B+\alpha)]^{C_-} - p(x_c)[-\alpha]^{C_-}]}{(-\alpha)^{C_+}[-(W_B+\alpha)]^{C_-} - (-\alpha)^{c_-}[-(W_B+\alpha)]^{C_+}}, \tag{D-39}$$

and

$$P_- = \frac{[p(x_c)[-\alpha]^{C_+} - p(x_e)[-(\alpha+W_B)]^{C_+}]}{(-\alpha)^{C_+}[-(W_B+\alpha)]^{C_-} - (-\alpha)^{c_-}[-(W_B+\alpha)]^{C_+}}. \tag{D-40}$$

We use this expression of $p(x)$ to calculate J_p given by

$$J_p = -qD_p(x)\frac{dp}{dx} + qD_p(x)\frac{k}{N_B(x)}p(x). \tag{D-41}$$

Since J_p is independent if x, we calculate J_p at x = x_e. After a few algebraic steps we obtain

$$J_p = q\frac{D_p^{eff}}{W_B}[p(x_e) - \tilde{p}(x_c)], \tag{D-42}$$

where

$$D_p^{eff} = D_p(x_e)(1-R)[\frac{\gamma+2}{1-R^{\gamma+2}}], \tag{D-43}$$

and

$$\tilde{p}(x_c) = R\,p(x_c), \tag{D-44}$$

where we have defined the dopant gradient, R as

$$R = \frac{N_B(x_c)}{N_B(x_e)}. \tag{D-45}$$

We note that in the limit of uniform doping across the base, R tends to unity and

$$\tilde{p}(x_c) = p(x_c), \tag{D-46}$$

and

$$\tilde{D_p}^{eff} = D_p(x_e). \tag{D-47}$$

In that case, Eq.(D-43) reduces to the well-known result

$$J_p = \frac{qD_p(x_e)}{W_B}[p(x_e) - p(x_c)]. \tag{D-48}$$

At the collector end of the base, we have the boundary condition

$$p(x_c) = \frac{J_p}{qv_s}, \tag{D-49}$$

where v_s is the hole saturation velocity. Hence, for the case of linear dopant grading, we can also write

$$\tilde{p}(x_c) = \frac{J_p}{qv_s^{eff}} \tag{D-50}$$

if we introduce an effective saturation velocity

$$v_s^{eff} = \frac{v_s}{R}. \tag{D-51}$$

Since $R < 1$ in the case of non-uniform doping, Eq.(D-51) implies that, it is as if the effective saturation velocity of hole is increased when non-uniform doping is used in the base region. Starting with Eq.(D-49), Eq.(D-43) becomes

$$J_p = qS_{dp}^{eff}(p(x_e) - \frac{J_p}{qv_s^{eff}}), \tag{D-52}$$

where we have defined $S_{dp}^{eff} = D_p^{eff}/W_B$.

Appendix E

Recombination Current Components

In this appendix, we derive explicitly the nonradiative (J_{br}) and radiative (J_{rr}) recombination currents. The nonradiative base recombination current is given by [69,70].

$$J_{br} = q \int_{x_e}^{x_c} \frac{[p(x) - p_o(x)]}{\tau_p(N_B(x))} dx, \tag{E-1}$$

where τ_p in nsec is given by

$$\tau_p(N_B(x)) = 10^{\delta - \vartheta log N_B(x)}, \tag{E-2}$$

as discussed in section 2.2.2. Using this last equation, we get

$$\frac{1}{\tau_p(N_B(x))} = \frac{N_B(x_e)^{\vartheta}}{10^{\delta}}, \tag{E-3}$$

where

$$N_B(x) = N_B(x_e) - k(x - x_e). \tag{E-4}$$

We rewrite Eq.(E-1) for J_{br} as $J_{br}^1 - J_{br}^2$ where

$$J_{br}^1 = q \int_{x_e}^{x_c} \frac{p(x)}{\tau_p(N_B(x))} dx, \tag{E-5}$$

and

$$J_{br}^2 = q \int_{x_e}^{x_c} \frac{p_o(x)}{\tau_p(N_B(x))}\ dx. \tag{E-6}$$

We first calculate J_{br}^1

$$J_{br}^1 = q10^{-\delta} \int_{x_e}^{x_c} N_B(x)^{\vartheta} p(x)\ dx. \tag{E-7}$$

The hole concentration was calculated explicitly in appendix D

$$p(x) = \frac{1}{[1 - R^{\gamma+2}]} \{A_1 z^{C_+} + A_2 z^{C_-}\} \tag{E-8}$$

where $A_1 = (1-R)^{\gamma+1}[p(x_e) - Rp(x_c)]$, $A_2 = \frac{R}{1-R}[p(x_c) - R^{\gamma+1}p(x_e)]$, and

$$z = -\frac{x - x_e}{W_B} - \frac{\alpha}{W_B}. \tag{E-9}$$

Rewriting $N_B(x)$ in terms of z

$$N_B(x) = kW_B[\frac{-\alpha}{W_B} - \frac{x - x_e}{W_B}] = kW_B z, \tag{E-10}$$

we obtain

$$J_{br}^1 = \frac{-qW_B 10^{-\delta}(kW_B)^{\vartheta}}{[1 - R^{\gamma+2}]} \int_{-\alpha/W_B}^{-(1+\alpha/W_B)} z^{\vartheta} \{A_1 z^{C_+} + A_2 z^{C_-}\} dz. \tag{E-11}$$

In the above integral the limits can be rewritten in terms of the dopant gradient from 1/1-R (lower limit) to R/1-R (upper limit). A straightforward but lengthy derivation leads to

$$J_{br}^1 = \frac{qW_B}{\tau(x_e)}[p(x_e)A(R) + p(x_c)B(R)], \tag{E-12}$$

where

$$A(R) = \frac{1}{(\gamma+\vartheta+2)(1-R)}\frac{(1-R^{\gamma+\vartheta+2})}{[1-R^{\gamma+2}]} - \frac{R^{\gamma+2}}{(1-R)}\frac{1}{\vartheta}\frac{1-R^{\vartheta}}{1-R^{\gamma+2}}, \tag{E-13}$$

and

$$B(R) = (\frac{R}{1-R})\frac{1}{1-R^{\gamma+2}}[\frac{1-R^{\vartheta}}{\vartheta} - \frac{1-R^{\gamma+\vartheta+2}}{(\gamma+\vartheta+2)}]. \tag{E-14}$$

Next, we calculate the second integral

$$J_{br}^2 = q\int_{x_e}^{x_c} \frac{p_o(x)}{\tau_p(N_B(x))}dx, \tag{E-15}$$

where

$$p_o(x) = \frac{n_{io}^2}{N_B(x)}, \tag{E-16}$$

is the hole concentration in the base. Substituting Eq.(E-16) into Eq.(E-15), we get

$$J_{br}^2 = q\int_{x_e}^{x_c} \frac{n_{io}^2}{N_B(x)\ \tau_p(N_B(x))}dx. \tag{E-17}$$

Now, using Eqs.(E-3), (E-9) and (E-10) we can write Eq.(E-18) as

$$J_{br}^2 = \frac{-qW_B n_{io}^2}{10^{\beta}}(kW_B)^{\vartheta-1}\int_{1/1-R}^{R/1-R} z^{\vartheta-1}\,dz. \tag{E-18}$$

Upon integrating we have

$$J_{br}^2 = \frac{qW_B n_{io}^2}{N_B(x_e)\tau_p(x_e)\vartheta}\frac{(1-R^{\vartheta})}{(1-R)}. \tag{E-19}$$

The contribution of J_{br}^2 is actually much less than J_{br}^1.

The radiative component of the base current is given by [69,70]

$$J_{rr} = qB\int_{x_e}^{x_c}[N_B(x)p(x) - n_i^2(x)]dx. \tag{E-20}$$

Once again, we split J_{rr} into two contributions

$$J_{rr} = J_{rr}^1 + J_{rr}^2, \tag{E-21}$$

We calculate J_{rr}^1 as

$$J_{rr}^1 = qB \int_{x_e}^{x_c} N_B(x) p(x) dx. \tag{E-22}$$

Using Eq.(E-10) for $N_B(x)$, Eq.(E-8) for $p(x)$ and Eq.(E-9), we write the above integral as

$$J_{rr}^1 = -qBN_B(x_e)(1-R)W_B \int_{1/1-R}^{R/1-R} [A_1 z^{\gamma+2} \ + \ A_2] \ dz. \tag{E-23}$$

Upon integrating we fixed,

$$\begin{aligned} J_{rr}^1 \ &= \ qBN_B(x_e)W_B[p(x_e)(\frac{1-R^{\gamma+3}}{(\gamma+3)(1-R)} - R^{\gamma+2})(\frac{1}{1-R^{\gamma+2}}) \\ &\quad + p(x_c)(\frac{R}{1-R^{\gamma+2}})[1 - \frac{1-R^{\gamma+3}}{(1-R)(\gamma+3)}]. \end{aligned} \tag{E-24}$$

.

The second integral J_{rr}^2 is simply

$$J_{rr}^2 = -qB \int_{x_e}^{x_c} n_i^2 dx = -qBn_i^2 W_B, \tag{E-25}$$

since n_i is constant across the quasi-neutral base region.

Appendix F

Calculation of Base Transit Time

The base transit time can be calculated using

$$\tau_b = \int_{x_e}^{x_c} \frac{dx}{v(x)}, \tag{F-1}$$

where v(x) is the average velocity of holes across the base and is related to the hole current J_p as follows

$$v^{-1}(x) = \frac{q}{J_p}(p(x) - p_o(x)). \tag{F-2}$$

In this last equation, $p_o(x)$ is the hole equilibrium concentration

$$p_o(x) = \frac{n_{io}^2}{N_B(x)}, \tag{F-3}$$

and

$$N_B(x) = N_B(x_e) - k(x - x_e), \tag{F-4}$$

where k is defined as

$$k = \frac{(N_B(x_e) - N_B(x_c))}{W_B}. \tag{F-5}$$

Using the above results, the integral for τ_b becomes

$$\tau_b = \frac{q}{J_p}\int_{x_e}^{x_c}(p(x) - p_o(x))dx. \tag{F-6}$$

We first calculate the contribution of $p_o(x)$ in the τ_b integral (we name it τ_2)

$$\tau_2 = -\frac{q}{J_p}\int_{x_e}^{x_c} p_o(x)dx. \tag{F-7}$$

Starting with Eqs.(F-3) and (F-5) we get

$$\tau_2 = -\frac{q}{J_p}\int_{x_e}^{x_c} \frac{n_{io}^2}{W_B k(\frac{-(x-x_e)}{W_B} + \frac{N_B(x_e)}{kW_B})}\, dx. \tag{F-8}$$

Introducing a new variable

$$z = -\frac{(x-x_e)}{W_B} - \frac{\alpha}{W_B}, \tag{F-9}$$

and using the definition of $\alpha = -\frac{N_B(x_e)}{k}$, the integral τ_2 becomes

$$\tau_2 = \frac{q}{J_p}\frac{n_{io}^2}{k}\int_{-\frac{\alpha}{W_B}}^{(-1+\frac{\alpha}{W_B})} \frac{dz}{z}, \tag{F-10}$$

which can be evaluated exactly

$$\tau_2 = \frac{q}{J_p}\frac{n_{io}^2}{k}\, lnR, \tag{F-11}$$

where R is the dopant grading given by $N_B(x_c)/N_B(x_e)$.

Next, we calculate the contribution of $p(x)$ in τ_b integral (we call it τ_1)

$$\tau_1 = \frac{q}{J_p}\int_{x_e}^{x_c} p(x)dx, \tag{F-12}$$

where

$$p(x) = \frac{1}{[1+R^{\gamma+2}]}\{A_1\{-(\frac{x-x_e}{W_B}) + \frac{1}{1-R}\}^{C_+} + A_2\{-(\frac{x-x_e}{W_B}) + \frac{1}{1-R}\}^{C_-}\}, \quad \text{(F-13)}$$

with

$$A_1 = (1-R)^{1+\gamma}[p(x_e) - Rp(x_c)], \quad \text{(F-14)}$$

and

$$A_2 = \frac{R}{1-R}[p(x_c) - R^{\gamma+1}p(x_e)]. \quad \text{(F-15)}$$

The relations between the constants C^+, C^- and γ are given in appendix D. Using Eq.(F-9), the integral τ_1 becomes

$$\tau_1 = \frac{-qW_B}{J_p(1-R^{\gamma+2})}\int_{1/1-R}^{R/1-R}(A_1 z^{C^+} + B_1 z^{C^-})dz. \quad \text{(F-16)}$$

Straight forward algebra leads to

$$\tau_1 = \frac{q}{J_p}W_B\{p(x_e)f(R) \; - \; p(x_c)g(R)\}, \quad \text{(F-17)}$$

where

$$f(R) = \frac{1}{\gamma+2}\frac{1}{1-\gamma} + \frac{R^{\gamma+2}}{1-R}(\frac{lnR}{1-R^{\gamma+2}}), \quad \text{(F-18)}$$

and

$$g(R) = \frac{R}{(\gamma+2)(1-R)} + \frac{R}{1-R}(\frac{lnR}{1-R^{\gamma+2}}). \quad \text{(F-19)}$$

The contribution of τ_2 to the base transit time is actually small compared to τ_1. In our numerical simulations, we ignore the contribution of τ_2. The expressions for τ_1 can be written in a more compact form with Eq.(D-52)

$$J_p = \frac{q}{W_B}D_p^{eff}[p(x_e) - \frac{J_p}{qv_s^{eff}}] \quad \text{(F-20)}$$

derived in appendix D. Solving this equation for $p(x_e)$ we get

$$p(x_e) = \frac{J_p W_B}{q D_p^{eff}}[1 + \frac{1}{W_B}\frac{D_p^{eff}}{v_s^{eff}}], \tag{F-21}$$

with the explicit expression for D_p^{eff} is given in appendix D. Furthermore, we have

$$p(x_c) = \frac{J_p}{q v_s}. \tag{F-22}$$

Substituting the last two expressions $p(x_e)$ and $p(x_c)$ in Eq.(F-17) for τ_1, we get a familiar compact expression for the base transit time

$$\tau_1 = \frac{W_B^2}{2\tilde{D_p}} + \frac{W_B}{\tilde{v_s}} \tag{F-23}$$

where we have introduced the effective diffusion coefficient

$$\tilde{D_p} = \frac{D_p^{eff}}{f(R)}, \tag{F-24}$$

and effective saturation velocity

$$\tilde{v_s} = \frac{v_s}{[Rf(R) - g(R)]}. \tag{F-25}$$